Design and In-Vitro Characterisation of Novel Sorbent Device for Extracorporeal Blood Filtration and Other Applications

Christopher R. Jackson

Biomedical Technology and Cell Therapy Research Laboratory
Department of Biomedical Engineering
Faculty of Medicine
McGill University
Montreal, Quebec, Canada

April 2012

A thesis submitted to McGill University in partial fulfillment
of the requirements of the degree of Master's in Biomedical Engineering

To Aunt Mary, for

never being scared to

ask questions.

Abstract

Patients suffering from chronic renal disease and acute liver failure may require extracorporeal blood filtration to clear toxins from their blood. Sorbent materials are used in re-circulating hemodialysis devices and hemoperfusion devices, but they can be expensive to manufacture. Current sphere and particle shaped sorbent materials create large pressure drops when subjected to a passing fluid, further reducing the practicality of their use. To address these problems, a novel sorbent material was developed in this thesis by co-depositing alginate and activated carbon onto a steel wire mesh using electrophoretic deposition.

A device was first created to perform electrophoretic deposition and to characterize the process as applied to three different grades of alginate. The properties of the resultant gels were compared, and the medium viscosity grade alginate was selected as the sorbent matrix. Alginate and activated carbon were co-deposited onto steel wire mesh to create a novel sorbent material. The sorbent gel physical properties were characterized. The process was analysed in context of dimensional optimization. A solution consisting of urea, uric acid, ammonia and creatinine was used to evaluate the sorbent performance of the material which was compared to other activated carbon immobilization techniques from literature. The material was shown to have promise as a blood toxin absorbent. The process outlines in this thesis is highly versatile, inexpensive, can easily be performed on an industrial scale, and could easily be adapted for a wide range of biomedical applications.

Résumé

Les patients souffrant de maladies rénales chroniques et de maladies hépatiques peuvent necessiter de la filtration sanguine extracorporelle pour éliminer les toxines de leur sang. Des matériaux absorbants sont utilisés dans les dispositifs d'hémodialyse recirculation et les dispositifs hemoperfusion, mais ils peuvent être coûteux à fabriquer. Les sphères et les particules de matériaux absorbants courramment utilisées créent de grandes chutes de pression quand ils sont soumis à un fluide circulant. Pour résoudre ces problèmes, un nouveau matériau absorbant a été développé dans cette thèse en déposant du carbone activé et de l'alginate sur un treillis d'acier inoxydable en utilisant un dépôt électrophorétique.

Un dispositif a d'abord été créé pour effectuer le dépôt électrophorétique et pour caractériser le processus tel qu'il est appliqué à trois types différents de l'alginate. Les propriétés des gels obtenus ont été comparées, et l'alginate de viscosité moyenne a été sélectionnée pour être utilisé dans le matériau sorbant. Les propriétés physiques du treillis sorbant ont été caractérisées. Le processus a été analysé dans le contexte de l'optimisation dimensionnelle. Le rendement des sorbants du matériel a été évalué pour l'urée, l'acide urique, l'ammoniac et de la créatinine, et il a été comparé à d'autres techniques d'immobilisation de carbone activée de la littérature. Le matériel a déjà été démontré pour être prometteur comme absorbant de toxine du sang. Le processus décrit dans cette thèse est très polyvalent, peu coûteux, peut facilement être réalisé à l'échelle industrielle, et pourrait facilement être adapté pour une large gamme d'applications biomédicales.

Acknowledgements

Thank you to Prof. Satya Prakash, research supervisor for the Masters project. Thank you to Dr. Hani Saleh Fadhl Al-Salami of McGill University for his help with statistical analysis. Thank you to Dr. Pavan M. V. Raja for his help and guidance throughout the project, as well as the other members of the Biomedical Technology and Cell Therapy Research Laboratory at McGill University. Pierre Ménard-Tremblay is to thank for performing the Gel Permeation Chromatography experiment and for running the analysis at l'Université de Montréal. The author would also like to acknowledge Dr. Jamal Daoud and Mina Mekhail of the Biomaterials Research Group at McGill University for helping out with the lyophilization procedure and the contact angle test, and SEM imaging respectively.

The author would also like to acknowledge the Canadian Institute of Health Research (CIHR) grant (MOP 93641) to Dr. S. Prakash, and for funding provided by the Natural Sciences and Engineering Research Council of Canada (NSERC).

Preface

In accordance with the McGill thesis preparation and submission guidelines, the thesis is written as a compilation of original papers. This section is provided in the McGill University Thesis Preparation and Submission Guidelines as follows: "As an alternative to the traditional thesis style, the research may be presented as a collection of papers of which the student is the author or co-author (i.e., the text of one or more manuscripts, submitted or to be submitted for publication, and/or published articles [not as reprints] but reformatted according to thesis requirements as described below). These papers must have a cohesive, unitary character making them a report of a single program of research."

The research articles presented in this thesis (chapters 3, 4 and 5) are divided into the following sections: Abstract, Introduction, Materials and Methods, Results, Discussion, and Conclusions. This thesis also includes a common Abstract, General Introduction, Literature Review, Summary of Results, General Discussion, Conclusions and Future Recommendations, and References. Prefaces are given to each of the research chapters to bridge concepts.

This thesis focuses on the development of a novel immobilization technique. Although there are numerous applications, this thesis focuses on extracorporeal blood filtration applications.

List of Abbreviations

AC	Activated Carbon
ALF	Acute Liver Failure
ANOVA	Analysis of Variance
Au	Gold
CRD	Chronic Renal Disease
ECBF	Extracorporeal Blood Filtration
EPD	Electrophoretic Deposition
ESKD	End Stage Kidney Disease
GPC	Gel Permeation Chromatography
HAlg	Alginic Acid
HV	High Viscosity
LV	Low Viscosity
MV	Medium Viscosity
Na-Alg	Sodium Alginate
Pd	Palladium
SEM	Scanning Electron Microscopy
TGA	Thermogravimetric Analysis

Symbols

Symbol	Units	Description
A_{open}	mm^2	Open area of the mesh
A_{tot}	mm^2	Total area of the mesh
C	g/L	Concentration
C_{p_A}	g/L	Concentration of chemical A in plasma
C_{u_A}	g/L	Concentration of chemical A in urine
C'	g/L	Critical concentration
E	V/cm	Electric field strength
K_{cell}	-	Pressure loss coefficient
L	cm	Distance between electrodes
m	g	Mass
m_0	g	Initial mass
M_n	kD	Number average molecular weight
M_w	kD	Weight average molecular weight
M_z	kD	Size average molecular weight
R_f	-	Resistivity ratio
R_{open}	-	Open area ratio
S	cm^2	Surface area
t	s	Time
t_{gel}	mm	Gel thickness
U_m	m/s	Fluid velocity
V	L, mL	Volume

Symbols (continued)

Symbol	Units	Description
V_{solid}	mL	Non-fluid volume of a material
V_{total}	mL	Total volume of a material
$\dot{V}_{p_A}$	L/h	Cleared volume of blood per unit of time
$\dot{V}_u$	L/h	Urine volume excreted per unit time
ΔP_{cell}	N/m^2	Pressure loss
ε	-	Porosity
$[\eta]$	mL/g	Intrinsic viscosity
μ_e	cm^2/Vs	Electrophoretic mobility
ρ	g/cm^3	Fluid density

A "-" is shown for all cases where the symbol is unitless

Table of Contents

Table of Figures

Table of Tables

Chapter 1: Introduction

Extracorporeal blood filtration (ECBF) is a technique used to filter waste from the blood and includes hemodialysis and hemoperfusion. ECBF is commonly used to treat chronic renal disease (CRD) and blood poisoning, and as a bridging treatment for acute liver failure (ALF).

In hemodialysis, blood is flowed through a network of capillaries. The capillary walls are made of a porous dialyser membrane so toxins may be transported freely from one side of the capillary wall to the other. Dialysate is flowed on the outside of the capillaries and absorbs toxins from the blood before it is disposed of [1]. CRD patients will typically undergo this treatment for up to 4 hours a day, 3 days a week [2]. With the hopes of one day creating a fully portable device, researchers are passing dialysate through sorbent cartridges to filter waste in order to safely recirculate the dialysate [1, 3]. This approach has already been taken in numerous systems [4-6] and is expected to greatly improve the quality of life of patients [7]. Reducing the weight of the system is nevertheless paramount to its future success. One possible approach is to reduce the drag created by the sorbent cartridge which would allow for designers to use smaller and lighter motors and batteries.

Alternatively, in hemoperfusion blood runs over a sorbent material which absorbs waste particles directly. This technique is popular in treating patients with ALF and acute poisoning, but is sometimes used in CRD patients as well [8, 9]. Although activated carbon (AC) is commonly used as a generalized sorbent due to its

large specific surface area and its high affinity for numerous blood toxins [10, 11], it cannot be in direct contact with the blood [12]. An immobilizing polymer such as alginate is commonly used to microencapsulate AC for this purpose [13]. This technique is nevertheless cumbersome and expensive, and although the packed bed of spheres will yield a large contact area with the blood [14-16], it also produces a large pressure drop. Small beads also require a large overhead to produce, and the process is poorly scalable.

To reduce the cost of production of sorbent materials for ECBF devices and to improve upon current design problems associated with recirculating hemodialysis devices, a novel sorbent material was developed and evaluated *in-vitro*.

Chapter 2: Literature Review

2.1 Extracorporeal Blood Filtration Techniques

2.1.1 Overview

Extracorporeal Blood Filtration (ECBF) is a treatment used to remove excess water and waste from the blood. The process is deemed necessary whenever it can increase the rate at which the body removes toxins by at least 30% [17] and it is commonly used in the treatment of Chronic Renal Disease (CRD), liver failure and blood poisoning [8, 9]. CRD patients typically undergo treatment for up to 4 hours a day and 3 days a week [2]. Although patients suffering from acute drug intoxication and patients that have recently suffered from liver failure may also undergo dialysis, their treatment can last for up to 48 hours, and is typically repeated only once or a few times [17].

2.1.2 Single-Pass and Recirculating Hemodialysis Systems

Hemodialysis is the most common extracorporeal blood filtration technique used for CRD patients. Blood is circulated through a network of synthetic capillaries made of dialyzer membrane. In single-pass systems, hundreds of litres of dialyser fluid pass in the opposite direction of the blood on the outside of the capillary. The porous nature of the capillary walls allows for ultrafiltration of the hemotoxins through the membrane into the dialyzer fluid, thereby removing waste from the blood [1]. See Figure 2.1.

Recent efforts have aimed at increasing the portability of the classic hemodialysis system with hopes of one day giving patients full mobility throughout the treatment. To accomplish this, recirculating systems were developed that clear the dialysate of toxins so that it can be recirculated. This greatly reduces the volume of dialysate required for treatment and eliminates the need to attach the dialysis machine to a drain (Figure 2. 2). This method was first suggested as an alternative to single pass proportioning dialysis systems by Reynolds after a similar approach was developed by NASA to recycle waste water in the 1960s [1].

In recirculating hemodialysis systems, sorbent dialyser-purifying cartridges are used such as the REDY cartridge developed by SORB technology (Oklahoma City, Oklahoma, US) [18]. Modern dialyser filters consist of four sections [1, 3]. In the first section, activated carbon is used to absorb heavy metals, oxidants, chloramines, creatinine, uric acid, and a number of organic waste molecules. In the second section, immobilized urease is used to break down urea. In the third section, zirconium phosphate exchanges its Na^+ and H^+ ions for K^+, Ca^{2+}, Mg^{2+}, metallic ions and ammonium. In the final section, zirconium phosphate is used to exchange Na^+, HCO_3^- and acetate for PO_4^{3-}, fluoride and heavy metals in the blood.

There are numerous advantages to the multi-pass dialyser systems over single-pass systems. As sorbent cartridges are disposable, the equipment requires less maintenance and is less susceptible to contamination. Only 6 L of tap water is required per treatment compared to over 120 L of highly sterilised fluid for a typical single-pass systems [3]. The smaller and more light-weight systems are more

practical for home use and are more versatile for on-site use in emergencies and for military applications. If a practical portable dialyser system were realized, the increased portability would facilitate increasing treatment frequencies and durations which has already been shown to eliminate patients' dependency on phosphate binders and blood pressure drugs, increase sodium retention, reduce hyperkalemia, hyperphosphosphatemia from bone disease, metabolic acidosis cardiovascular disease, strokes, hypertension, anemia, morbidity and mortality, and help increases patients' appetite, nutrition, volume control, serum albumin levels and quality of life due to liberalization of the diet and fluid restrictions [7].

There are currently a number of multi-pass dialysers either in development or on the market. Some of these include the Allient® system (Renal Solutions In. Warrendale, Pa, USA) [4], the Xcorporeal® Wearable Artificial Kidney (The WAK, Los Angeles, CA, USA) [5] and the Molecular Adsorbent Recirculating System (Gambro, Stockholm, Sweden) [6].

2.1.3 Peritoneal Dialysis

One of the most common alternatives to hemodialysis for patients suffering from CRD is peritoneal dialysis. In this method, patients add a sterile fluid to their abdominal cavity. Toxins diffuse into the fluid via the peritoneal membrane. The fluid is drained and replaced for periodic clearance of the blood.

2.1.4 Hemoperfusion

Hemoperfusion is commonly used to help treat patients suffering from acute liver failure and acute drug intoxication. Although it is not as popular as hemodialysis, it has also been used to treat CRD.

In hemoperfusion, blood is passed directly over a sorbent material. Immobilised activated carbon (AC) is commonly used as the generalized sorbent material due to its high porosity, high specific surface area and its relatively low cost. See Figure 2.3. AC is an excellent sorbent material for removing middle molecules, uric acid, creatinine, and other organic compounds from the blood [10, 11]. In general, it has been shown to have a strong affinity for molecules with low charge and with molecular weights greater than 100 [3].

2.2 Applications of Extracorporeal Blood Filtration Devices

2.2.1 Kidney Function and Disease

The kidneys are two symmetrical organs that form part of the urinary system and are located within the abdominal cavity. Approximately 20% of the cardiac supply is diverted through the renal arteries into the kidneys where waste is removed from the blood [19]. Waste is dissolved in the urine which is diverted to the bladder and excreted through the urinary tract [20].

The kidneys play an important role in the reabsorption of water, glomerular filtration and the control of the blood inorganic ion composition, volume and pressure [21]. The kidneys are responsible for gluconeogenesis, the production of

glucose from amino acids and various precursors, as well at the production of hormones such as erythropoietin, renin, and 1,25-dihydroxyvitamin D.

The kidney filtration rate is calculated separately for each chemical, and represents the volume of blood that is completely cleared of a chemical per unit of time [21]. This is calculated as:

Eq. 1

$$\dot{V}_{p_A} = \frac{C_{u_A}\dot{V}_u}{C_{p_A}}$$

where $\dot{V}_{p_A}$ is the cleared volume of blood per unit of time [L/h], C_{u_A} is the concentration of chemical A in the urine [g/L], $\dot{V}_u$ is the volume of urine excreted per unit time [L/h], and C_{p_A} is the concentration of chemical A in the plasma [g/L].

Chronic renal disease (CRD) is characterised by the progressive loss of renal function over time and affects between 1.9 and 2.3 million Canadians [22]. In the United States, CRD is estimated to cost $24 billion dollars annually [23]. Patients showing signs of CRD are screened for blood levels of creatinine which is an indicator of the kidney glomerular filtration rate. Patients are often at risk of CRD if they have high blood pressure, diabetes, or if they have blood relatives with CRD.

Symptoms of CRD include increase in blood pressure, reduction in erythropoietin production, azotemia, uremia, potassium accumulation, fluid volume overload, hyperphosphatemia and metabolic acidosis. Symptoms can be mitigated through supplements, a tight control over nutrition, medication, and through

extracorporeal dialysis. Currently, the only permanent solution is through kidney transplantation [24].

2.2.2 Acute Liver Failure

Patients are at risk of acute liver failure (ALF) when their liver becomes severely damaged. This occurs when liver cells no longer function which causes cardiovascular collapse, encephalopathy, and other symptoms [6, 25]. There are over 100 different forms of liver diseases including hepatitis, liver cancer, poisoning and cirrhosis [26]. In 2009, over 100,000 Americans died of cirrhosis alone [27].

Spontaneous recovery from ALF is possible, and the probability of occurrence depends on the stage of the disease. Spontaneous recovery occurs in 65-70% of stage II, 40-50% of stage III, and 20% of stage IV ALF patients [28]. Although there are medications under development such as acetylcysteine [29, 30] and various stem cell approaches are being explored [31-33], the long term survival of patients is not currently possible without transplantation unless spontaneous recovery occurs. Due to the scarcity of donors, only 20% of patients that require liver transplants in the United States receive them [34]. Only recently have techniques been developed that can remove the albumin-bound toxins that are normally cleared by the liver [35]. Thus, to prolong the patient's life long enough for either a donor to become available or for spontaneous recovery to occur, patients may be subjected to extracorporeal flood filtration. This allows for the clearance of toxins no longer cleared by the failing liver that would further harm the body if not removed. Moreover, in certain cases, it may remove a poison whose presence was preventing

spontaneous recovery. Spontaneous recovery is the preferred outcome as it avoids many of the complications of liver transplantation [28]. Liver dialysis is still a relatively new technique.

2.3 Current Limitations in Extracorporeal Blood Filtration Techniques

2.3.1 Multi-Pass Hemodialysis Limitations

Multi-pass dialyser systems are an emerging technology, and costs are still too high for widespread use. Currently, there are numerous design challenges associated with the systems. The filters use small sorbent particles which result in a large pressure drop when the dialyser fluid passes through it. Stronger pumps and larger batteries are required to overcome large pressure drops which add to the mass of the system. Cartridges are also expensive, driving up the cost of operating the system.

2.3.2 Peritoneal Dialysis

Peritoneal dialysis requires a highly invasive procedure. Although this procedure gives patients greater autonomy, replacing the fluid is cumbersome. One approach to reduce the frequency with which the fluid is replaced is to circulate it through a sorbent filter such as the REDY system [36]. Citing the need to reduce the resistance caused by the small particle sizes of the sorbent filter, Ofsthun and Stennett proposed immobilizing the sorbent particles on the inner walls of long hollow tubes [37]. Further work is still required before clinical trials can be performed.

2.3.3 Hemoperfusion

When a sorbent particulate such as AC is used for hemoperfusion it must be free from particulate fines and it must resist attrition [38]. AC should not be in direct contact with the blood as it causes thrombocytopenia and neutropenia [12]. To satisfy the above criteria, an immobilization agent is often used [13]. Microcapsules are popular for this purpose as they can be produced on the micron scale, ensuring a high surface-area-to-volume ratio [14-16]. Although microencapsulation will yield a sorbent material with a large contact area with the blood for a given volume, it requires an expensive secondary polymer to form the beads. Moreover, for smaller beads with improved surface area to volume ratios, a large overhead is required and the process may be poorly adapted for large scale production. The spherical geometry is also not ideal as it creates a considerable pressure drop in passing fluid when compared with other geometries that have equivalent absorptive behaviour.

Hemodialysis is highly efficient at removing excess water and molecules smaller than 500 D from the blood [38]. Nevertheless, molecules in the range of 1-50 kD are poorly removed due to the nature of the high flux dialysis membrane. It has been shown that their continued presence in the patients' blood has been linked to amyloidosis and cardiovascular disease [39-41]. In one study, the enhanced removal of middle molecules increased patients' survival by 5 % [42]. It has recently been suggested that the removal of an additional spectrum of molecules can only be achieved through direct contact of sorbent material with the blood [10]. A combination of hemoperfusion and hemodialysis may be required in order to

efficiently remove low molecular weight toxins while also removing middle-molecules [43].

An alternate to the generalized sorbent approach is to use resins developed to bind to specific molecules such as β_2-Microglobulin [44]. Although such resins can be tailored with high biocompatibility, there are at least 100 uremic toxins that have been discovered, rendering the molecular specific resin approach unrealistic for most applications [45].

2.4 Design Criteria for Novel Extracorporeal Blood Filtration Sorbent Material

There are numerous design criteria for sorbent material to be used in ECBF. As general sorbents are more practical than specific sorbents, the material should be able to absorb a variety of blood toxins. The absorptive capability of a given material in light of a given chemical depends on the concentration of the chemical in the solution in contact with the material. As the concentration increases, so does the absorptive capability. There is no standard set of conditions in which sorbent materials are evaluated *in-vitro* for ECBF, however the initial concentration of the toxins being absorbed must be higher that physiological conditions for the data to be useful in predicting *in-vivo* behaviour. Creatinine and uric acid are commonly evaluated *in-vitro* using either blood or a saline solution; other chemicals that have been evaluated include uric acid, nembutal, albumin and inulin [46-48]. A general sorbent material should have pores larger than the chemicals to be absorbed.

The surface area over which the blood or dialysate flows must be large in order to facilitate the toxin diffusion into the material. The ideal geometry should result in the smallest possible pressure drop in the passing fluid while optimising mass transfer.

2.5 Background on Method for Designing Novel Sorbent Material

2.5.1 Electrophoretic Deposition

2.5.1.1 Overview

Electrophoretic deposition (EPD) was first performed in 1808 by Ruess on clay particles suspended in water. The process was developed slowly and it wasn't until 1933 that the first patent was issued for an EPD process for the deposition of thoria particles onto a platinum substrate [49]. At that time, EPD gained attention in academia with extensive research performed by Hamaker who was the first to model deposition rates [50]. In the last 20 years, researchers have focused on EPD as a means of creating advanced materials including functional and structural ceramic coatings, laminated ceramics, biomaterials, composites, porous materials, thin films and nanostructured materials [51]. Today, EPD is considered a relatively inexpensive method of forming uniform layers or bi-layers on substrates with complex geometries.

EDP is carried out by first suspending particles or dissolving ions in solution. A substrate and counter-electrode are placed in the solution and an electric field is induced between them, driving the particles/ions towards the substrate as shown in Figure 2.4. The particles/ions then form a solid film on the substrate through a

number of possible mechanisms including flocculation through accumulation [52], particle charge neutralization [53], particle coagulation [51], and electrical double layer thinning [54]. As long as particles can be suspended in a stable solution and are free to migrate towards the electrode, they can be used as a deposition material. Fine powders, metals, polymers, ceramics and glass have all been used for EPD, although in many cases a heat-treatment or sintering step is required post-deposition [54-57].

EPD has been used on a number of biomaterials such as bioceramics, bioactive materials such as hypoxyapatite [58, 59], biodegradable materials such as Bioglass® powder [60], nanoparticles and nanocomposites [61], and hydrogels [62-64]. Porous materials, composites, and textured layers have all been produced for biomedical engineering purposes using EPD [62].

2.5.1.2 Modelling

EPD deposition rates were first modelled by Hamaker [50] who obtained the following relation describing the process:

Eq. 2
$$\frac{dm}{dt} = \mu_e CSE$$

where μ_e is the electrophoretic mobility [cm^2/Vs], C is the concentration [g/cm^3], S is the surface area of the substrate [cm^2], E is the electric field strength [V/cm], and m is the mass of the deposit [g]. This relation indicates that for a constant geometry, concentration and electric field strength, the deposition rate would remain constant.

Although this relationship was true for short deposition times, it was found that the deposition rate may decrease with time.

To explain this phenomenon, Sarkar et al. noted that longer depositions could be modelled either under constant current/constant voltage and constant concentrations/variable concentrations conditions [54]. For the constant voltage/constant concentration condition, the reduction in deposition rate is primarily caused by the buildup of a resistive layer of deposit which decreases the effective electric field strength between the solid/liquid deposition surface and the counter electrode. For constant current/variable concentrations, the reduction in concentration reduces the deposition rate as would be predicted by the Hamaker equation. Although a resistive layer builds up, the current passing through the solution and solution resistivity do not change, so the electric field strength remains constant as well. Such a process was first modelled by Zang et al. for naturally depleting solutions [65]. Under constant voltage/variable concentration conditions, both the buildup of deposit and the change in concentration reduce the deposition rates. Only under constant current/constant concentration does the deposition rate remain fixed. Equations for each case are shown in Table 2.1.

2.5.2 Alginate

2.5.2.1 Overview

Sodium alginate is a polysaccharide copolymer made of (1-4)-linked β-D mannuronate (M) and C-5 epimer α-L-guluronate (G) blocks. The hydrogel is derived from brown algae and has many uses in a variety of fields including tissue

engineering. Alginate can be used for both *in-situ* gelation and immobilization-through-microencapsulation to create injectable tissue engineering scaffolds [66]. Such methods have already been used for bone tissue repair [67], cartilage repair [68], skin repair [69] and in neural tissue repair [70]. Recently, alginate has been used to prevent adverse tissue remodelling in damaged myocardial tissue [71]. Alginates are also used for drug delivery [72], cell delivery, enzyme encapsulation and wound dressing [73]. The popularity of alginate in the field of biomedical engineering is widely attributed to its non-toxicity, biodegradability, and its excellent biocompatibility [72].

Sodium alginate is readily available in powder form. It is typically dissolved in water and a gel matrix is formed through cross-linked using di- or trivalent cations such as calcium, barium or iron [74, 75]. Cross-linking generally occurs in a random manner, resulting in the final gel form. Gelation can be reversed by exposing the gel to salts containing monovalent cations such as sodium citrate. Typically, the gels have to be exposed to positively charged polymers such as poly-l-lysine or chitosan to form secondary layers. There are several grades of alginate viscosities available which, along with the G/M block ratio, the concentration of cations and the cation species employed during the cross-linking process, greatly affect the gel's mechanical and swelling properties [72, 76]. The weight average molecular weight has been correlated with viscosity [77] which was shown to have a large impact on the drug release rate of the gel under neutral pH [78-80]. The erosion of the gel has been shown to vary depending on the acidity of the environment [80, 81].

2.5.2.2 EPD of Alginate

The negatively charged alginate ions are amenable to EPD and yield a uniform alginate-gel film on the desired substrate [52, 69, 82, 83]. The polymer undergoes an anodic deposition, and the mechanism has been previously described in literature by Yokoyama et al. [82]. The application of electric current causes a hydrolysis reaction in the water, reducing the pH around the anode through the following mechanism:

Eq. 3
$$H_2O \rightarrow \frac{1}{2}O_2 + 2H^+ + 2e^-$$

The electric field causes sodium alginate particles to migrate towards the anode where they undergo the following reactions:

Eq. 4
$$Na - Alg \rightarrow Na^+ + Alg^-$$

$$Alg^- + H^+ \rightarrow HAlg$$

where Na-Alg is sodium alginate and HAlg is alginic acid. A solid phase is formed due to the hydrogen bonding interaction between alginic acid particles. Cross-linking can also be used to further solidify the gels if desired. It is possible to add subsequent layers without requiring secondary polymers simply by changing the contents of the deposition solution.

The process was first performed on a platinum wire over a span of 6 hours to create a bulk gel [82]. The deposition rate, sodium content and polymer molecular weights were characterized as a function of radial distance from the substrate. EPD

has since been used to co-deposit a number of materials with alginate using significantly smaller deposition times. Hydroxyapatite and TiO_2 were co-deposited to obtain a novel bone tissue replacement which could be formed over a layer of cathodically-deposited chitosan to improve the corrosion resistance of the substrate [84]. The EPD of alginate has also been used to bind hypoxyapatite and carbon nanotubes while avoiding a damaging sintering process [85]. Carbon nanotubes reinforce the hypoxyapatite and were shown to increase its mechanical strength [86]. Although such a material has direct applications in bone tissue engineering, the toxicity of carbon nanotubes is still in question for *in-vivo* applications [87]. A biosensor has been formed through the co-deposition of horseradish peroxidase and alginate, and its selectivity to hydrogen peroxide showed favourable results [88]. In another study, $CaCO_3$ was added to the deposition solution to carry out EPD under less harsh conditions allowing for the entrapment of E. coli cells [83]. While this was also the first study to induce cross linking post-deposit using a $CaCl_2$ solution, the effects of cross-linking were not extensively examined on the electrophoretically deposited alginate gels.

2.5.3 Stacked Wire Mesh Materials

2.5.3.1 Heat Exchangers

Simple two dimensional wire meshes can be stacked to form three dimensional materials with open pores and highly controlled geometries. In heat exchanger studies, channels were packed with stacked wire mesh in order to improve the heat exchange rate between a passing fluid and the wall by up to 40%

[89, 90]. These improvements are due to both the increase in contact surface area of the heat exchanger and the introduction of a localized turbulent flow. Tian et al. studied the effects of porosity and orientation of stacked wire mesh on heat transfer efficiency when a current was applied directly to the mesh. They found that there was an optimal porosity of approximately 0.75 [91]. As the porosity increases, the mass transfer of passing fluid increases whereas the contact surface area of the mesh decreases. These factors change the heat transfer rate in opposite directions for a given change in porosity. Similar results were obtained by Xu et al. [90].

Conductive heat transfer represents the heat flowing into a body caused strictly by the diffusion of heat, and is the only means of heat transfer between two solid bodies. Convective heat transfer represents the heat flowing into a body in the presence of a flowing fluid, and consists of conductive and advective heat transfer. Convection only occurs when a fluid has movement. Natural convection occurs when the movement of the fluid is induced through differences in fluid density caused by fluid temperature gradients. Forced convection occurs whenever an external force causes the bulk flow of the fluid.

The Nusselt number is a dimensionless number representing the ratio of convective to conductive heat transfer. Studies have already shown Nusselt numbers above 100 are readily achieved in stacked wire mesh heat exchangers for Reynolds numbers as low as 500 [90].

2.5.3.2 EDP on Stacked Wire Mesh for Mass Exchange Applications

Heat and mass transfer are analogous to one another. Wire meshes have gained attention for use in mass exchangers and for solid state catalytic applications. For these, EPD has proven to be a useful process in saving costs and in improving performance [92]. Meshes made of bulk-catalyst-material wires have been used such as in the production of nitric acid from ammonia and formaldehyde [93]. Alternatively it is significantly less expensive to coat stainless steel wire mesh with powdered catalyst using EPD [92]. Stainless steel wire meshes have been coated with aluminum particles for catalytic applications such as the oxidation of 1,2-dichlorobenzene (*o*-DCB) [92, 94-96]. Ti [97, 98] and TiO_2 [99] were also deposited on wire mesh for catalytic applications.

EPD can also be used to increase the surface area of bulk mesh material by creating micropores. In one case, Ti particles were deposited onto a Ti mesh to increase the specific surface area by almost 4 times to improve the electrical generation of hydrogen peroxide [98].

2.5.3.3 Pressure Loss with Passing Fluid

Studies have examined the effects of wire mesh dimensions on the pressure drop in passing fluid for both heat exchangers and mass exchangers, and a number of correlations have been established [90, 100, 101]. A stacked wire mesh is advantageous over a packed bed of spheres in that its dimensions can be controlled to obtain better heat transfer efficiencies with smaller pressure drops [102].

One study performed by Tian et al. examined the effect of open cross sectional area on the pressure loss coefficient K_{cell} over a short distance [91]. The pressure loss coefficient is defined as

Eq. 5
$$K_{cell} = \frac{\text{Pressure loss}}{\text{Dynamic Pressure}} = \frac{\Delta P_{cell}}{\frac{\rho U_m^2}{2}}$$

where ΔP_{cell} is the pressure loss of the passing fluid [N/m^2], ρ is the fluid density [kg/m^3], and U_m is the fluid velocity [m/s]. The open area ratio for a given geometry is

Eq. 6
$$R_{open} = \frac{\text{Open area}}{\text{Total area}}$$

It was found that for a given R_{open} the pressure coefficient could be approximated by

Eq. 7
$$K_{cell} = \left(\frac{1 - R_{open}}{R_{open}}\right)^2$$

This shows that although the heat transfer rate increases with porosity until 0.75 [90], the pressure will always decrease.

The Sherwood number is a dimensionless mass transfer number analogous to the Nusselt number. Using both experimental and modelling approaches, Kołodziej et al. showed that the Sherwood and Nusselt numbers for stacked wire meshes could be converted from one to another using empirical relations [103]. Moreover, it was shown that in their specific example, Sherwood numbers above 100 could be

obtained using stacked wire mesh for Reynolds numbers as low as 500. Further research is still required as their relations were only shown for gaseous fluids under a narrow range of conditions.

2.6 Research Justification

Although the use of sorbent technology is widespread in ECBF, there is a need for new and innovative sorbent immobilization techniques. This thesis investigated electrophoretic deposition of alginate and AC onto stacked wire meshes as a method to produce a novel sorbent material with a large macro-porosity. Appropriate steps were taken to model the deposition process in order to obtain a control over the material dimensions. The material was evaluated under *in-vitro* conditions and showed promising results.

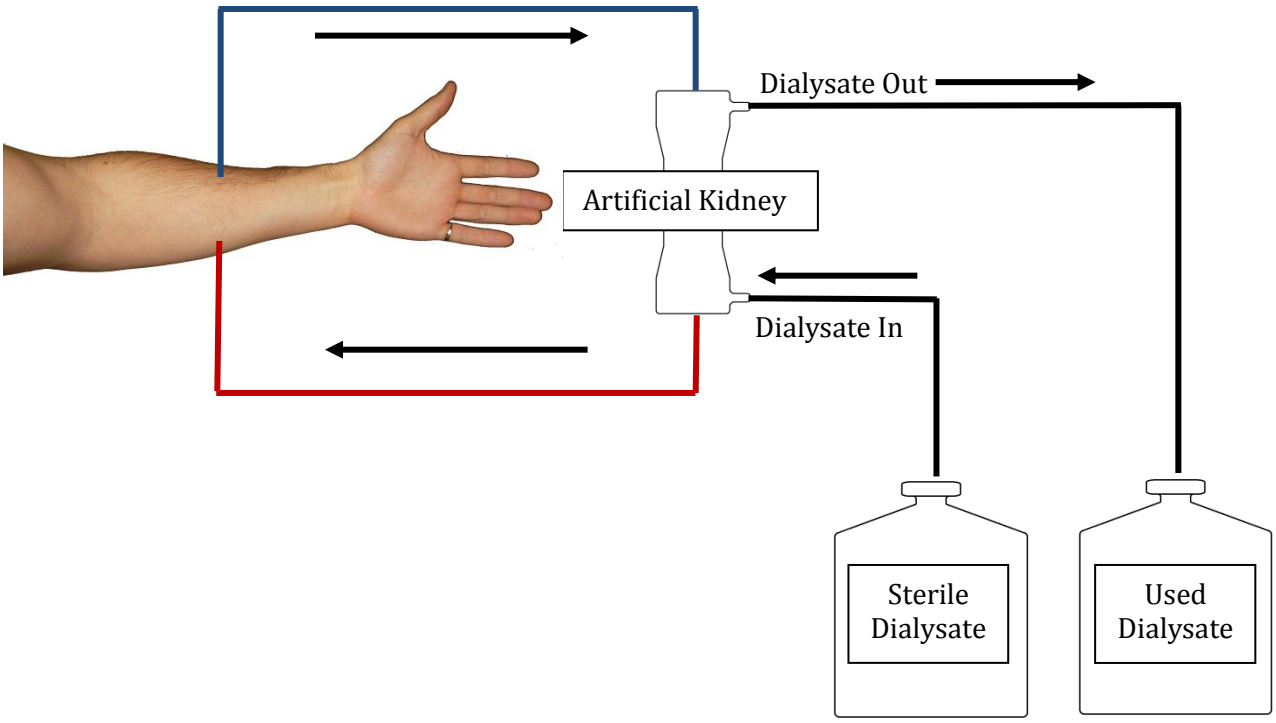

Figure 2.1 Simplified Single-Pass Hemodialysis System. Blood leaves the arm (blue) and is passed through an artificial kidney. This clears the blood of toxins (red) before it is re-introduced to the circulatory system. A sterile solution is used as dialysate and is disposed of once used.

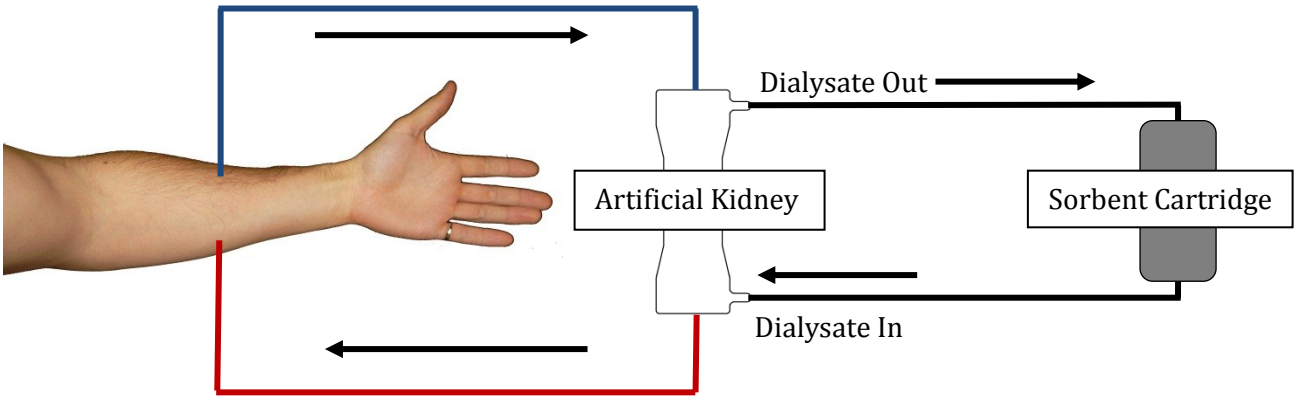

Figure 2.2 Simplified Re-Circulating Hemodialysis System. This is the same as hemodialysis, except tap water is used as a dialysate. Salts are introduced into, and waste is removed from the dialysate via a sorbent cartridge.

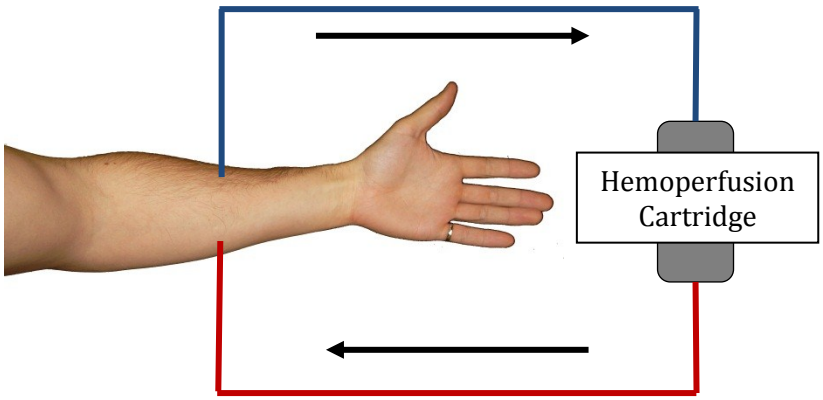

Figure 2.3 Simplified Hemoperfusion System. Blood leaves the body and is filtered through a hemoperfusion cartridge.

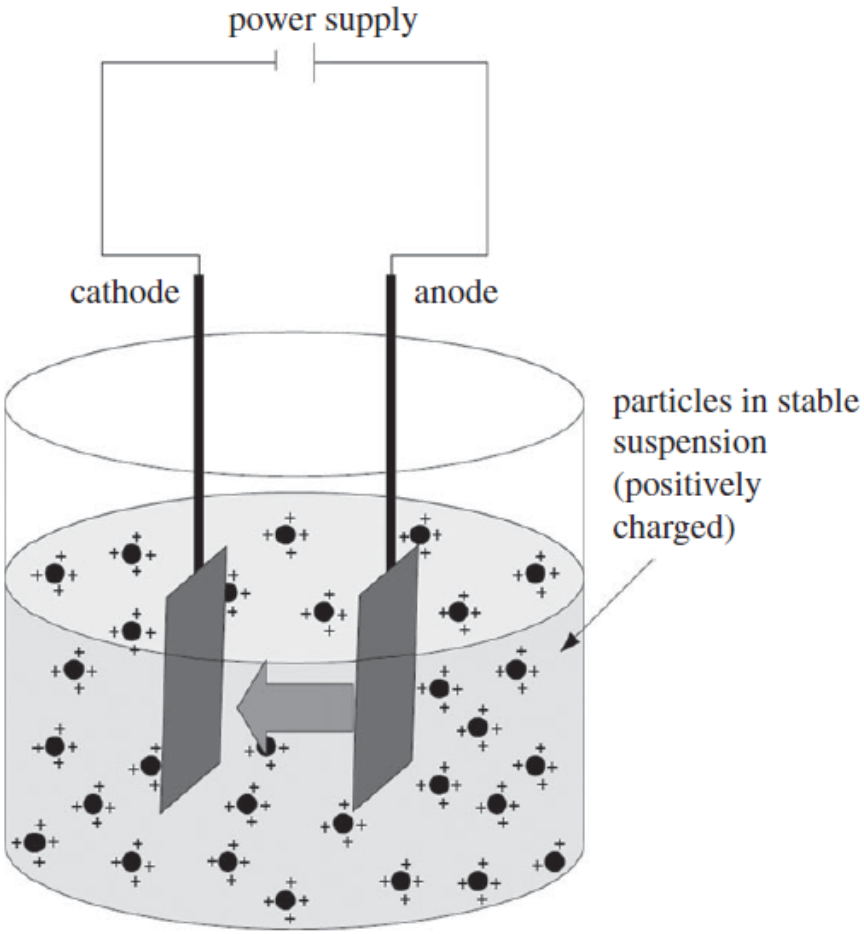

Figure 2.4 Cathodic Electrophoretic Deposition. Positively charged particles are first suspended in solution. A voltage difference is applied between two electrodes, and the particles are then driven towards the cathode where they form a deposit [62].

Conditions	Mass Equation	Reference
Constant Current/ Constant Concentration	$m = \mu_e CSEt$	[50]
Constant Current/ Variable Concentration	$m = m_0\left(1 - e^{\frac{-\mu_e SE}{V}t}\right)$	[54]
Constant Voltage/ Constant Concentration	$m = \frac{L\rho S}{2(R_f - 1)}\left(-1 + \sqrt{\frac{4(R_f - 1)\mu_e m_0 E}{VL\rho}t + 1}\right)$	[54]
Constant Voltage/ Variable Concentration	$\frac{(R_f - 1)}{\rho S}m + \left(\frac{(R_f - 1)}{\rho S}m_0 + L\right)\ln\left(\frac{m_0 - m}{m_0}\right) + \frac{S\mu_e EL}{V}t = 0$	[54]

Table 2.1 Mass of Electrophoretically Deposited substance as a Function of Time for Various Conditions. V is the volume of the solution [mL], L is the distance between electrodes [m], $\mathbf{R_f}$ is the resistivity ratio [unitless], and $\mathbf{m_0}$ is the initial mass of deposition material in solution [g].

Co-Deposited Particle	Potential Applications	Reference
Carbon Nanotubes - Hypoxyapatite	Bone tissue replacement	[85]
Cells (E. coli)	Tissue engineering applications, *in-vitro* modelling, biosensor	[83]
Proteins		
Horseradish Peroxidase	Peroxide biosensor	[88]
Haemoglobin	Implant surface modifications	[104]
Hypoxyapatite	Bone tissue replacement	[84]
Albumin	Culture matrix, unspecified	[105]
TiO_2	Bone tissue replacement	[84]

Table 2.2 Substances Co-Deposited With Alginate and their Various Applications.

Preface to Chapters 3, 4, and 5

In accordance with the McGill thesis preparation and submission guidelines, the thesis is written as a compilation of original papers. Subsequent chapters are original research articles and I am the first author on each. Chapter 3 examines the design of a novel device used to electrophoretically deposit alginate onto a flat substrate. Low, medium and high viscosity grade alginates were examined and medium viscosity grade alginate was selected for use in chapters 4 and 5. In Chapter 4, an alginate-activated carbon gel was deposited onto a steel wire-mesh substrate to create a novel sorbent material. Dimensional analysis was carried out and the gel properties were obtained. In Chapter 5, the sorbent properties of the novel sorbent material were evaluated and compared with other methods.

Formatting was used as per the journal requirements for each article. Exceptions were made in order to better integrate the manuscripts with the thesis. The placement of the figures and the numbering of each section were both changed.

Hypothesis and Research Objectives

Hypothesis

A novel sorbent material can be produced for extracorporeal blood filtration by applying electrophoretic co-deposition of alginate and activated carbon onto a steel wire mesh substrate.

Research Objectives

The primary goal of this thesis is to develop a novel sorbent material with potential use in recirculating hemodialysis sorbent cartridges or as a hemoperfusion device that meets the following criteria: (i) low cost of production with high scalability, (ii) highly controllable geometry and dimensions, and (iii) high affinity for blood toxins. The specific objectives are:

1. To perform an extensive literature review on the design problems currently associated with the production of extracorporeal blood filtration devices, and on potential methods that can be used to design a novel sorbent material for this purpose.
2. Design a method to produce a novel sorbent material that is highly scalable and select appropriate sub-materials.
3. Investigate the dimensional constraints of the system.
4. Evaluate *in-vitro* the ability for the sorbent materials to absorb toxins.

In the following sections, we will discuss experiments and results to meets the above specific objectives.

Research Articles Presented in Chapters 3, 4 and 5:

1. **Chris R. Jackson**, Pavan M. V. Raja, Satya Prakash, A novel electrophoretic deposition device: effects of alginate viscosity grade on deposition kinetics, Journal of Biotechnology and Biomaterials, February 29, 2012. Published.

2. **Chris R. Jackson**, Satya Prakash, Development and geometric evaluation of a novel sorbent material for extracorporeal blood filtration, Journal of Biotechnology and Biomaterials, 2012. Under preparation.

3. **Chris R. Jackson**, Satya Prakash, *In-Vitro* absorption of blood toxins into novel sorbent material for use in extracorporeal blood filtration devices, Journal of Biotechnology and Biomaterials, 2012. Under preparation.

Chapter 3: A Novel Electrophoretic Deposition Device: Effects of Alginate Viscosity Grade on Deposition Kinetics

Chris R. Jackson, Pavan M. V. Raja, Satya Prakash*

Biomedical Technology and Cell Therapy Research Laboratory
Departments of Biomedical Engineering, Physiology, and Artificial Cells and Organs Research Center,
Faculty of Medicine, McGill University, Duff Medical Building

3775 University Street, Montreal, Qc, H3A 2B4, Canada

*Corresponding author - Phone: 514-398-2736, Fax: 514-398-7461,

E-mail: satya.prakash@mcgill.ca

Preface

The present study focuses on the development of a device used to study electrophoretic deposition as applied to hydrogels. Three viscosity grades of alginate were tested, and their rates were modelled using previously established relations. Gel properties were also evaluated. Co-authors (Pavan M. V. Raja and Satya Prakash) contributed to the design of the experiments and gave project oversight.

Contributions of Authors

The thesis author was responsible for designing and performing experiments, data analysis and preparing manuscripts. Dr Satya Prakash was reported as the last author in all articles and supervised the research. Dr. Pavan M. V. Raja, a post-doc in the Biomedical Technology and Cell Therapy Research Laboratory at McGill University, gave direction to various aspects of the project including suggestions in designing and performing experiments.

A Novel Electrophoretic Deposition Device: Effects of Alginate Viscosity Grade on Deposition Kinetics

3.1 Abstract

A novel device was designed to perform electrophoretic deposition under tightly controlled conditions. The device physical parameters were investigated by depositing three different viscosity grades of sodium alginate hydrogels. A thin metallic rectangular substrate was used to obtain the various time dependant deposition rates of the gels. The resulting deposition curves showed the effective electrophoretic mobilities of the low, medium and high viscosity grade gels were 0.0610 cm^2/Vs, 0.0584 cm^2/Vs and 0.0909 cm^2/Vs and that the ratios of gel deposit to solution resistivities were 21.0, 16.2 and 47.5 respectively. Following electrophoretic deposition, the gels were cross-linked in a 0.1 M $CaCl_2$ solution in order to further solidify the gels. Cross-linking reduced the masses of the gels to 50.9 ± 1.8%, 26.7 ± 2.0%, and 28.5 ± 1.3% of their initial masses respectively. Lyophilization was applied to the gels to determine the alginate content of the gels. Immediately after deposition the alginate mass fractions of the low, medium and high viscosity grade gels were 2.92 ± 0.49%, 2.70 ± 0.08% and 2.94 ± 0.15% respectively. Cross-linking caused the mass fraction of alginate to increase significantly to 5.59 ± 0.07%, 7.11 ± 0.37% and 7.02 ± 0.24% respectively. The device in this study provided sufficient data to model the electrophoretic deposition rates. The technique can be expanded to other hydrogel species which can be used in a variety of biomedical and biotechnological applications.

3.2 Introduction

Electrophoretic deposition (EPD) is a relatively inexpensive method of forming uniform layers or bi-layers on substrates with complex geometries. It has gained much attention in the last 20 years in the development of advanced materials including functional and structural ceramic coatings [106], laminated ceramics [106], biomaterials [62, 107], composites [51, 107-109], porous materials, thin films, and nanostructured materials [51].

In this method, particles are suspended or ions are dissolved in solution before they are driven towards a substrate through the application of an electric field. The particles/ions then form a solid film on one of the electrodes through a number of possible mechanisms including flocculation through accumulation [52], particle charge neutralization [53], particle coagulation [51], and through electrical double layer thinning [54]. EPD has been used on a number of biomaterials such as bioceramics, bioactive materials, nanoparticles, and hydrogels [62]. Porous materials, composites, and textured layers have all been produced for biomedical engineering purposes using this technique.

Sodium alginate is a polysaccharide copolymer made of (1-4)-linked β-D mannuronate and C-5 epimer α-L-guluronate blocks. To date, our laboratory has focused on the therapeutic applications of encapsulated alginate systems. The hydrogel is derived from brown algae and has many uses in a variety of fields including tissue engineering. Alginate can be used for both *in-situ* gelation and immobilization-through-microencapsulation to create injectable scaffolds [66]. Such

methods have already been used for bone tissue repair [67], cartilage repair [68], skin repair [69] and in neural tissue repair [70]. Recently, alginate has been used to prevent adverse tissue remodelling in damaged myocardial tissue [71]. Alginates are also used for drug delivery [72], cell delivery, enzyme encapsulation and wound dressing [73]. This class of materials is widely used for its non-toxicity, biodegradability, and excellent biocompatibility [72].

There are several alginate viscosity grades available which, along with the G/M block ratio, the concentration of cations and the cation species employed during the cross-linking process, greatly affect the gel mechanical and swelling properties [72, 76]. The weight average molecular weight has been correlated with viscosity [77] which was shown to have a large impact on the drug release rate of the gel under neutral pH [78-80]. The erosion of the gel has been shown to vary depending on the acidity of the environment [80, 81]. Previous research has also focused on the importance of cross linking with either Ca^{2+} or Ba^{2+} ions in order to improve the mechanical stability of alginate gels [74].

The negatively charged alginate particles are amenable to EPD which results in the formation of a thin uniform alginate-gel film on the desired substrate [52, 69, 82, 83]. Previous studies have focused on the EPD of sodium alginate for biosensor, tissue engineering, and corrosion resistance applications [73, 83, 84, 88]. Sodium alginate undergoes an anodic deposition, and the mechanism has been previously described in literature [82].

Although the feasibility of alginate deposition and co-deposition has been well established, more research is needed to better understand the characteristics of the deposition itself. To the best knowledge of the authors, no study has yet been published that investigated the electrophoretic mobility and the resistivity ratio between the deposited gel and the solution, both of which are required to model the deposition rates. This would allow for a more precise control over the gel thickness which is important for industrial applications. Moreover, the impact of alginate viscosity on EDP has not yet been addressed even though it greatly affects properties such as drug release rate, swelling, and mechanical strength of the gel when it is prepared through direct cross-linking alone.

3.3 Materials and Methods

3.3.1 Materials

Three alginate viscosity grades were used for deposition: low viscosity (LV) alginic acid sodium salt (MP Biomedicals, Solon, Ohio, USA) which was rated at 250 cP at 2% aqueous, medium viscosity (MV) alginate (Sigma Aldrich, St. Louis, Montana, USA) which was rated at 3,500 cP at 2% aqueous, and a high viscosity (HV) alginate (Sigma Aldrich, St. Louis, Montana, USA) which was rated at 14,000 cP at 2% aqueous. The alginates were chosen in order to span the viscosity grades that are commonly manufactured. All alginates were derived from the kelp species *M. pyrifera*.

3.3.2 Method for Determining Alginate Deposition Rates

The EPD device was used to investigate the deposition rates of the three different viscosity grades of alginate. After alginate was deposited on the substrate, the film was rinsed in deionized water before it was briefly exposed to compressed lab air to remove droplets from the surface. The mass was measured before and after deposition using a Mettler Toledo AG204 DeltaRange scale (Mettler-Toledo, Greifensee, Switzerland). The mass of the substrates and films were recorded at 1, 2, 3, 5 and 10 minutes. Approximately 1.5 L of solution was used to ensure the alginate concentration remained approximately constant. Depositions were carried out in triplicate at room temperature under static conditions.

3.3.3 Method for Cross-Linking and Evaluation of Mass

Cross-linked gels were obtained by submerging the post-deposit-gels in a 0.1 M $CaCl_2$ (ACP, Montreal, Quebec, Canada) solution overnight at 4°C. The gel masses were evaluated before and after cross-linking and samples were obtained in sextuplicate while the gels were still attached to the substrate.

3.3.4 Method for Lyophilization and Dry Gel Mass

After deposition, sample gels were removed from the substrate, weighed, and placed in petri dishes. A ThermoSavant ModulyoD-115 (Thermo Fisher Scientific, Waltham, Massachusetts, USA) was used to freeze-dry the samples over the span of two days after which changes in mass were recorded. Samples were obtained in triplicate.

3.3.5 Method for Determining Molecular Weight through Gel Permeation Chromatography

Gel permeation chromatography (GPC) was used to differentiate the alginate powders by molecular weight. Experiments were performed courtesy of the Laboratoire de Caractérisation des Matériaux Polymères au Département de Chimie at L'Université de Montreal. The weight average molecular weight (M_w), the number average molecular weight (M_n) and the size average molecular weight (M_z) of the three alginate powders were obtained. Samples were dissolved in a 0.1M $NaNO_3$ solution at a concentration of 10 mg/ml, and experiments were carried out at 35°C. A Polysep-5000 GPC setup (Phenomenex, Torrance, California, USA) with an Ultrahydrogel 500 (Waters, Milford, Massachusetts, USA) column was used with Breeze v.3.20 software (Waters, Milford, Massachusetts, USA). The molecular weights were subsequently used to calculate the viscosities of the different alginate grades using the Mark-Houwink-Sakurada equation.

3.3.6 Method for Determining Contact Angles of Dried Alginate Gels

Contact angles were obtained using a VCA Optima (Billerica, Massachusetts, USA) goniometer with 0.25 μL water droplets. Gels were allowed to dry overnight under vacuum before experimentation. A sample size of 12 was used.

3.3.7 Statistical Analysis

Statistical analysis was performed using Minitab software (Minitab, Version 15; Minitab Inc, Pennsylvania, USA). Values are expressed as mean ± standard error. Statistical comparisons were carried out by multiple analyses of variance (ANOVA) or by student t-test where appropriate. Randomized independent sampling was

assumed and statistical significance was set at $p < 0.05$. All interaction terms were treated as fixed terms. Sample sizes varied between 3 and 12, as indicated per experiment.

3.4 Results

3.4.1 Design of EPD Device

A 10 x 10 x 25 cm box was constructed out of chemically welded acrylic as a means of holding the deposition solution. The 3 x 8 x 0.1 cm rectangular metallic substrate was submerged in the deposition solution and was held in place via a simple holding device that was also constructed out of chemically welded acrylic. To keep the substrate mechanically stable, the 3 cm side of the substrate was pinched between two surfaces whose widths were 0.3 cm. The area exposed to the deposition solution was therefore 43.2 cm^2. An electric field was supplied via an Abra AB-3000 (Abra, Champlain, New York, USA) voltage source which remained at a constant voltage of 10.0 V throughout the experiment. Two rectangular counter-electrodes were placed parallel 4 cm from either side of the substrate to obtain a uniform electric field of 2.5 V/cm, which was sufficient to induce alginate deposition. A long thin metallic strip that ran along the side of the substrate holder was used as the contact surface between the voltage source and the substrate. It was positioned such that it was not exposed to the solution. An overview of the device design is shown in Figure 3.1. In preliminary experiments, it was observed that highly concentrated solutions formed deposits with poor thickness uniformity, so the deposition concentration was kept at 0.4% for all experiments in this paper.

3.4.2 Alginate Deposition Rates

The EPD device was used to deposit alginate on a flat geometry. The device was designed to be flexible such that other hydrogels can easily be substituted in the deposition solution. Moreover, a co-deposition can also be performed with another particle. The device is an excellent tool for modelling the deposition rates as the solution is geometrically constrained to the same cross-section as the substrate, ensuring the electric field is approximately constant over the substrate surface. Moreover, a large volume of deposition solution can be held by the device, allowing for a constant-concentration approximation assumption to be taken, although it must be supported with rigorous calculations based on the mass of the deposit layer formed.

The mass of the alginate films increased approximately linearly for the first few time points, but over time the deposition rates decreased. The surface was smooth for low deposition times, but dimples and variations in colour concentration appeared as deposition time approached 10 minutes.

Figure 3.2 shows the alginate film mass as a function of time. For the first 180 seconds, the LV and MV grade alginates deposited at the same rate which was slightly below that of the HV grade alginate. By 10 minutes, the HV gel had the lowest mass, implying that the HV grade alginate deposition rate was most severely slowed down in the later stage of the deposition. By the end of the deposition, the LV and MV gels had different masses, with the MV being the higher of the two. All three gels were found to be significantly different from one another with p-values < 0.005.

3.4.3 Cross Linking Mass Reduction

The cross-linked-gel mass was calculated as a percent of the initial mass and is shown in Figure 3.3. The MV and HV gels had similar changes in mass (p-value = 0.508) with a reduction to 72.3 ± 1.2%. The LV gel mass decreased the most with a reduction to 49.1 ± 1.8%.

3.4.4 Gel Description

All un-cross-linked gels were opaque, with a yellow tint. The side of the gel that was exposed to the deposition solution had bumps, while the substrate side of the gel was flat. The opacity of the un-cross-linked gels decreased with viscosity. The cross-linked gels were more opaque than their un-cross-linked counterparts. Images of gels obtained after 5 minute depositions are shown in Figure 3.4. A water displacement test was performed on the gels and showed they all had a density of approximately 1.0 g/cm^3.

3.4.5 Effect of Lyophilization on Alginate Gels Mass

The dry alginate mass was calculated as a percent of the post-deposit gel mass. The dry alginate contents were statistically similar (p-values > 0.266) for all three gels with dry mass fractions of 2.85 ± 0.46%. When the gels were cross-linked, their water contents were reduced. The MV and HV gels had similar dry masses (p = 0.839) of 7.07 ± 0.46%, while the LV gel has a dry mass of 5.59 ± 0.07%. See Figure 3.5.

3.4.6 Molecular Weight through Gel Permeation Chromatography

The values of M_n, M_z and M_w are shown in Table 3.1. It was shown that for all measurements except M_n, the molecular weight increased with viscosity grade. This indicates that although the majority of the mass of the HV alginate was found in the higher molecular weight range, there was a larger presence of smaller molecules. Increased molecular weights are associated with higher alginate viscosity [110, 111], and the relation between the two have been discussed in literature [112, 113].

3.4.7 Dried Alginate Gels' Contact Angles

Contact angles are expressed from the water side of the droplet, so angles <90° are hydrophilic. All gels had statistically similar (p-values > 0.193) contact angles of 47.4 ± 1.1° except for the cross-linked HV gel whose contact angle was 37.2 ± 6.38°. As the dried gel is both highly hydrophilic and porous, droplets would absorb quickly, which warped the surface of the dried gels. Contact angles were therefore taken quickly after droplets were deposited before warping occurred. See Figure 3.6.

3.5 Discussion

3.5.1 Electrophoretic Deposition Device

EPD devices commonly employ large baths of deposition solution while completely neglecting the effects of solution geometry on the local electric field strength. For substances that deposit relatively much quicker than ceramics such as hydrogels, this means that an uneven deposition can become very pronounced, which can skew the results for modelling purposes. Boccaccini et al. for example

describe an EPD device in which the substrate was held in an excessively large solution bath [62]. Although such a container is flexible in that unspecific substrate geometries can be used, it is not ideal for modelling the deposition rates. Non-uniform coatings may also have played a role in the non-linear correlation between chitosan concentration and deposition rate [114]. In another study, quartz crystal microbalance method of measuring deposit mass was used to yield significantly more time points [84], but it cannot be used for extensive deposition times where the deposit resistance becomes significant.

The device presented in this study overcomes the above mentioned obstacles. The container shape forces the deposition solution into a geometry such that the electric fields are parallel, ensuring the electric field strength is uniform over the surface of the substrate. The ability to weigh deposits after extended deposition times allowed for the characterization of gel deposition rate well beyond the non-linear range which has not been attempted before for alginate. The device could easily be used with other charged polymers, hydrogels, ceramics and nanoparticles as well as other suspension mediums such as ethanol and other organic solvents as long as the electric field strength and direction is controlled appropriately.

3.5.2 Alginate Deposition Rates

EPD rates were first modelled by Hamaker [50] who obtained the following relation describing the process:

Eq. 8

$$\frac{dm}{dt} = \mu_e CSE$$

where μ_e is the electrophoretic mobility [cm^2/Vs], C is the concentration [g/cm^3], S is the surface area of the substrate [cm^2], E is the electric field strength [V/cm], t is time [s] and m is the mass of the deposit [g]. Although this relationship was true for short deposition times, the deposition rate slowed down throughout longer deposition times.

To explain this phenomenon, longer depositions are modelled either as constant current or constant voltage conditions. These are further classified into the two scenarios where the deposition solution concentration is or isn't kept constant. Under constant voltage/constant concentration conditions, the buildup of a resistive layer of deposit slows down the deposition rate with time. Sarkar et al. used the Hamaker equation to obtain the relation for deposit mass under these conditions [54]:

Eq. 9

$$m = \frac{1}{\alpha}\left(-1 + \sqrt{2\alpha\beta t + 1}\right)$$

$$\alpha = \frac{2(R_f - 1)}{L\rho S}$$

$$\beta = \mu_e SCE$$

where L is the distance between electrodes [cm], R_f is the ratio of deposit resistivity to the suspension resistivity, and ρ is the density of the deposit [g/cm^3].

In many EPD processes including those involving ceramics, the solute is the only species deposited on the substrate. In the case of hydrogels, however, the solvent also forms part of the deposited mass. It is therefore more practical to model the deposition rate in terms of the total mass of the deposited hydrogel and not just the polymer species. The alginate deposition curves obtained from our EPD device were fit to the above Sarkar equation using MatLab R2010a (MathWorks, Natick, Massachusetts, USA) cftool function and the results are shown in Figure 3.2. Values for α and β, as well as the calculated values of μ_e and R_f are shown in Table 3.1. It was found that μ_e and R_f for the LV and MV grade alginates were similar, however both values were noticeably higher for the HV gel.

The first two terms of the Maclaurin series for the above equation yields:

Eq. 10
$$m = \beta t\left(1 - \frac{\alpha\beta t}{2}\right)$$

As the Maclaurin series for the Sarkar equation is an alternating series, this equation can be used to show that the error associated with the Hamaker equation is negligible for values of $t \ll \frac{2}{\alpha\beta}$.

The electrophoretic mobility is an empirical value that results from the balance between the electrostatic forces and the friction forces exerted on the particle. Although the viscosity grade is a good indicator of the friction forces resisting particle motion towards the substrate, the electrostatic force is much more complex, and depends on particle charge, inter-particle interactions, and local pH which varies along the distance between the electrodes [49]. The viscosity of the HV

gel indicated that the friction force would have been higher during EPD compared to the other two gels. The HV μ_e was nevertheless greater, indicating that the increased friction was overcome by an even greater increase in electrostatic force. The HV gel deposition rate slowed down the most throughout the run due its larger R_f.

3.5.3 Cross-Linking

The MV and HV gels had a larger mass reduction following cross-linking than did the LV gel. This is because the MV and HV alginate particles were larger, offering more sites for Ca^{2+} bridging. This resulted in a higher degree of cross-linking, and therefore a reduction in swelling properties. In literature, dry alginate and alginate microcapsules were also shown to have changes in mass increase with viscosity grade when they were moved from cross-linking solutions to water [80, 115, 116]. When alginate microcapsules produced through an emulsion technique were placed in water [117], a slightly higher change in mass was observed compared to gels produced using EPD subjected to a cross-linking solution.

All gels had approximately the same density so the change in volume was the same as the change in mass. Gel opacity was caused by micro-bubbles formed at the cathode. As bubble transportation from the cathode to the anode increased as viscosity decreased, it follows that opacity also increased as viscosity grade decreased. Gels were qualitatively observed to have improved mechanical properties following cross-linking. This was especially true for the LV grade alginate. Future works should focus on a qualitative assessment of the gel mechanical properties.

3.5.4 Contact Angle

The HV gels contact angle following cross-linking was likely smaller due to Ca^{2+} uptake. All surfaces were shown to be highly hydrophilic, with contact angles below 47.4°. Hydrophilic materials are ideal for mammalian cell cultures [118] due to an uptake in adhesive proteins [119-121]. As hydrophobic materials are commonly antithrombotic and resistant to fibrin sheath formation [122], the gels may have potential in tissue engineering and implant coating applications due to their increase biocompatibility. EPD would be especially useful as it would be possible to coat arbitrarily shaped tissue engineering scaffolds, so long as they are conductive. The hydrophilic surface is also ideal for immobilizing hydrophilic proteins.

3.5.6 Viscosity Calculations from Molecular Weights

It was shown that cross-linking reduced the mass for the MV and HV grade alginates to a greater extent than it did for the LV grade alginate. This is in accordance with previous studies that have shown a greater degree of cross-linking in alginates of higher molecular weight [123]; however it may also be due to differences in the fraction of G blocks in the polymer, which also have a higher affinity for Ca^{2+} ions. The viscosity grade increased with M_w as shown in previous studies [77]. The loss of mass that occurred during cross-linking was least extreme in the LV gels, which resulted in them having the smallest change in water mass fraction after cross-linking out of the three gels.

The viscosities of the solutions used in the experiments were approximated using the relation obtained by Morris et. al [112] whereby the concentration dependent viscosity of a random coil polysaccharide varied as $C^{3.3}$ and $C^{1.4}$ for dilute and highly concentrated solutions respectively. The transition between dilute and highly concentrated solution occurs at concentration C':

Eq. 11
$$C' \approx \frac{4}{[\eta]}$$

where [η] is the intrinsic viscosity [ml/g]. Values of [η] were calculated from experimentally obtained values of M_w using the Mark-Houwink-Sakurada relation [112, 113]:

Eq. 12
$$[\eta] = KM^a$$

where K and a are the Mark-Houwink-Sakurada constants. As the molecular weights for all alginates were above 300 kDa, values of 0.0305 and 0.66 were used for K and a respectively [112, 113]. Viscosities of 2% solutions provided by the respective manufacturers were used to calculate the viscosities of the solutions at the critical concentrations and at 0.4% by scaling accordingly. Relevant values are shown in Table 3.2. It was thus shown that the viscosities of the 0.4% solutions spanned a total of 1.5 orders of magnitude.

3.6 Conclusion

A novel EDP device was designed to effectively deposit alginate on a flat substrate. Alginate films were then produced on thin steel rectangles using three

alginates of different viscosity grades. The deposition mass was quantified and was used to show that the process could be modelled using the Sarkar equation for a constant voltage/constant concentration EPD. A change in mass was observed following cross-linking using $CaCl_2$ solution, with the LV grade alginate having the smallest change in mass. The dry alginate content was similar for all samples before cross-linking, but it was lower for the cross-linked LV grade alginate than for the other two. Although the viscosity grade affected the deposition rate, the Sarkar model was still accurate as long as appropriate μ_e and R_f values were used. Although results indicated that many properties varied with viscosity grade, it is possible that properties may become more extreme with a larger range of grades. These results will be useful in the design and manufacturing of devices that incorporate EPD of sodium alginate. Moreover, the methods outlined in this paper can be extrapolated to model and understand other hydrogel systems.

3.7 Acknowledgements

A special thank you is given to Dr. Hani Saleh Fadhl Al-Salami of McGill University for his help with statistical analysis. Pierre Ménard-Tremblay is also to thank for performing the Gel Permeation Chromatography experiment and for running the analysis at l'Université de Montréal. The authors would also like to acknowledge Dr. Jamal Daoud of McGill University for helping out with the lyophilization procedure and the contact angle test.

The authors would also like to acknowledge the Canadian Institute of Health Research (CIHR) grant (MOP 93641) to Dr. S. Prakash, and for funding provided by NSERC.

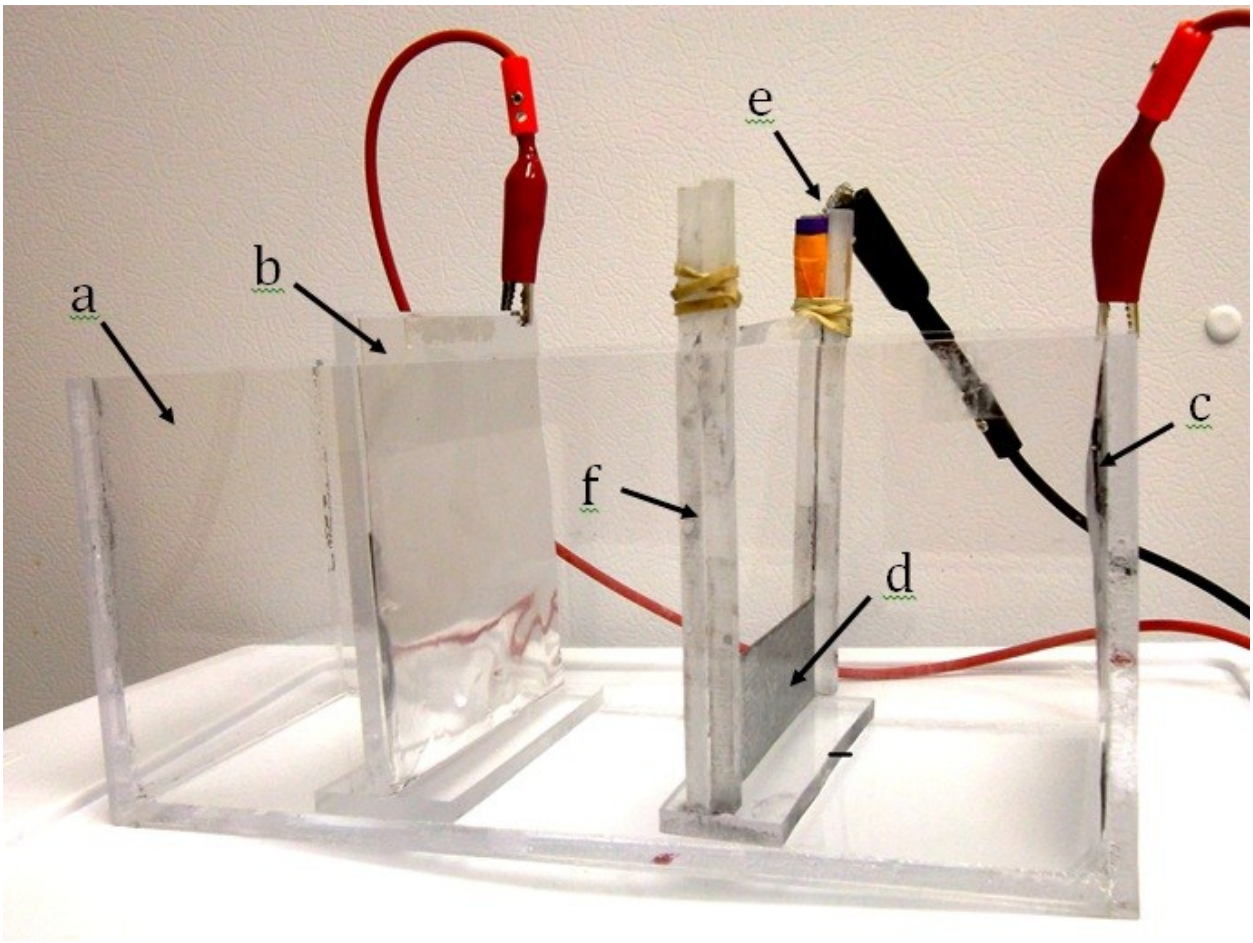

Figure 3.1 Electrophoretic Deposition Device. Acrylic container (a) is 2.5 L in volume. This is sufficiently large to hold the deposition apparatus and the deposition solution. Metallic counter-electrodes (b, c) are suspended parallel to the substrate (d). A 10 V potential is applied between the substrate and the electrodes which drives alginate in the solution towards the substrate to forms a solid gel layer. A metallic ribbon (e) acts as a contact between the substrate and the voltage source but is not exposed to the solute. An acrylic holding device (f) immobilizes the substrate and ensured that it is flush against the contact strip.

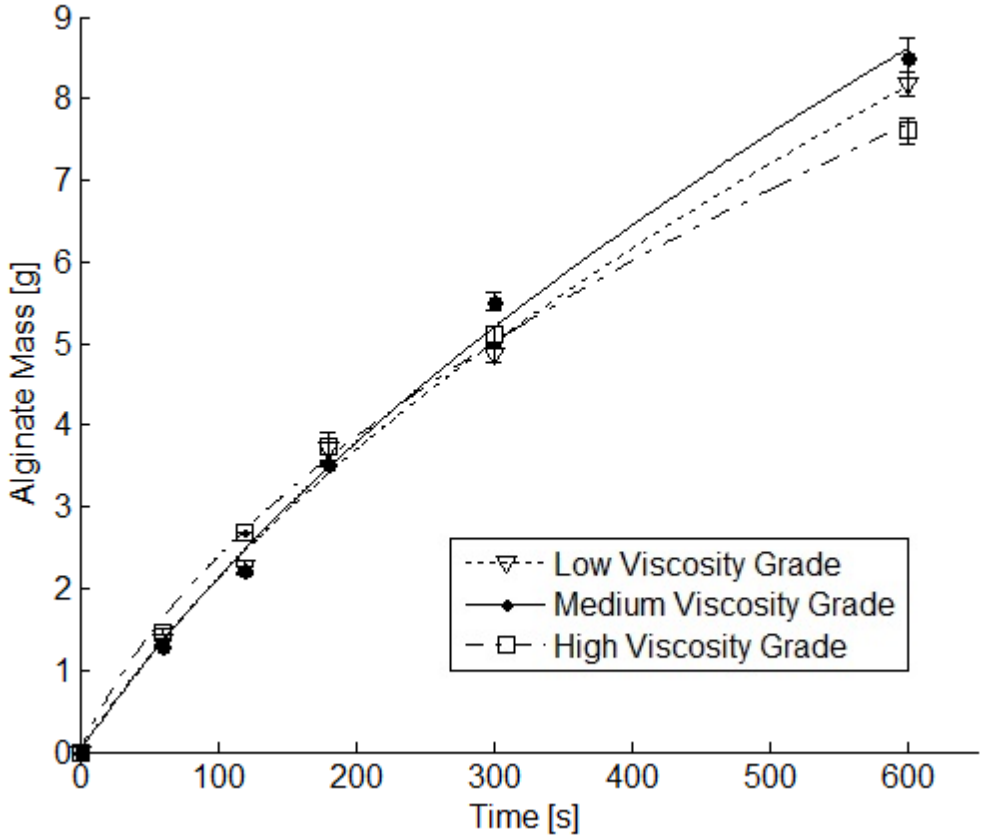

Figure 3.2 Mass of Alginate Film Based On Deposition Time. Three different alginate viscosity grades were electrophoretically deposited on thin rectangular substrates. By 1 minute, the LV and MV grade alginates did not have dissimilar masses (p-value = 0.163) and were 1.31 ± 0.02 g. The HV grade alginate was heavier (p-value = 0.011) with a mass of 1.47 ± 0.03 g. By 10 minutes, the LV and MV grade gels were similar (p-value = 0.347) with masses of 8.33 ± 0.15 g. The HV grade alginate was then lighter (p –value = 0.010) than the other gels with a mass of 7.60 ± 0.16 g. The Sarkar model was used to fit the LV (R^2 = 0.9914), MV (R^2 = 0.9886) and HV (R^2 = 0.9907) data. Error bars are in S.E.M., n = 3.

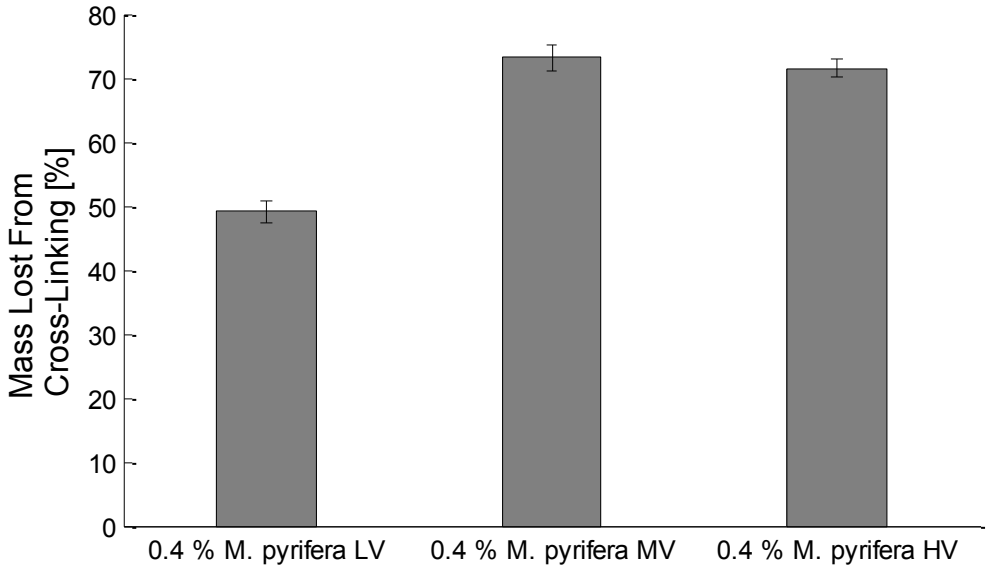

Figure 3.3 Effect of Viscosity Grade on Gel Mass Following Cross-Linking. Alginate gels were placed in a 0.1 M $CaCl_2$ solution overnight at 4°C which cross-linked the polymer and reduced the gel mass. The LV grade alginate shrank the least by 49.1 ± 1.8%. The MV and HV grade alginate gel mass reductions were not statistically dissimilar (p-value = 0.508) and were 72.3 ± 1.2%. Error bars are in S.E.M., n = 6.

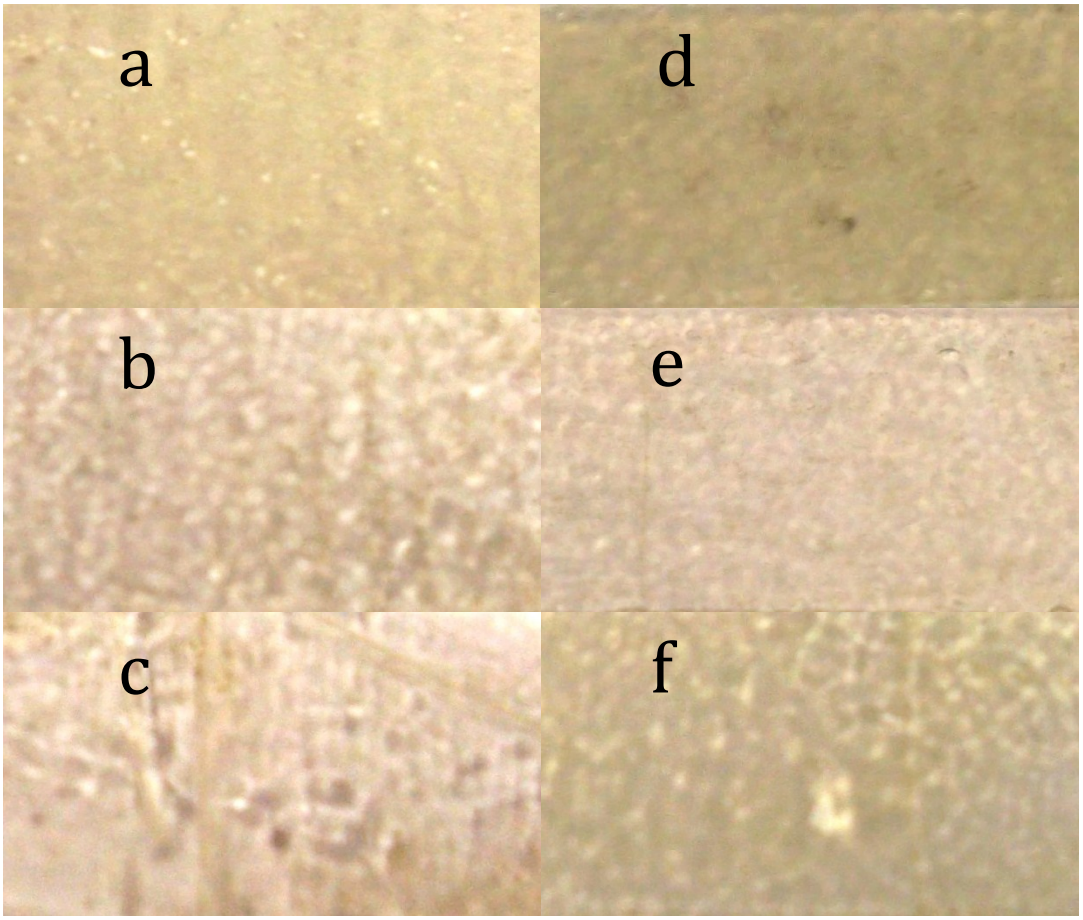

Figure 3.4 Photographs of Alginate Gels. (a-c) Un-cross-linked and (d-f) cross linked (a, d) low viscosity, (b, e) medium viscosity and (c, f) high viscosity grade gels formed through electrophoretic deposition are shown.

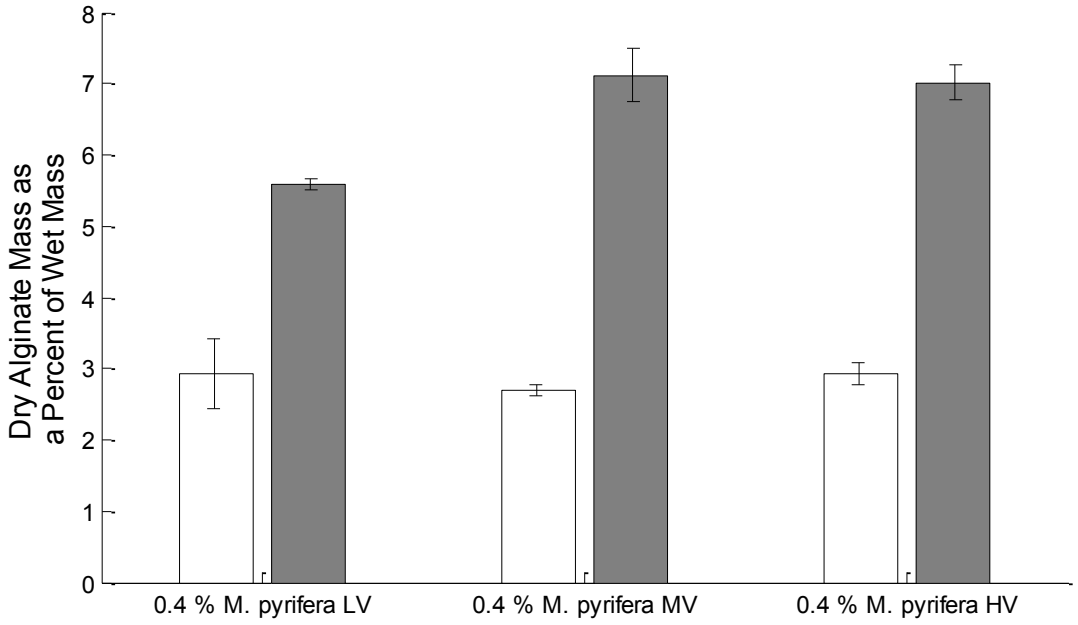

Figure 3.5 Effect of Viscosity Grade on Dry Alginate Mass. Alginate gels were lyophilized for 2 days either before or after cross-linking. The dry alginate masses of the un-cross-linked (white) and cross-linked (grey) gels are represented above. Un-cross-linked gels had statistically similar dry masses (p-values > 0.266) of 2.85 ± 0.46%. Cross-linking increased all of the dry masse with p-values < 0.033. Error bars are in S.E.M., n = 3.

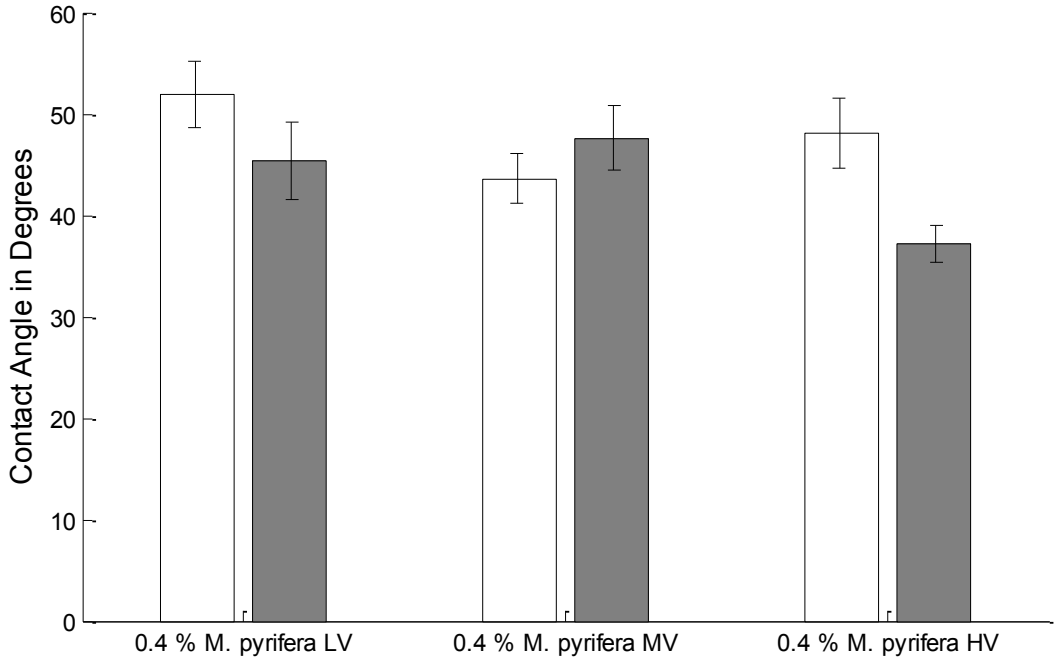

Figure 3.6 Effect of Alginate Viscosity Grade on Dry Gel Contact Angle. Gels from three different viscosity grades of alginate were produced using electrophoretic deposition, and they were dried overnight in vacuum. The contact angles were then obtained by depositing a 0.25 μL drop of water on the dried gel surface. Un-cross-linked (white) and cross-linked (grey) gel contact angles are represented above. All gels had similar contact angle (p-values > 0.193) of 47.4 ±1.1° except for the cross-linked HV grade alginate (p-value < 0.001) that had a contact angle of 37.2 ± 6.38°. Error bars are in S.E.M., n = 12

Alginate Grade	**M_n**	**M_w**	**M_z**	**[η]**	**C'**	**$\eta_{2\%}$**	**$\eta_{0.4\%}$**
Units	**[kDa]**	**[kDa]**	**[kDa]**	**[ml/g]**	**[%]**	**[cP]**	**[cP]**
0.4% M. pyrifera LV	196	643	1,652	208	1.92	250	24.4
0.4% M. pyrifera MV	196	779	2,055	236	1.70	3500	269
0.4% M. pyrifera HV	178	981	2,446	275	1.46	14,000	805

Table 3.1 Viscosities of Deposition Solutions The molecular weights of the three sample alginates were obtained courtesy of the Laboratoire de Caractérisation des Matériaux Polymères au Département de Chimie at L'Université de Montréal. From M_w , [η] was calculated using the Mark-Houwink-Sakurada equation [113], which allowed for the calculation of the critical concentration C'. Using the viscosities of the 2% solutions which were provided by the manufacturers, the 0.4% viscosities were then calculated.

Alginate Grade	**α**	**β**	**μ_e**	**R_f**
Units	**[1/g]**	**[g/s]**	**[cm^2/Vs]**	**[unitless]**
0.4% M. pyrifera LV	0.2302	0.02634	0.0610	21.0
0.4% M. pyrifera MV	0.1759	0.02524	0.0584	16.2
0.4% M. pyrifera HV	0.5377	0.03927	0.0909	47.5

Table 3.2 Deposition Rate Modelling Parameters. Values of α and β were obtained by curve-fitting the mass vs. time curves shown in Figure 3.2 with the Sarkar equation for constant-voltage/constant-concentration deposit mass. From this, the electrophoretic mobility (μ_e) and deposit-solution resistivity ratios ($\boldsymbol{R_f}$) were obtained.

Chapter 4: In-Vitro Characterization of a Novel Sorbent Device for Extracorporeal Blood Filtration

Chris R. Jackson, Satya Prakash*

Biomedical Technology and Cell Therapy Research Laboratory
Departments of Biomedical Engineering, Physiology, and Artificial Cells and Organs Research Center,
Faculty of Medicine, McGill University, Duff Medical Building

3775 University Street, Montreal, Qc, H3A 2B4, Canada

*Corresponding author - Phone: 514-398-2736, Fax: 514-398-7461,

E-mail: satya.prakash@mcgill.ca

Preface

In the present study, a novel sorbent material was first created by depositing alginate and activated carbon onto a stainless steel wire mesh using electrophoretic deposition. Knowledge of deposition rates as well as alginate swelling properties obtained in the previous chapter was used to select the medium viscosity grade alginate. Throughout this chapter, the research focused on the impact of deposition time and cross-linking on the final material dimensions.

Contributions of Authors

The thesis author was responsible for designing and performing experiments, data analysis and preparing manuscripts. Prof. Satya Prakash was reported as the last author in all articles and supervised the research.

In-Vitro Characterization of a Novel Sorbent Device for Extracorporeal Blood Filtration

4.1 Abstract

Sorbent materials are used in re-circulating hemodialysis devices and hemoperfusion devices to clear toxins from dialysate and the blood respectively. In this paper, a novel method of creating sorbent materials was developed by co-depositing alginate and activated carbon onto a stainless steel wire mesh using electrophoretic deposition. A 0.668% ± 0.006% carbon loading was obtained, and the gel deposition rate was investigated. Dimensional analysis was carried out and showed that deposited gel filled the mesh holes after 70 second. Cross-linking increased the size of the macro-pores while reducing the size of the micro-pores from 32.9 ± 1.1 nm to 15.6 ± 0.8 nm. The novel sorbent material has potential use in dialysis where it may be used as a low-cost alternative to current sorbent materials.

4.2 Introduction

4.2.1 Sorbents in Hemodialysis

The most common extracorporeal blood filtration method is hemodialysis and involves passing blood over a semi-permeable membrane. Toxins pass through the membrane and into a counter-flowing dialyser fluid which is then removed through a drain.

Recent efforts have aimed at developing portable dialysis machines to give patients mobility during the treatment. To reduce the weight of the system, the dialysate is cleared of toxins and recirculated. Current devices use just 6 L of tap-

water compared to the 120 L of sterile fluid required for single pass hemodialysis systems [3]. To date, over 2,000,000 treatments have been carried out using this technology.

Sorbent cartridges that are used to filter the dialysate make use of fine powders for their high specific surface area. Small powders create large pressure drops which require larger and more powerful pumps and batteries to overcome, adding to the overall weight of the system. Cutting down the weight of systems is paramount if it is to become the primary form of dialysis. One approach taken to mitigate this problem has been to put sorbent particles in the shell side of the dialyser membrane [37]. Although this resulted in a smaller device, no experimental data showing the viability of the system has yet been published.

4.2.2 Sorbents in Hemoperfusion

In hemoperfusion, blood is passed directly over a sorbent material to remove toxins. When sorbent particulates are used for hemoperfusion, they must be free from particulate fines and resist attrition [38]. Activated carbon (AC) is commonly employed but it cannot be in direct contact with the blood as it causes thrombocytopenia and neutropenia [12]. A polymer such as alginate is often used to immobilize AC [13]. Microcapsules are popular for this purpose as they can be produced on the micron scale ensuring a large contact surface with blood is obtained for a given volume [14-16]. Microencapsulation nevertheless requires a large overhead and an expensive secondary polymer to form the beads, and the process is poorly scalable.

4.2.3 Stacked Wire Mesh in Heat and Mass Exchangers

Two-dimensional wire mesh can be stacked to form three dimensional materials with open pores and highly controllable dimensions. These materials have gained attention in mass exchangers and for use as solid state catalysts. Electrophoretic deposition (EPD) has proven to be a useful process in reducing costs and improving overall performance in these materials [92]. Although wire meshes made of bulk catalyst material have been used such as in the production of nitric acid from ammonia and formaldehyde [93], it is significantly less expensive to coat stainless steel mesh with powdered catalyst using EPD [92]. In one example, stainless steel wire meshes were coated with aluminum particles for catalytic applications such as the oxidation of 1,2-dichlorobenzene (*o*-DCB) [92, 94].

Previous studies have examined the effects of wire mesh dimensions on pressure drops for both heat exchangers and mass exchangers, and a number of correlations have been established [90, 100, 101]. Stacked wire mesh material is advantageous over a packed bed of spheres in that it can be tailored to yield superior heat and mass transfer efficiencies with significantly smaller pressure drops [102].

In this paper, a novel sorbent material with highly a controllable macro-pore size is developed for extracorporeal blood filtration purposes. EPD is used to co-deposit a hydrogel with sorbent particles onto a wire mesh. AC was chosen due its dark colour which is easily identifiable under an optical microscope, and because it is one of the most effective general sorbents of blood toxins [3].

4.3 Materials and Method

4.3.1 Materials

Medium viscosity grade alginic acid (Sigma Aldrich, St. Louis, Montana, USA) was dissolved in deionized water with 1000 m^2/g AC powder (Sigma Aldrich, St. Louis, Montana, USA) [124]. A 2% alginate – 1% AC solution was used for all experiments. Both alginate and AC were used for their high biocompatibility. A 20 gauge T316 stainless steel wire mesh (TWP, Berkley, California, USA) was used as a substrate for all depositions. Mesh holes were 1.041 mm wide and the wires were 0.2286 mm in diameter.

4.3.2 Method for Depositing Gel onto Mesh Substrate

Meshes were cut into 5 cm x 10 cm rectangles prior to deposition. A holding apparatus was used that covered 0.3 cm of each of the shorter sides of the mesh, so the area of mesh affected by the deposition was 47 cm^2. The same EPD device has previously been used in our laboratory (see Chapter 3). A 2.5 V/cm electric field was supplied via an Abra AB-3000 (Abra, Champlain, New York, USA) voltage source.

4.3.3 Method for Determining Mesh Hole Open Area and Gel Thickness

The AC-alginate gels were deposited up to 70 seconds and samples were collected at 10 second intervals. Images were taken of samples at 4 x magnification using a Leica ICC50 (Leica Microsystems, Wetzlar, Germany) with a DM500 attachment. Sample gels were cross-linked in a 0.1 M $CaCl_2$ solution overnight at 4°C before they were re-imaged. The hole open areas of the mesh before and after cross-

linking were analysed using ImageJ 1.44p (National Institutes of Health, USA). Depositions were carried out in triplicate, and 9 holes were imaged per deposition.

For gel thickness calculations, the deposit was modelled as being perfectly centered with square edges. Thus

Eq. 13
$$t_{gel} \approx \frac{\sqrt{A_{tot}} - \sqrt{A_{open}}}{2}$$

where t_{gel} is the gel thickness [mm], A_{tot} is the total area of the mesh [mm^2], and A_{open} is the post-deposition open hole area [mm^2].

4.3.4 Method for Evaluating Gel Mass Deposition Rate

Steel wire mesh masses were obtained before deposition using a Mettler Toledo AG204 DeltaRange scale (Mettler-Toledo, city, Ohio, USA). Following deposition, the gels were cross-linked overnight. Water droplets were removed using compressed lab air and the gel mass was obtained. The mass was only obtained following cross-linking because the non-cross-linked alginate could not be cleared of droplets without mechanical damage to the gel. Depositions were carried out in triplicate.

4.3.5 Method for Evaluating Activated Carbon Loading

The gel AC loading was obtained via two independent methods; gel dissolution followed by filtration, and thermogravimetric analysis (TGA).

4.3.5.1Gel Dissolution and Filtration

Gel samples were massed and re-dissolved in sodium citrate. The resulting solution was passed through a grade 1 filter paper (Whatman, Maidstone, Kent, UK). Once the filter was dried, the mass was recorded.

The mass of AC powder caught by the filter paper is not expected to be the same as the mass of AC loaded in the gel, as some of the AC was smaller than the pore size of the filter paper. Moreover, the mass of the particles would either increase or decrease due to alginate attachment and sodium citrate corrosion. Thus, a known mass of AC was added to a sodium citrate – alginate solution and was filtered using the same method in order to proportion the mass of the powder caught by the filter versus the mass of AC in the gel.

4.3.5.2 Thermogravimetric Analysis

Thermogravimetric Analysis was carried out using a Q500 (TA Instruments, New Castle, Delaware, USA) on a 2% alginate gel, a 2% alginate-1% AC gel, and on the AC powder. A ramp speed of 20°C/min was used in all experiments, and a temperature range between 40°C and 1000°C was observed. The mass fraction of AC in the gel was computed graphically using ImageJ software.

4.3.6 Method for Determining Pore Size Using Scanning Electron Microscopy

Critical point drying was used to remove water from the gels without altering the pore sizes. Sample gels were washed in 30%, 50%, 70%, 80%, 90%, 95% and 100% ethanol solutions for 10 minutes each. They were then washed in 25%, 50%,

75% and 100% solutions of amyl acetate in ethanol for 15 minutes each. The gels were removed from their substrates and critical point drying was performed using a Leica ME CPD030 (Leica Microsystems, Wetzlar, Germany). The dried gels were coated in Au/Pd for 5 minutes using a Hummer VI sputter coater (Anatech, Union City, California, USA).

SEM images were obtained using a Hitachi Cold FE SU-8000 (Roche Diagnostics Corps., Indianapolis, Indiana, USA) with an accelerating voltage of 2 kV and 10 μA. Images were analysed using ImageJ 1.44p (National Institutes of Health, USA) software to obtain the pore size distribution. Pores were measured over a 1.5 μm square area.

4.3.7 Statistical Analysis

Statistical analysis was performed using Minitab software (Minitab, Version 15; Minitab Inc, Pennsylvania, USA). Values are expressed as mean ± standard error. Statistical comparisons were carried out by multiple analyses of variance (ANOVA) or by student t-test where appropriate. Randomized independent sampling was assumed and statistical significance was set at $p < 0.05$. All interaction terms were treated as fixed terms. Sample sizes varied between 3 and 18, as indicated per experiment.

4.4 Results

4.4.1 Mesh Hole Open Area and Gel Thickness

When there was no AC in the deposition solution, the boundary of the gel was not distinguishable from the water droplet using the light microscopy. With the addition of AC, the boundary was clearly visible.

The deposit was not uniform and was thicker at the extremities of the mesh. The resulting mesh was therefore divided into two sections; the central area of the mesh and the area near the edges. Holes were imaged from the central area, which accounted for the majority of the mesh. Figure 4.1 shows the steel wire mesh before and after depositions.

Examples of light microscope images are shown in Figure 4.2. For all time points before 70 seconds, the holes were larger post-cross-linking due to the reduction in gels volume as shown in Figure 4.3. Once holes closed at 70 seconds, cross-linking did not reopen them. Gel thickness is shown in Figure 4.4.

4.4.2 Gel Mass Deposition Rate

The gel mass increased steadily with deposition time, and is shown in Figure 4.5. The gel mass per unit area is shown as a function of time in Table 4.1.

4.4.3 Activated Carbon Loading

4.4.3.1 Gel Dissolution and Filtration

When a known mass of AC was dissolved in the alginate-sodium citrate solution, 58% of the initial mass was recovered. The gel AC loading was 0.67% ± 0.0058%.

4.4.3.2 Thermogravimetric Analysis

The TGA curves for AC powder, 2% alginate gel, and for the 2% alginate - 1% AC gel are shown in Figures 4.6, 4.7 and 4.8 respectively. The AC powder curve showed that the majority of the mass was lost at approximately 670°C and that 13.0% of the mass remained by 1000°C. The 2% alginate gel initially lost 95.0% of its mass below 180°C. The differential curve indicated that there was another loss in mass at 310°C and again at 570°C, and that 1.6% of the mass remained after the run. For the 2% alginate - 1% AC gel, 72.5% of the mass was lost below 110°C. The differential curve indicated that there were four more peaks at 280°C, 450°C, 530°C and 650°C. The final peak at 650°C accounted for a 0.84% change in mass due to AC. There was a final residue of 6.6% at 1000°C.

4.4.4 Pore Size Using Scanning Electron Microscopy

Gel images at 30,000 x and 100 x magnification are shown in Figures 4.9 and 4.10 respectively. For the alginate gel, the pores were ellipsoid, and their long axis was unidirectional. The alginate gel was found to have an average pore size of 32.9 ± 1.1 nm. When AC was added to the gel, pores were round and their size was reduced to 15.6 ± 0.8 nm. Images of the AC-gel at 100 x magnification revealed that AC was

scattered along the surface. Histograms of the pore sizes were produced with 5 nm bins and are shown in Figure 4.11.

4.5 Discussion

4.5.1 Mesh Hole Open Area and Gel Thickness

A tight control over the post-deposit mesh hole size is desired for optimization. Increasing the deposit mass will increase the total mass of AC available for toxin absorption, but will negatively affect mass transfer efficiencies if too high [90]. Too small a hole will render the mesh susceptible to clogging. The pressure drop has previously been shown to increase with the square of the open area ratio [91]. An ideal hole size therefore depends on numerous factors including AC loading, absorption rate, toxin concentration, pump strength and run-time.

4.5.2 Gel Mass Deposition Rate

The mass of the gel increased linearly with deposition time. Figure 4.5 shows that a fit was obtained with the equation

Eq. 14 $$m = 0.0366t$$

where m is the mass of the gel [g] and t is the deposition time [s], with an R^2 value of 0.9834.

4.5.3 Activated Carbon Loading

The AC loading value obtained using the filtration method was compared to the value obtained using the TGA. Similar values of 0.668% ± 0.006% and 0.84% were obtained respectively. The TGA results were likely overestimated as there was

significant overlap with other peaks in the differential curves. The filtration method was likely more accurate, although the electrophoretic deposition selectivity to particle size should be evaluated to ensure accurate proportioning.

Alginate gel residue following the TGA run was largely due to the formation of Na_2CO_3, as reported previously in literature [125]. AC residue was likely due to impurities in the powder and unreacted carbon.

The loading obtained using electrophoretic deposition was significantly lower than using other immobilizing techniques such as chitosan matrix encapsulation [47] and polyhydroxy ethyl methacrylate encapsulation [48] who achieved 40% and 75% loading respectively. Future works needs to address the high electrophoretic mobility of alginate when compared to activated carbon in order to increase loading.

4.5.4 Pore Size Using Scanning Electron Microscopy

The co-deposition of carbon significantly reduced the average pore size (p-value < 0.001). This has been previously seen in the production of alginate-activated carbon microcapsules [126]. Pore sizes for alginate gels produced using EPD were a full order of magnitude larger than for alginate gels produced using a dissolution technique. Creatinine is a common marker for chronic renal disease found in the blood. With dimensions smaller than 0.53 nm, it should easily be transported through the gel pores [127]. Diffusivity increases with particle size, so EPD alginate is expected to have significantly improved diffusional characteristics over alginate

microcapsules [89, 128]. Histograms revealed that the pore size distribution was more homogeneous for gels with no AC than it was for the alginate alone.

4.6 Conclusion

In this study, alginate was electrophoretically co-deposited with AC onto a stainless steel wire mesh to form a novel sorbent material with high macro-porosity for potential use in extracorporeal blood filtration. A high degree of control over the deposition rate was obtained and will allow for hole size optimization. A 2.5 V/cm electric field was applied to a 20 gauge stainless steel mesh in a 2 % alginate – 1% AC deposition solution, and holes were completely filled with deposited gel within 70 seconds. The resulting gel had a carbon loading of 0.67% ± 0.0058%.

Although this paper outlined the general approach taken to make the novel sorbent material, there is still much room for optimization. It is likely possible to increase the mass fraction of AC in the resulting gel by increasing its concentration in the deposition solution [55]. It would then also be important to establish the effect of AC loading on the mechanical properties of the gel to ensure that it is not significantly weakened. It is also important to validate the materials' ability to absorb blood toxins.

4.7 Acknowledgements

Thank you to Dr. Pavan M. V. Raja for his help in experimental design, as well as the other members of the Biomedical Technology and Cell Therapy Research Laboratory at McGill University for their valued input. Thank you to Mina Mekhail of the Biomaterials Research Group at McGill University for helping out with the SEM

images. Thank you to Petr Fiurasek of the Centre for Self Assembled Chemical Structures for aiding with the TGA. The authors would also like to acknowledge the Canadian Institute of Health Research (CIHR) grant (MOP 93641) to Prof. S. Prakash, and for funding provided by NSERC.

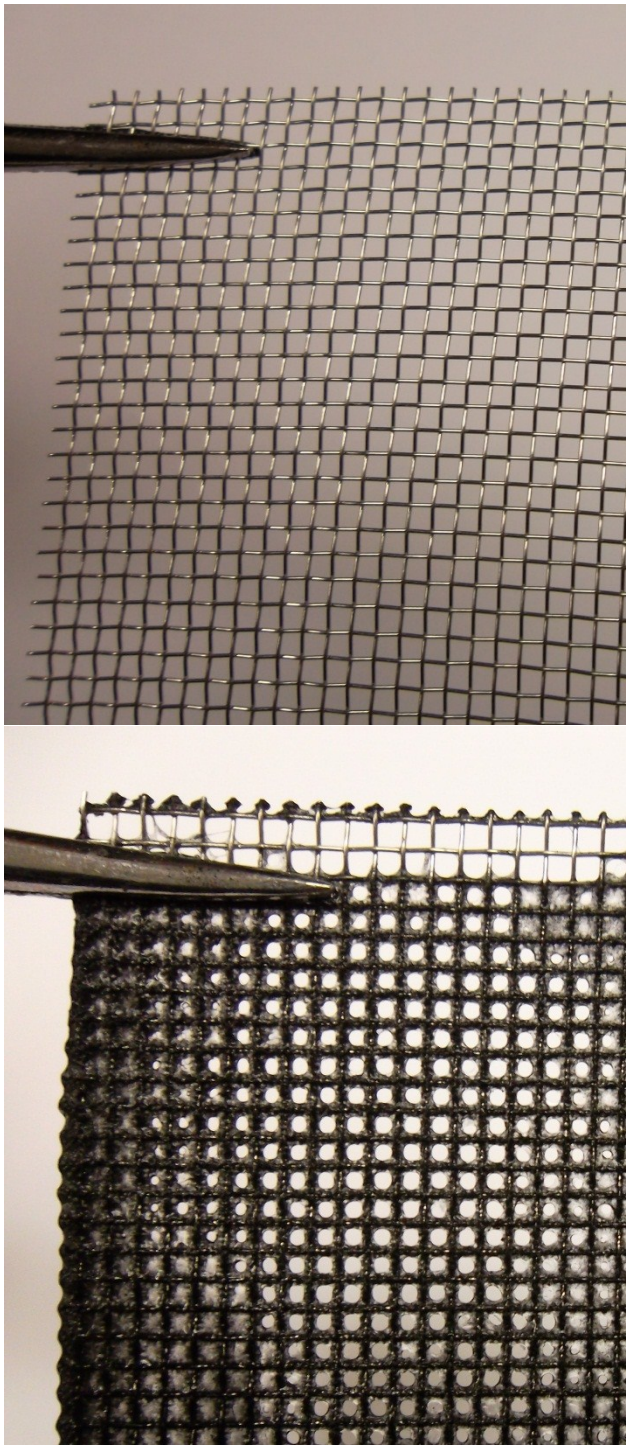

Figure 4.1 Photograph of 20 Gauge Stainless Steel Mesh. Images are shown (top) before and (bottom) after deposition.

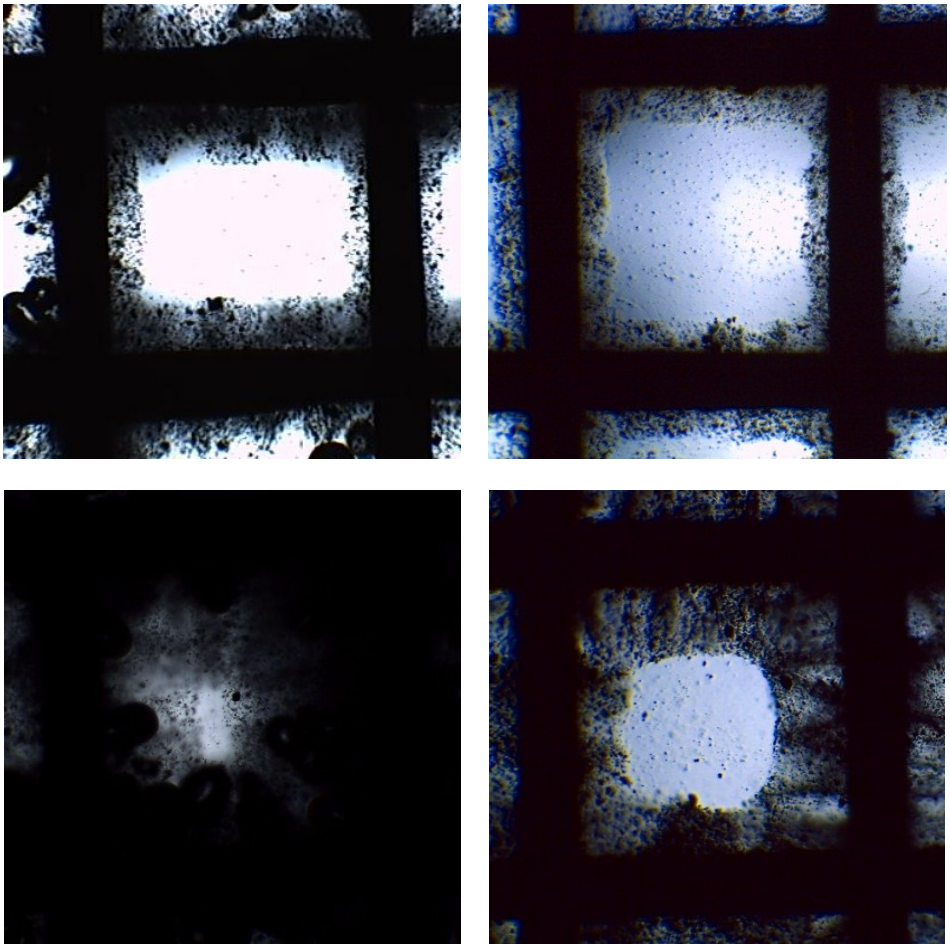

Figure 4.2 Light Microscope Images of Sorbent Material at 4 x Magnification. Mesh Holes are shown after deposition times of (a, and b) 20 seconds and (c and d) 60 seconds for (a and c) non-cross-linked and (b and d) cross-linked gels. The stainless steel wire is clearly visible as solid black, while the gel is gray with black AC particles. The central white area is the hole open area.

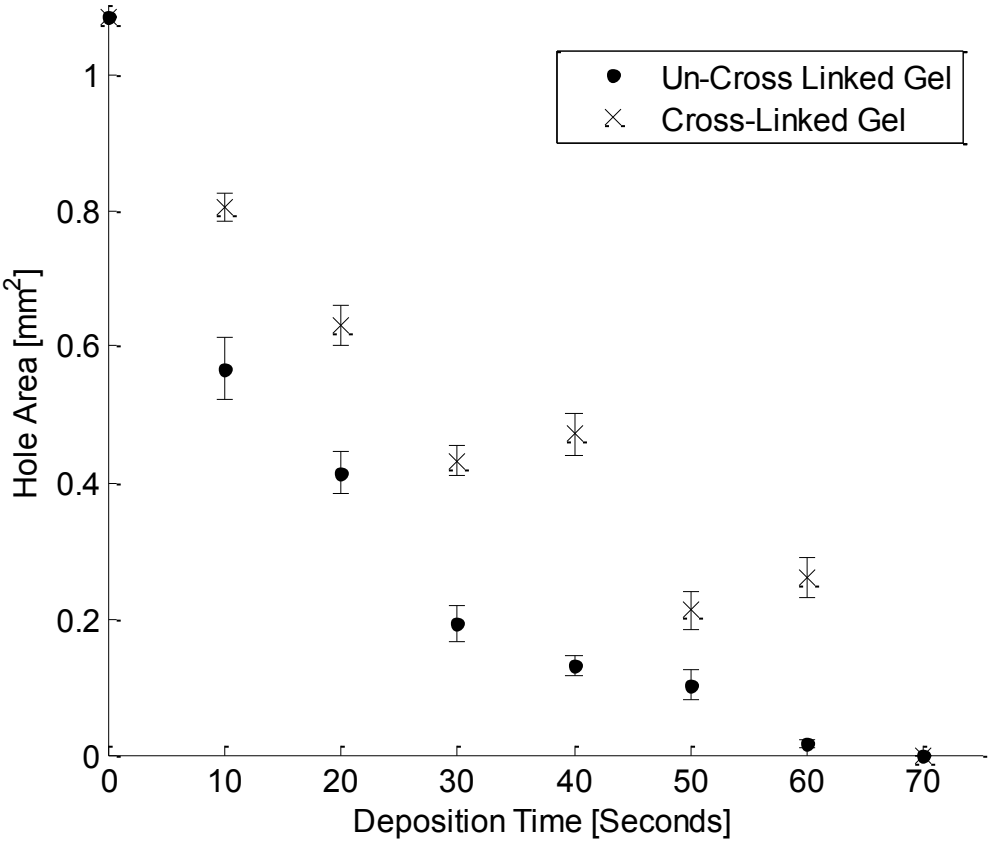

Figure 4.3 Hole Open Area Depending on Deposition Time. Meshes were photographed after 10, 20, 30, 40, 50, 60 and 70 second deposition times. Cross-linked open hole areas were larger due to gel shrinking. Error bars are in S.E.M., n = 18.

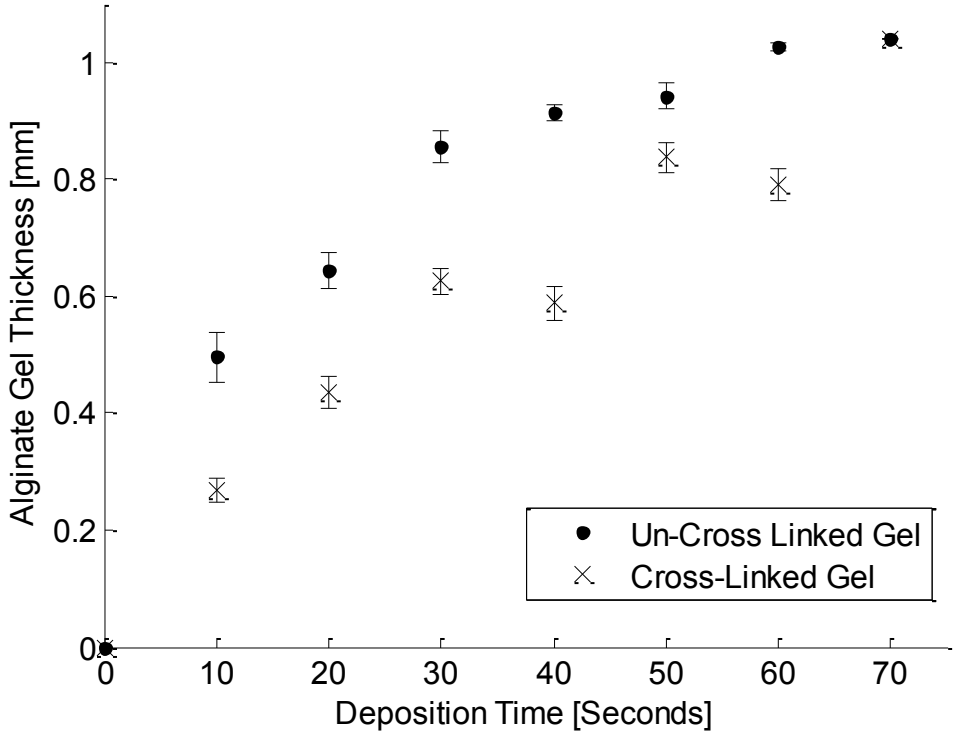

Figure 4.4 Gel Thickness Depending On Deposition Times. The gel thicknesses were calculated using the hole open area. Both gels increased with time, and the cross-linked gel was thinner than the un-cross-linked gel due to shrinking. Error bars are in S.E.M., n = 18.

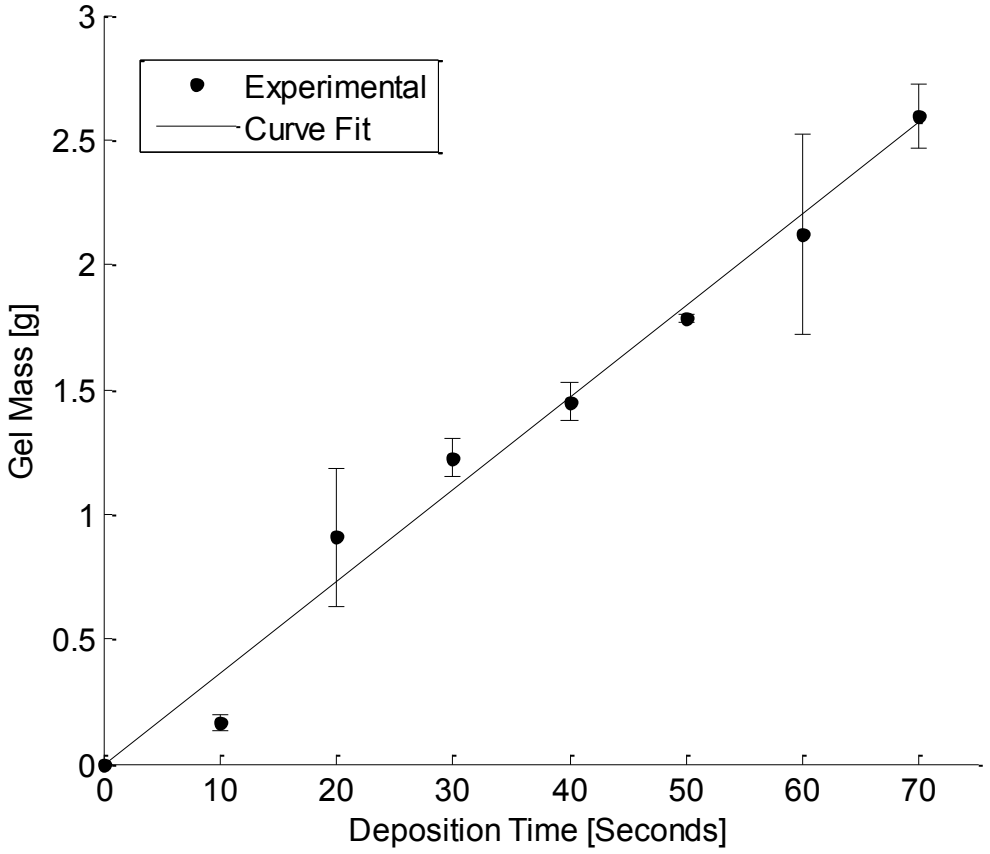

Figure 4.5 Gel Mass Depending On Deposition Time. The mass of the deposit is represented above for the given deposition times. The mass of the gels increased approximately linearly until a final mass of 2.59 ± 0.13 g was obtained at 70 seconds. A curve fit is shown with a slope of 0.0336 g/s. Error bars are in S.E.M., n = 3.

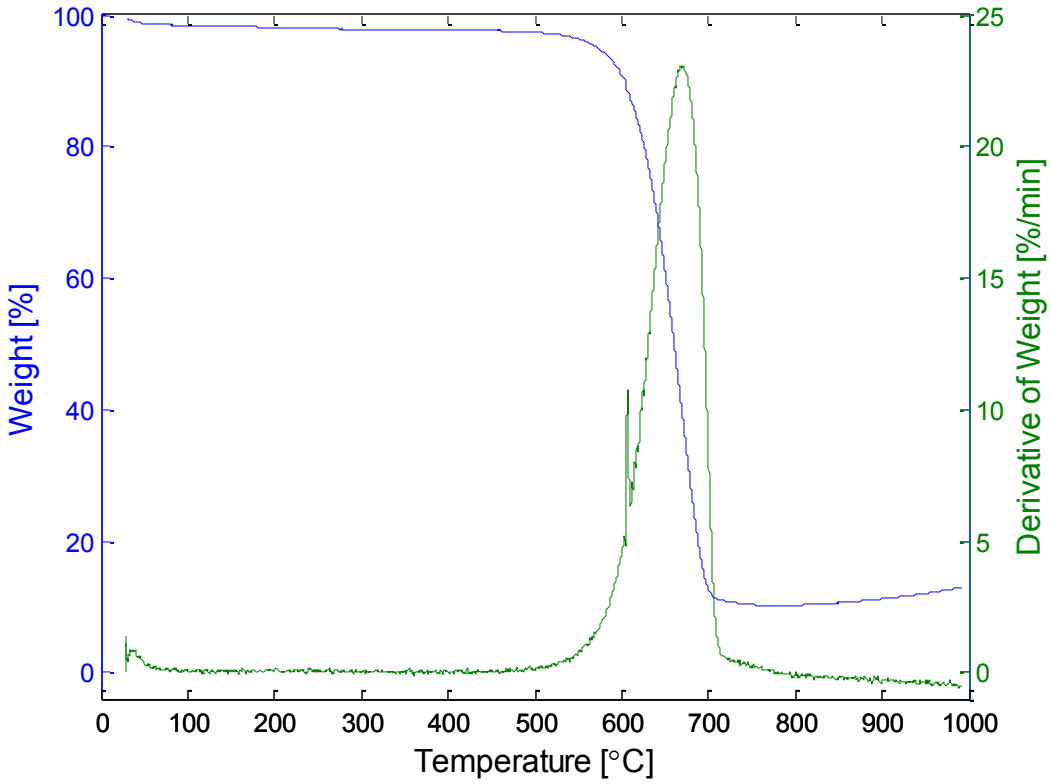

Figure 4.6 Thermogravimetric Analysis of AC Powder. Most of the powder reacted at 670°C, and 13.0% of the mass remained as residue by 1000°C.

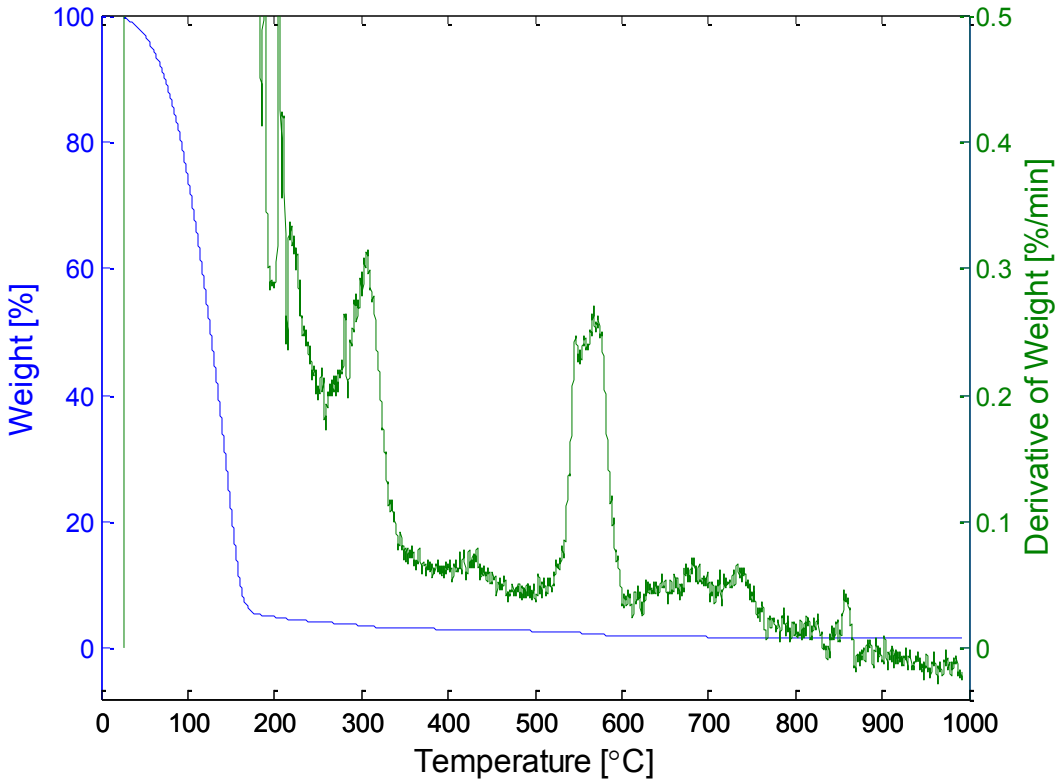

Figure 4.7 Thermogravimetric Analysis of 2% Alginate Gel. The water fraction of the gel was lost before 180°C. Alginate reacted at 310°C and at 570°C, and 1.6% of the mass remained as residue.

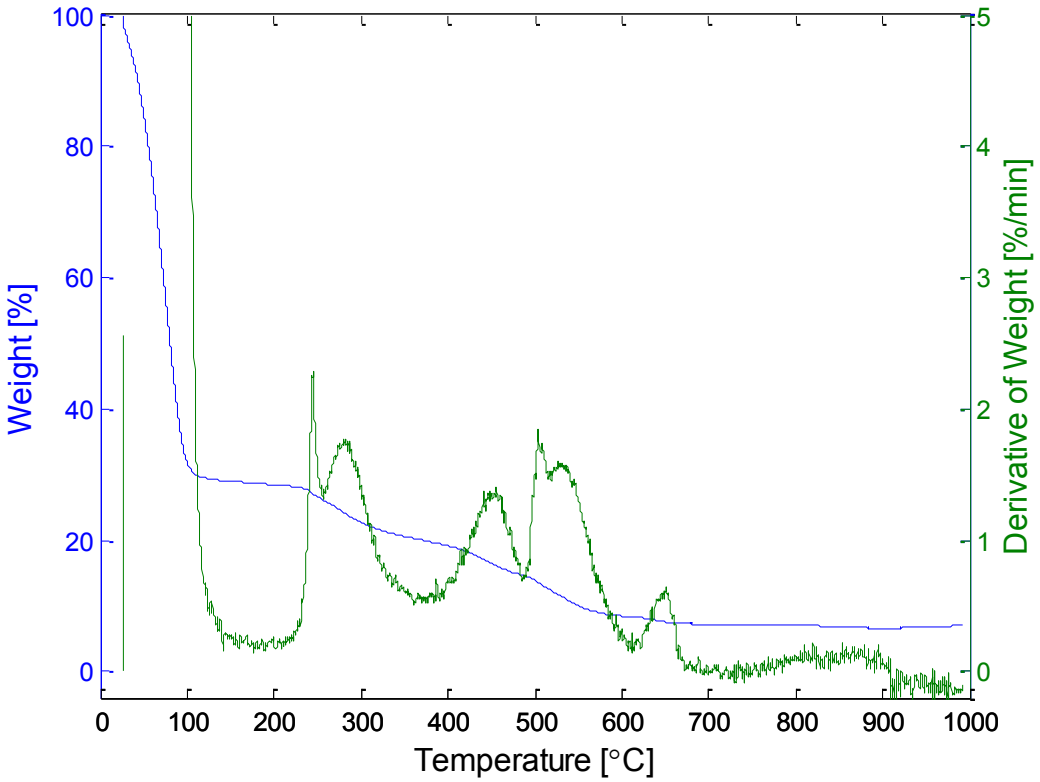

Figure 4.8 Thermogravimetric Analysis of 2% Alginate – 1% AC Gel. The water fraction of the gel evaporated below 110°C. Peaks at 280°C, 450°C, and 530°C accounted for the algiante gel, and the peak at 650°C accounted for AC powder.

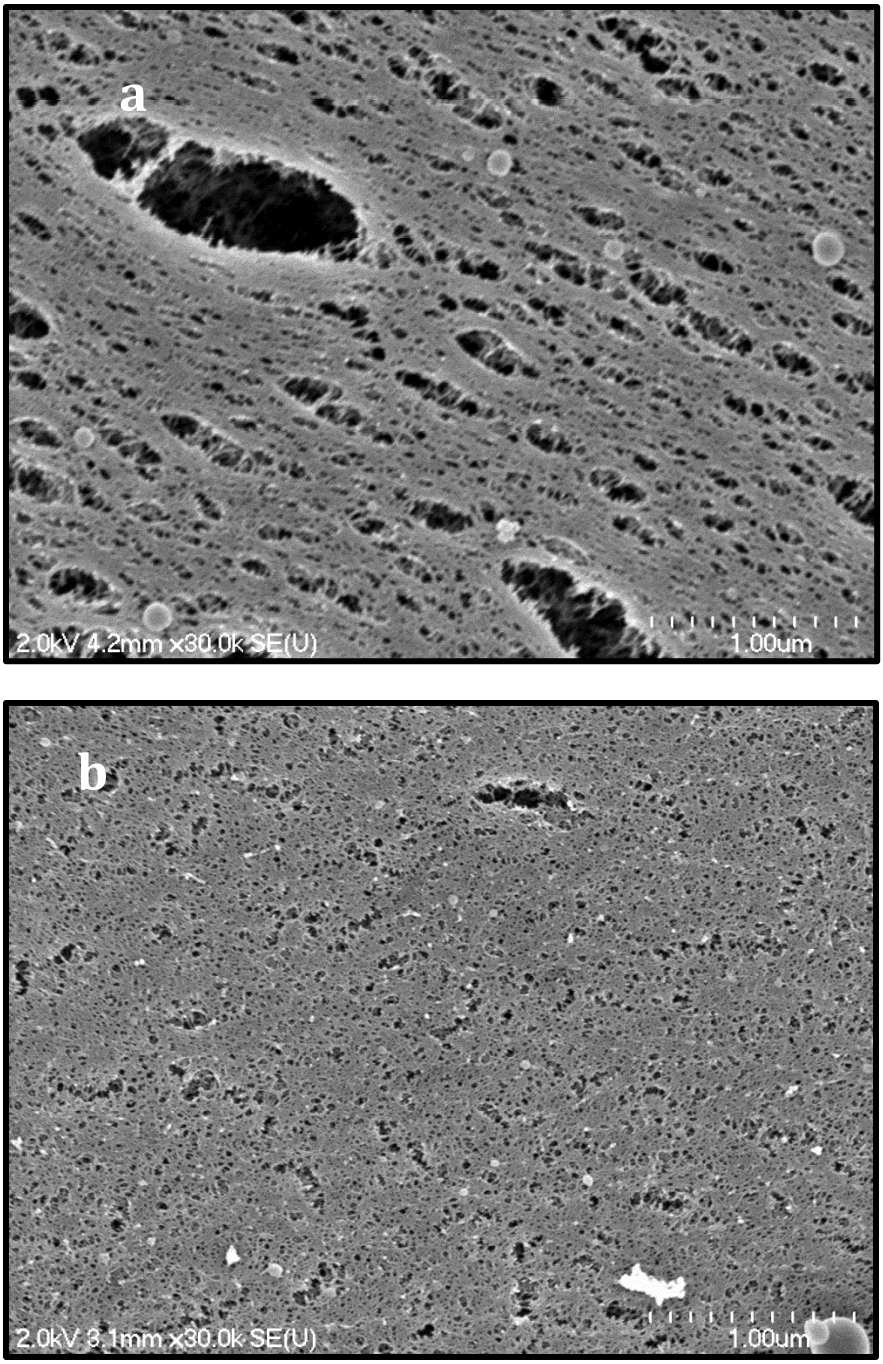

Figure 4.9 SEM Images of Gels. (a) 2% Alginate and (b) 2% Alginate - 1% AC gels were prepared using electrophoretic deposition. Images were taken at 30,000 x magnification, and were used to obtain the pore sizes of the two gels.

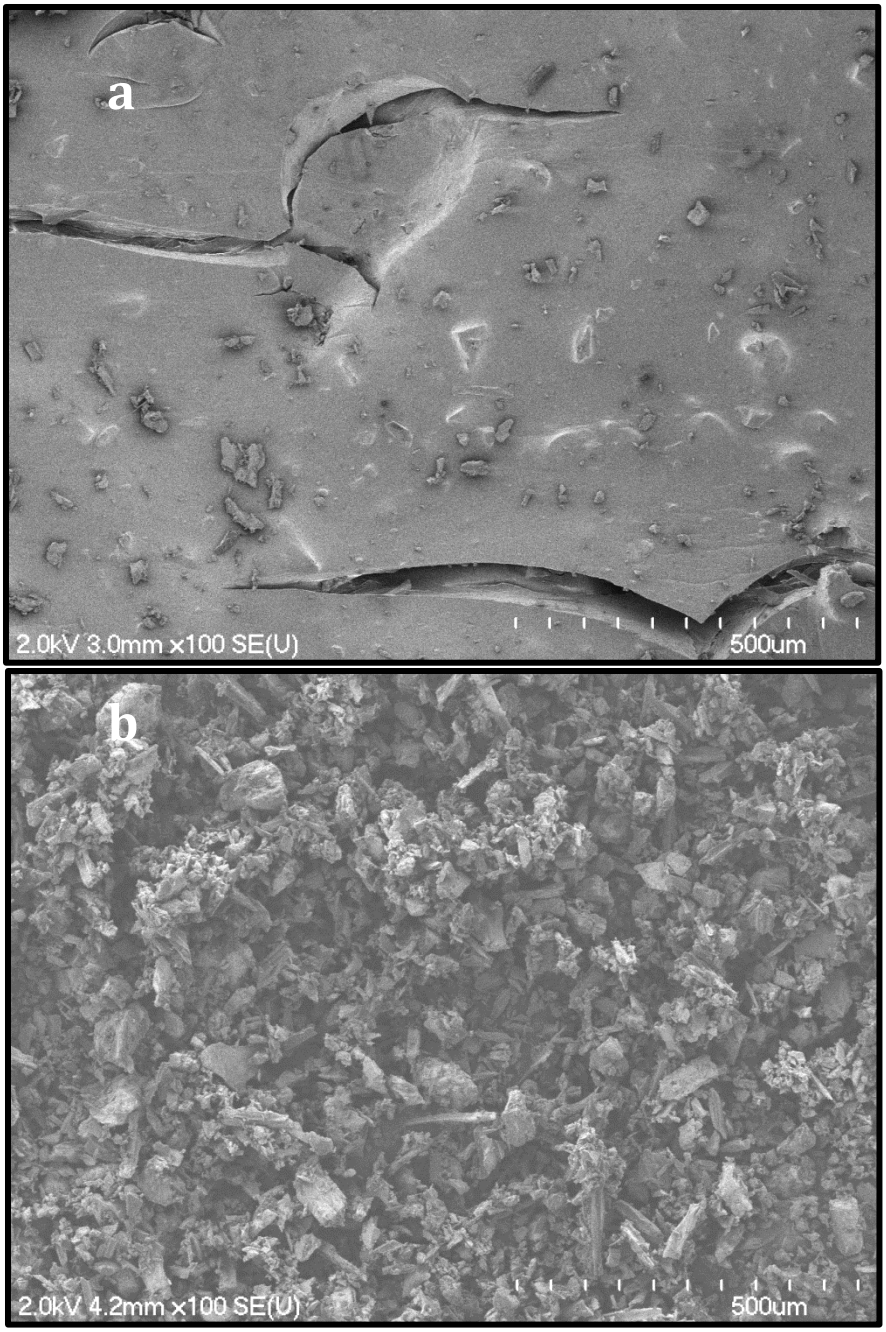

Figure 4.10 SEM Images of Alginate-AC Gel and AC Particles (a) Alginate – AC gel and (b) AC particles were imaged using SEM at 100 x magnification. AC Particles are clearly visible embedded along the surface and within the gel.

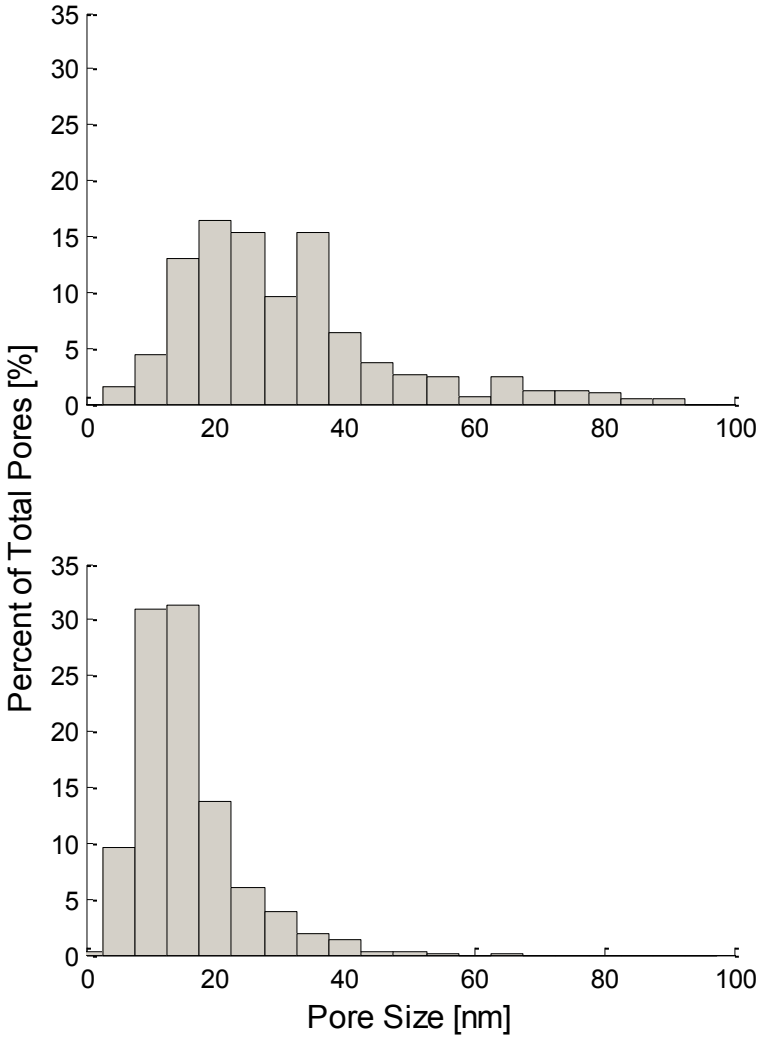

Figure 4.11 Pore Size Distributions of Alginate and Alginate-AC Gels. The alginate-AC (bottom) gel has smaller pores and a narrower pore-size distribution than the alginate gel (top).

Deposition Time [s]	Un-Cross Linked		Cross Linked		
	Hole Area [mm^2]	Gel Thickness [mm]	Gel Mass [mg/cm^2]	Hole Area [mm^2]	Gel Thickness [mm]
0	1.084	0	0	1.084	0
10	0.568 ± 0.045	0.496 ± 0.043	3.5 ± 0.7	0.805 ± 0.020	0.268 ±0.019
20	0.414 ± 0.031	0.643 ± 0.030	19.3 ± 5.9	0.631 ± 0.029	0.434 ±0.028
30	0.193 ± 0.028	0.856 ±0.027	26.1 ± 1.7	0.432 ± 0.023	0.626 ± 0.022
40	0.131 ± 0.014	0.915 ±0.013	30.9 ± 1.6	0.472 ± 0.031	0.588 ± 0.030
50	0.103 ± 0.022	0.942 ±0.021	37.9 ± 0.4	0.212 ± 0.028	0.837 ± 0.027
60	0.016 ± 0.008	1.025 ±0.006	45.2 ± 8.5	0.260 ± 0.030	0.791 ± 0.029
70	0	1.041	55.2 ± 2.8	0	1.041

Table 4.1 Physical Characteristic of Sorbent Material per Unit Area, Depending on Deposition Time. Gels were formed on 20 gauge stainless steel substrates through EPD. The size of the holes and gel thicknesses were evaluated using graphical methods. Values are shown with ± S.E.M., with n = 3 for gel mass and n=18 for hole size and gel thickness.

Chapter 5 *In-Vitro* Investigation of Efficacy of Novel Sorbent Device for Removal of Uremic Blood Toxins

Chris R. Jackson, Satya Prakash*

Biomedical Technology and Cell Therapy Research Laboratory
Departments of Biomedical Engineering, Physiology, and Artificial Cells and Organs Research Center,
Faculty of Medicine, McGill University, Duff Medical Building

3775 University Street, Montreal, Qc, H3A 2B4, Canada

*Corresponding author - Phone: 514-398-2736, Fax: 514-398-7461,

E-mail: satya.prakash@mcgill.ca

Preface

A deposition time was selected using the dimensional data made available in the previous chapter. The ability for the sorbent meshes to absorb a selection of blood toxins was evaluated and compared to encapsulation techniques reported in literature.

Contributions of Authors

The thesis author was responsible for designing and performing experiments, data analysis and preparing manuscripts. Dr Satya Prakash was reported as the last author in all articles and supervised the research.

In-Vitro Investigation of Efficacy of Novel Sorbent Device for Removal of Uremic Blood Toxins

5.1 Abstract

Alginate and activated carbon were co-deposited onto 20 gauge stainless steel wire meshes to produce a novel sorbent material. In this paper, the sorbent performance was evaluated using selected blood toxins. After a 150 minutes experimental run, the uric acid concentration decreased by 99.0 ± 1.1%, the creatinine concentration decreased by 38.3 ± 1.1%, the ammonia concentration decreased by 13.7 ± 2.2%, and the urea concentration decreased by 3.7 ± 1.0%. The novel sorbent material shows promise for use in extracorporeal blood filtration devices.

5.2 Introduction

5.2.1 Dialysis

Patients suffering from chronic renal disease (CRD), liver failure, and acute drug intoxication are all likely to be subjected to extracorporeal blood filtration to remove toxins from their blood. There are nearly 900,000 CRD patients worldwide [2] that must undergo treatment for up to 4 hours a day, 3 days a week. Patients suffering from acute drug intoxication or liver failure may also require extracorporeal dialysis with treatments lasting as long as 48 hours [17]. Extracorporeal dialysis is justified whenever it can increase the rate at which the body removes toxins by at least 30% [17].

5.2.2 Sorbents in Dialysis

Hemoperfusion is commonly used to help treat patients following liver failure, patients suffering from acute drug intoxication, and occasionally CRD patients. In this method, blood is passed directly over a sorbent material. Immobilised activated carbon (AC) is commonly used as a generalized sorbent material for its extremely high specific surface area, low cost, and high affinity for a number of blood toxins including middle molecules, uric acid, creatinine, and other organic compounds [10, 11]. AC has been shown to have a strong affinity for molecules with low charge and molecular weights greater than 100 [3].

When a sorbent particulate is used for hemoperfusion, it must be free of particulate fines and it must resist attrition [38]. When AC is used, it must not be in direct contact with the blood as it causes thrombocytopenia and neutropenia [12]. To satisfy the above criteria, an immobilization agent is used [13]. The naturally occurring di-polymer alginate derived from seaweed is commonly used for this purpose [129]. Microencapsulation of AC is popular because a high contact area with the blood can be achieved for a given volume [14-16]. To obtain large specific surface areas, however, small microcapsules must be used which require a large overhead. A secondary shell polymer must also be used that adds a diffusion layer and is often expensive. Moreover, microcapsules are produced one at a time, so the process can be difficult to scale for mass production.

An alternative approach to generalized sorbents is to use resins developed to bind to specific molecules such as β_2-Microglobulin [44]. Although such resins can be tailored with high biocompatibility, there are at least 100 uremic toxins that have been discovered, so molecule-specific binders are not likely to replace unspecific binders for most applications [45].

5.2.3 Hydrogel Electrophoretic Deposition

Electrophoretic deposition (EPD) is a technique used to deposit layers of material onto electrically conductive substrates. The method is commonly used in ceramics and has recently gained attention in developing biomaterials. EPD is relatively inexpensive, highly controllable, and results in the uniform coating on the substrate. Alginate has recently gained attention for anodic EDP and has already been successfully co-deposited with ceramics [84], proteins [88], cells [83] and carbon nanotubes [85].

To the knowledge of the author, no sorbent material with stacked wire mesh geometry has been used for extracorporeal blood filtration. With the potentially small pressure drop, high versatility, and small overhead required for production, this material warrants further research. In this study we test the sorbent performance of the electrophoretically co-deposited alginate-AC gel.

5.3 Materials and Methods

5.3.1 Materials

The alginate-AC gel coated mesh was developed using methods outlines in chapter 4. Medium viscosity grade alginic acid (Sigma Aldrich, St. Louis, Montana, USA) and AC (Sigma Aldrich, St. Louis, Montana, USA) were dissolved in deionised water and co-deposited on 5 x 10 cm rectangles of 20 gauge T316 stainless steel wire mesh (TWP, Berkley, California, USA). EPD was carried out under a 2.5 V/cm electric field for 40 seconds to ensure that a large mass of gel was deposited without clogging the pores. A 2% alginate - 1% AC solution was used in sufficient quantities that the concentration remained approximately constant throughout the deposition. Following EPD, the material was placed in 0.1 M $CaCl_2$ solution overnight at 4°C to induce cross-linking.

5.3.2 Method for Evaluating Sorbent Performance

A solution was prepared with approximately double physiological concentrations of urea (Sigma Aldrich, St. Louis, Montana, USA), uric acid (Sigma Aldrich, St. Louis, Montana, USA), creatinine (Sigma Aldrich, St. Louis, Montana, USA), ammonium chloride (Sigma Aldrich, St. Louis, Montana, USA). The initial concentrations of each are shown in Table 5.1. In order to imitate physiological blood pH, a 2 M NaOH (Sigma Aldrich, St. Louis, Montana, USA) solution was added drop-wise until a pH of 7.4 was achieved.

For each experimental run, the 5 x 10 cm alginate-AC coated steel meshes were cut into four 5 x 2.5 cm rectangles. Twenty of these smaller meshes were

added to 200 mL of the toxin solution under mixing conditions. Solution samples were extracted for analysis in 500 μL volumes at 0, 5, 10, 20, 45, 90 and 150 minutes. The toxin concentrations were obtained using a Hitachi 911 Automatic Analyser (Roche Diagnostics Corps., Indianapolis, Indiana, USA).

5.3.3 Method for Evaluating Volumetric Porosity

The volumetric porosity of a material is a fraction of a material that consists of fluid and can be determined through the following;

Eq. 15
$$\varepsilon = \frac{V_{total} - V_{solid}}{V_{total}}$$

where ε is the porosity, V_{total} is the total volume of the material [mL], and V_{solid} is the volume occupied by the solid portion of the material [mL]. V_{total} was obtained by measuring length, height and width of 15 stacked meshes. V_{solid} was obtained immediately after the absorption test and was carried out by first removing droplets from the surface of the individual meshes and then performing a water displacement test.

The sorbent material was weighed before and after the absorption experiment using a Mettler Toledo AG204 DeltaRange scale (Mettler-Toledo, Greifensee, Switzerland) to indicate if the gel deteriorated throughout the experiment.

5.3.4 Statistical Analysis

Statistical analysis was performed using Minitab software (Minitab, Version 15; Minitab Inc, Pennsylvania, USA). Values are expressed as means ± standard error. Statistical comparisons were carried out by multiple analyses of variance (ANOVA). Randomized independent sampling was assumed and statistical significance was set at $p < 0.05$. Sample sizes with $n = 3$ were used.

5.4 Results

5.4.1 Sorbent Performance

The urea concentration decreased by 3.7 ± 1.0% throughout the 150 minutes experimental run as shown in Figure 5.1. The experimental uric acid concentration was shown to decrease throughout the run with a total reduction of 98.9 ± 1.1%, while the control increased steadily by 30 ± 1.4% as shown in Figure 5.2. Although the ammonia concentration decreased very rapidly by 13.7 ± 2.2% within the first 5 minutes, there was little change in concentration afterwards as shown in Figure 5.3. The creatinine concentration decreased throughout the run by 38.3 ± 1.1% as shown in Figure 5.4. Other than uric acid which increased, there was no change in toxin concentration in the control groups. All observations were statistically significant with p-values < 0.037.

5.4.2 Volumetric Porosity

The material was found to have a volumetric porosity of 0.51. The sorbent mesh mass increased by 8.7 ± 1.7 % following the absorption experiment.

5.5 Discussion

5.5.1 Sorbent Performance

Urea was poorly absorbed as commonly seen in AC based hemoperfusion devices [46]. The protein urease is commonly used in addition to AC in order to break down urea in sorbent cartridges [1, 3]. Although experimentation is still required, proteins have already been electrophoretically co-deposited with alginate [88], so it is likely that the method described in this paper could also be used for this purpose.

Although uric acid has a larger molecular weight and was more concentrated than creatinine, it was nevertheless found to absorb faster. Such results were expected when comparing the Langmuir adsorption isotherms for the two chemicals for charcoal binding as reported by Ash [3]. A higher gauge mesh would likely help in removing creatinine, as it would expose the solution to a larger surface area over which the creatinine would absorb. The increase in uric acid in the control group was likely due to a slow dissolution rate.

Although uric acid was sufficiently absorbed, creatinine and ammonia were still present above physiological concentrations after 150 minutes. Ammonia was unique because although it absorbed very quickly, it saturated the AC within the first 5 minutes. Increasing the mass of AC should be used to increase creatinine and ammonia absorbance. This may be achieved by either using a higher concentration of AC in the deposition solution, or by using a larger surface area of sorbent mesh. Higher gauge meshes would not likely have a large impact on the ammonia

absorption as it was limited by AC saturation and not by diffusion through the alginate matrix.

Table 5.1 compares the performance of the alginate-sorbent mesh with various other immobilization techniques used in literature. In all cases, the sorbent mesh absorbed more creatinine and uric acid per gram of AC, though a lower concentration was used. This may be in part due to toxin absorption into the alginate matrix, which was negligible for the other techniques. The overall performance was nevertheless inferior due to the significantly smaller AC loading achieved with the electrophoretic deposition. The results are nevertheless promising, and indicated that an increase in AC loading should be considered in future research. Although only Uric Acid was reduced to within the physiological concentrations during the experimental run, with the proper ratio of activated carbon to absorbed chemical it should be possible to achieve physiological concentrations throughout a large spectrum of chemicals. Although the final concentration of uric acid was below physiological concentration, it may be possible to pre-load activated carbon to levels just before saturation, reducing its absorbance.

5.5.2 Volumetric Porosity

Preliminary experiments showed that un-cross-linking gels deteriorated when exposed to mixing conditions. Cross-linking strengthened the gel and significantly reduced this effect. Exposing the gel to the lowly-saline solution (when compared to the cross-linking solution) caused the gels to swell which is not desirable, and must be taken into account when packaging the sorbent material.

Moreover, the deposition time should be altered to obtain a final porosity of 0.75 which is ideal for hydrodynamic and mass transfer considerations [91].

5.6 Conclusion

The sorbent performance of the mesh material was evaluated by exposing it to a blood toxin solution under mixing conditions. The urea, uric acid, creatinine and ammonia absorption was evaluated. Uric acid had the highest of absorption a 98.9 ± 1.1% absorption. Hard to remove middle molecules in the range of 1-50 kD should be evaluated in future works.

Further research is required to optimize the sorbent material. Altering the composition of the deposition solution, the mesh gauge and dimensions, electrophoretic deposition parameters, and post-deposition processes should be investigated for improving mesh performance. The volumetric porosity was found to be 0.51, which is lower than the optimal 0.75, implying that there is further research required to optimize the deposition time. Although the functionality of the material was shown under *in-vitro* conditions, the performance must be improved before *in-vivo* evaluation.

5.7 Acknowledgements

Thank you to Dr. Pavan M. V. Raja for his initial guidance on the project, as well as the other members of the Biomedical Technology and Cell Therapy Research Laboratory at McGill University for their valued input. The authors would also like to acknowledge the Canadian Institute of Health Research (CIHR) grant (MOP 93641) to Dr. S. Prakash, and for funding provided by NSERC.

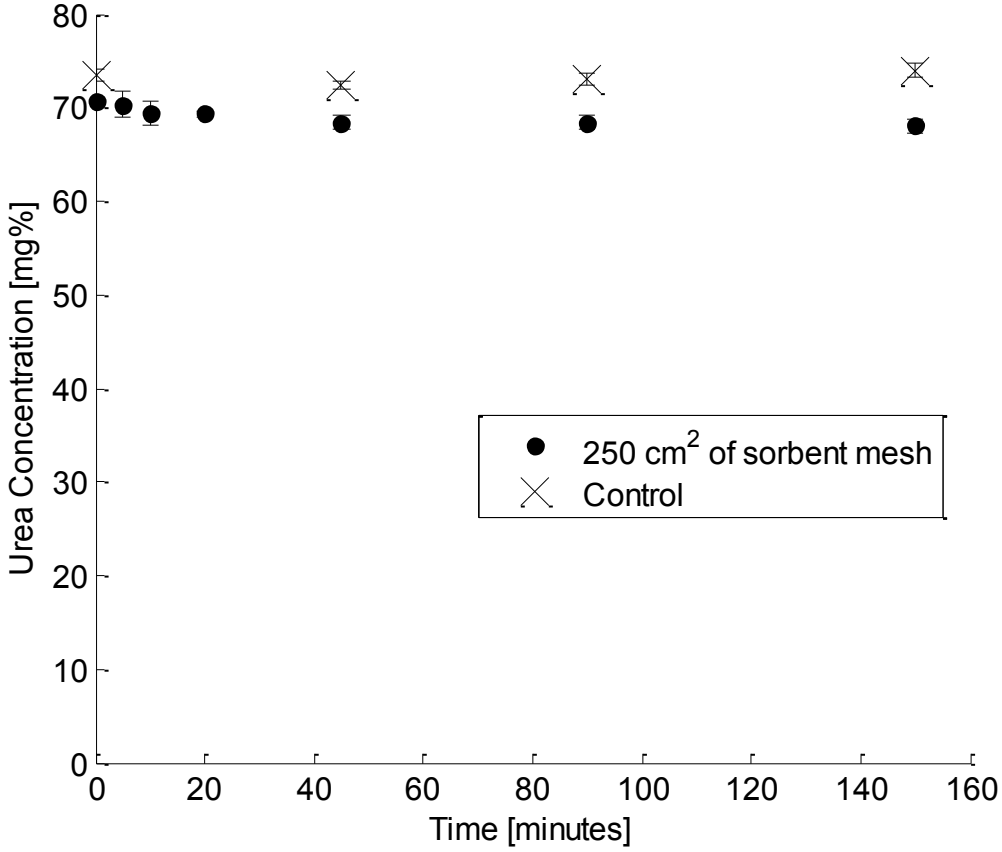

Figure 5.1 Urea Filtration Efficacy. A 200 mL volume of blood toxin solution was exposed to 250 cm^2 of sorbent mesh under mixing conditions. The solution initially had double physiological concentrations of blood toxins. The initial and final urea concentrations were 70.71 ± 0.34 mg% and 68.05 ± 0.69 mg% respectively. Error bars are in S.E.M., n = 3.

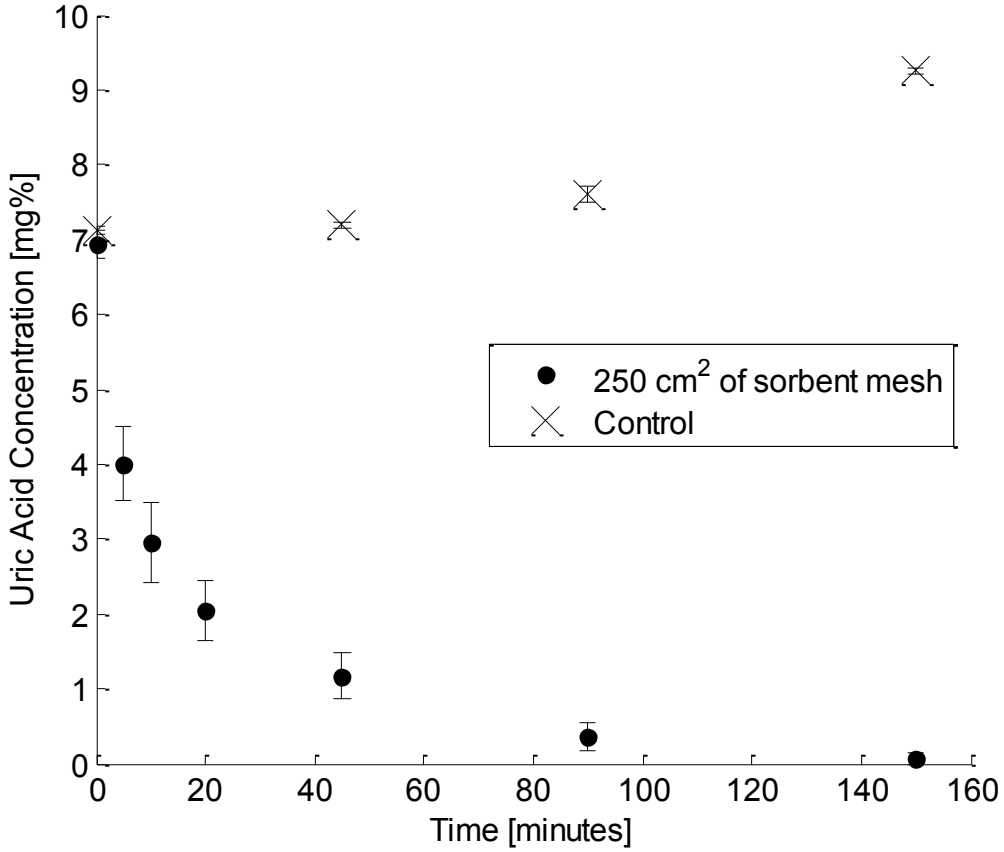

Figure 5.2 Uric Acid Filtration Efficacy. The uric acid concentration decreased steadily with time in the experimental group. The initial and final uric acid concentrations were 6.93 ± 0.19 mg% and 0.070 ± 0.076 mg% respectively. Error bars are in S.E.M., n = 3.

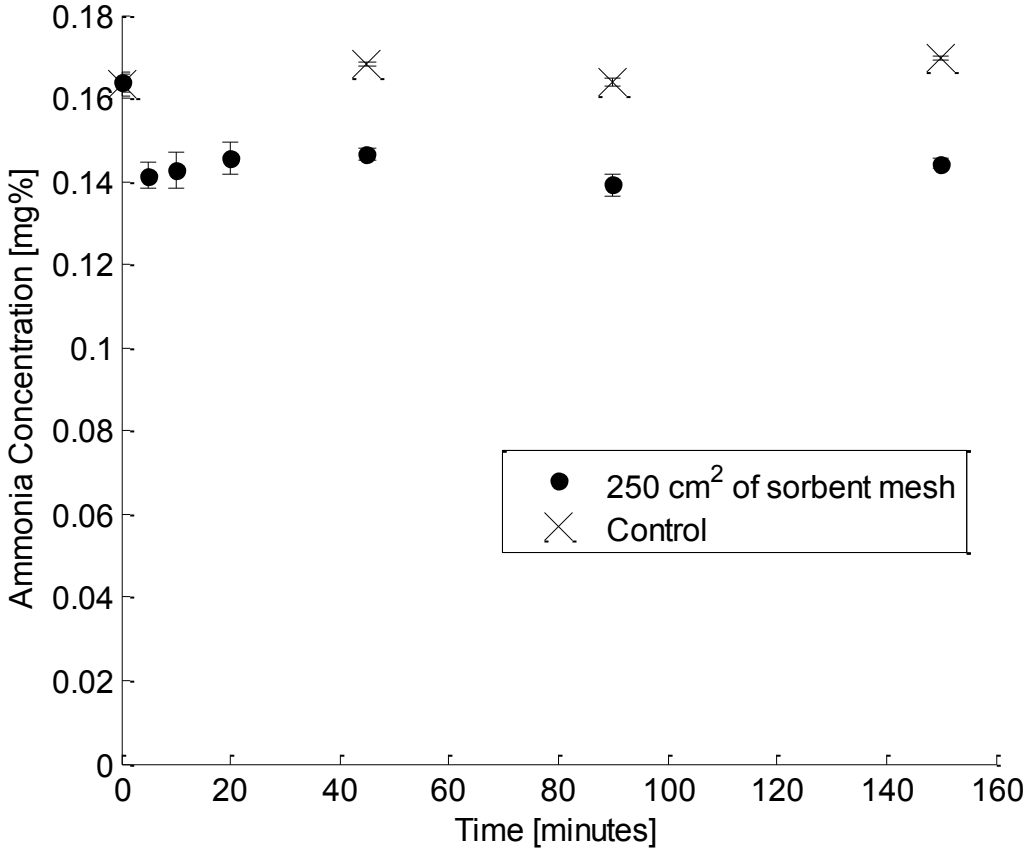

Figure 5.3 Ammonia Filtration Efficacy. The initial experimental concentration was 0.1640 ± 0.0023 mg% and dropped within the first 5 minutes to 0.1413 ± 03.0032 mg%. The final ammonia concentration was 0.1444 ± 0.0011 mg%. Error bars are in S.E.M., n = 3.

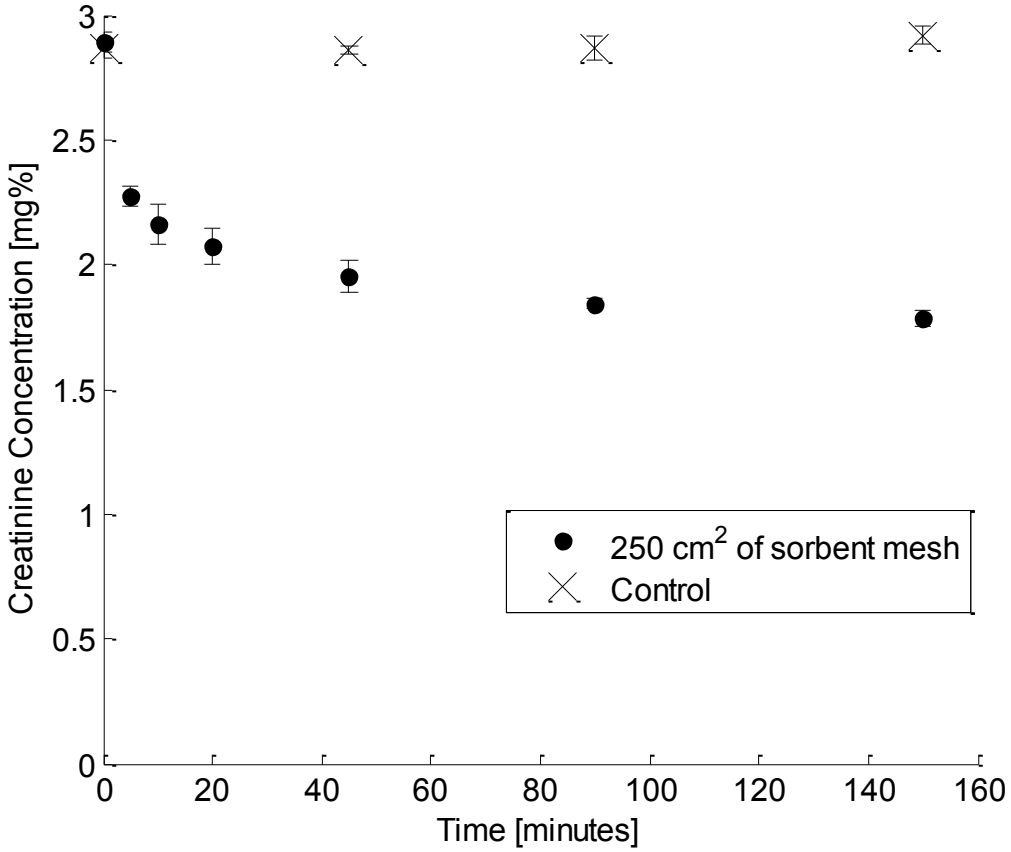

Figure 5.4 Creatinine Filtration Efficacy. Creatinine concentration decreased throughout the experiment, and the initial and final creatinine concentrations were 2.893 ± 0.038 mg% and 1.784 ± 0.031 mg% respectively. Error bars are in S.E.M., n = 3.

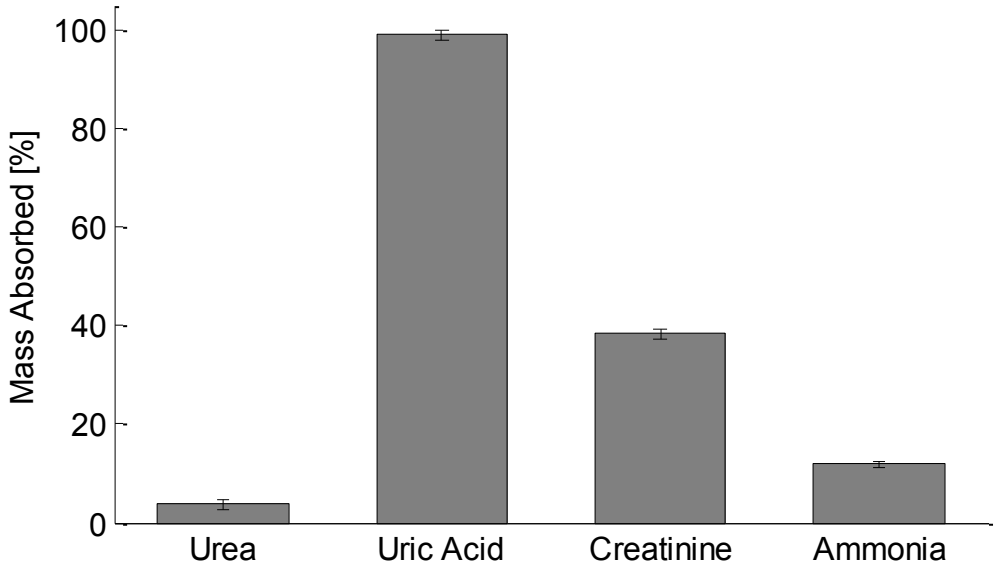

Figure 5.5 Percent of Toxin Mass Absorbed. The mass fraction of each toxin absorbed by the sorbent material after 150 minutes. Uric acid was absorbed the most with 98.9 ± 1.1 % and urea was absorbed the least with 3.7 ± 1.0. Error bars are in S.E.M., n = 3

Chemical	Concentration [mg %]			
	Initial	Final	Physiological [130]	Pathological
Urea	70.71 ± 0.34	68.04 ± 0.69	21-43	>43
Uric Acid	6.932 ± 0.188	0.070 ± 0.075	1.5-8.0	>8.0
Creatinine	2.892 ±0.038	1.784 ± 0.031	<1.5	>1.5
NH_3	0.1639 ± 0.0024	0.144 ± 0.001	0.010-0.080	>0.080

Table 5.1 Toxin Concentrations. Initial and final concentration of blood toxins in solution, physilogical concentration ranges, and pathological concentration ranges.

			Sorbent Mesh	ACCB [47]	PHEMA [48]	ACAC [46]
Run Time		[min]	150	360	120	120
Activated Carbon Loading		[% mass]	0.67	40	75	-
Creatinine	concentration tested	[mg%]	2.892	10	5	21
	absorbed per unit mass of carbon	[mg/g_{carbon}]	48.5	15	15	6.6
	absorbed per unit mass of gel	[mg/g_{gel}]	0.329	6	11.5	-
Uric Acid	concentration tested	[mg%]	6.932	10	9	11
	absorbed per unit mass of carbon	[mg/g_{carbon}]	303*	40	24	3*
	absorbed per unit mass of gel	[mg/g_{gel}]	2.0301*	16	18	-

Table 5.2 Comparative Creatinine and Uric Acid Absoprtion. The creatinine and uric acid absorption is compared for the sorbent mesh, chitosan matrix (ACCB) [47], activated charcoal encapsulated with polyhydroxy ethyl methacrylate (PHEMA) [48], and albumin-coated activated carbon [46]. A (*) indicates that the toxin was fully absorbed before the end of the experimental run. In all experiments, gels were placed in contact with toxin solutions. The experimental run time, toxin concentration, and the activated carbon loading is included for each when available.

Chapter 6 Summary of Observations

Viscosity grade was shown to affect alginate electrophoretic deposition characteristics and the resulting gel properties. An alginate grade was selected and a novel sorbent material was developed for use in dialysis. The material was characterized and evaluated *in-vitro*. The following observations were made:

1) Novel Electrophoretic Deposition Device

A novel electrophoretic deposition device was designed to quickly deposit hydrogels onto flat substrates for analysis. The device was able to hold approximately 2 L of deposition solution, and would effectively deposit hydrogels onto flat substrates whose dimensions did not exceed 10 cm x 10 cm. The electric field strength could easily be controlled by changing the position of the counter-electrodes relative to the substrate and by controlling the voltage produced by the voltage source.

2) Electrophoretic Deposition of Alginate

Low, medium and high viscosity grade alginates were deposited onto steel substrates. The deposition rates were modelled using the Sarkar equation for constant voltage-constant concentration conditions. Electrophoretic mobilities of 0.0610, 0.0584, 0.0909 cm^2/Vs and resistivity ratios of 21.0, 16.2 and 47.5 were found for the low, medium and high viscosity grade alginates respectively. Molecular weight was found using gel permeation chromatography and increased with

viscosity grade. Cross-linking the gels in 0.1 M $CaCl_2$ solution reduced the weight of the low viscosity grade gel by 49.1 ± 1.8% and the medium and high viscosity grade gels by 72.3 ± 1.2% (p-value = 0.508). Lyophilization was used to show that all three un-cross-linked gels had dry mass fractions of 2.85 ± 0.46% (p-values > 0.266). Cross-linking increased the dry mass-fraction of the low viscosity grade gel to 5.59 ± 0.07% and the medium and high viscosity grade gels to 7.07 ± 0.46% (p = 0.839). All dried gels had similar contact angles (p-values > 0.193) of 47.4 ± 1.1° except for the cross-linked high viscosity grade alginate with a contact angle of 37.2 ± 6.38°.

3) Development Of A Novel Sorbent Material

To produce a novel sorbent material, alginate and activated carbon were co-deposited onto a wire mesh using electrophoretic deposition. A 2.5 V/cm electric field was applied between a 20 gauge stainless steel wire mesh and two counter-electrodes in a 2% alginate – 1% activated carbon solution. A dark gel formed around the wires mesh and grew with time. Light microscopy was used to image the mesh holes and to relate holes size to deposition time. At 4 x magnification, the gel was clear with black specks which represented the activated carbon powder. Holes closed up after 70 seconds. Cross-linking was performed and increased the size of the holes in all cases except for once the holes were closed. Gel thickness was calculated from hole-open areas and decreased with cross-linking. Droplets were removed from the surface of the gels using compressed lab air. This was only performed following cross-linking as it would otherwise damage to gels. The mass-deposition rate was steady at 0.0336 g/s throughout the experimental run.

4) Activated Carbon Loading

Gels were dissolved in sodium citrate and the resulting solution was passed through filter paper. The change in mass of the dried filter paper correlated with a gel loading of 0.67% ± 0.0058%. Thermogravimetric analysis was also performed on activated carbon powder, alginate gel, and the sorbent alginate-activated carbon gel. The activated carbon peak was found at 670°C. Graphical analysis was used to show that activated carbon accounted for 0.84% of the mass. The mass fraction values found in both methods were similar, although the filtration method is considered more accurate than the graphical thermogravimetric analysis.

5) Scanning Electron Microscopy

Electrophoretic deposition was used to deposit alginate and alginate-activated carbon gels. Gels were cross-linked, and their surfaces were imaged using scanning electron microscopy. At 100 x magnification, activated carbon was seen clearly embedded along the surface of the alginate-activated carbon gel. The alginate gel pores were elongated and unidirectional with an average small-axis width of 32.9 ± 1.1 nm. The alginate-activated carbon gel had round pores with an average width of 15.6 ± 0.8 nm. Pore size histograms showed that alginate-activated carbon gels had a tighter pore size distribution than did the alginate gels alone.

6) Sorbent Performance

The performance of the novel sorbent material was evaluated *in-vitro*. A toxin solution was prepared and was left in contact with the material under mixing

conditions for 150 minutes. The urea concentration decreased by 3.7 ± 1.0% throughout the run. The uric acid concentration and creatinine concentration decreased steadily by 98.9 ± 1.1% and 38.3 ± 1.1% respectively. The ammonia concentration decreased within the first 5 minutes by 13.7 ± 2.2%, and remained steady throughout the rest of the run. Throughout the experiment, the gel mass increased by 8.7 ± 1.7 % due to swelling.

Chapter 7 General Discussion

Extracorporeal blood filtration (ECBF) includes hemodialysis and hemoperfusion and is widely used in treating liver failure, chronic renal disease, and blood poisoning. Activated carbon is commonly encapsulated in microspheres for this purpose, but encapsulation has many drawbacks. Single spheres have the smallest surface area to volume ratio of any geometry. This is overcome by using progressively smaller and smaller spheres, which vastly increases the surface area to volume ratio but at the expense of increasing the pressure drop in the passing fluid.

A radically different immobilization technique was developed in this thesis, and resulted in a stacked-wire mesh sorbent material. To the best knowledge of the author, this thesis marks the first time that such an approach has been taken to produce sorbent materials for ECBF. Dimensional analysis was carried out and indicated that further optimization is possible. The material was exposed to a toxin solution and the sorbent properties were evaluated, as is common for materials of this nature. Although single and multi-pass tests were not carried out, this thesis offers valuable insight into how the material is expected to perform under those conditions. A thorough literature review on stacked wire mesh in heat and mass exchangers was conducted to better understand the dimensional optimization of the material.

Results are discussed in light of the development of the novel material, with focus on material selection, design considerations, novel material geometric and physical parameters, and sorbent performance.

1) Effect of Viscosity Grade on Electrophoretic Deposition Characteristics of Alginate

Three different viscosity grades of alginate were deposited onto rectangular substrates using electrophoretic deposition (EPD). The electrophoretic mobilities were calculated to be 0.0610, 0.0584 and 0.0909 cm^2/Vs for the low, medium and high viscosity grade alginates respectively. The resistivity ratios between the deposited gels and the solution were 21.0, 16.2, and 47.5 respectively. This indicates that the low and medium viscosity grade alginates will deposit slower for short deposition times and faster for longer deposition times than the high viscosity grade alginate.

The viscosity grade affected the swelling properties of the gels following cross-linking. The dry alginate mass fractions and the change in mass following cross-linking indicated that the medium and high viscosity grade alginates underwent similar degrees of cross-linking.

2) Alginate Selection

A 20 gauge stainless steel mesh was used as a substrate for immobilizing the gel. The mesh opening side was 1.041 mm while the wire was 0.2286 mm in diameter. A tight control over the post-deposition hole size was desired, so the

medium viscosity grade alginate was selected. This allowed for a low deposition rate with a high degree of shrinking following cross-linking. Low viscosity grade alginate was also rejected as it was qualitatively observed to have a lower toughness than the other two gels.

3) Development of A Novel Sorbent Mesh Material

A 2% alginate – 1% activated carbon solution was deposited onto the steel wire mesh to create a novel sorbent material. A tight control over the deposit mass was obtained as it took 70 seconds for the mesh openings to completely fill. Longer depositions increase the total mass of AC available for toxin absorption, but inhibit mass transfer for single and multi-pass dialysis systems [90].

The deposited gel was thicker in the region near the edges of the mesh, but it was uniform around the centre. The edge of the mesh would be discarded in single and multi-pass dialysis due to the lack of uniformity. For industrial applications, a larger surface area of mesh should be used to reduce waste which increasing the uniformity of the final product. The mesh would then be cut into appropriate sizes.

4) Sorbent Gel Physical Properties

The activated carbon loading was found using a dissolution-filtration method and was 0.668% ± 0.006%. This is significantly smaller than encapsulation techniques [47, 48], and will need to be addressed in future works. It is clear that a significantly larger activated carbon-to-alginate ratio should be used in the deposition solution.

The pressure drop increases with the square of the open area ratio [91]. As a low pressure drop is desired when a fluid passes through the mesh, the open area ratio should be as large as possible. In this thesis, a large deposition was used to evaluate the sorbent properties of the material owing to the larger mass of activated carbon present on the mesh. If the activated carbon loading were increased, this may not be required. Mesh with thinner wires may also be used.

The addition of carbon to the deposited gel significantly reduced the average pore size (p-value < 0.001). Similar results were seen in the production of alginate-activated carbon microcapsules [126]. Pore sizes for alginate gels produced using EPD were a full order of magnitude larger than for alginate gels produced using a dissolution-microencapsulation technique. The larger pore sizes will result in an improved diffusion of toxins into the gels [89, 128], but the benefits will be limited due to the small carbon loading. Increasing the activated carbon loading may further reduce the pore sizes, which is not desired but may be necessary.

5) Sorbent Performance

Urea was poorly absorbed as commonly seen in AC based hemoperfusion devices [46]. The protein urease is generally used in addition to AC in order to break down urea [1, 3]. Although further research is required, proteins have already been co-deposited with alginate using EPD [88], so the method described in this paper may also be used for this purpose.

Although uric acid has a larger molecular weight and was more concentrated than creatinine, it was nevertheless found to absorb faster. Such results were expected when comparing the Langmuir adsorption isotherms for the two chemicals for carbon binding as reported in by Ash and is due to particle charge [3]. A higher gauge mesh would help remove creatinine, as it would expose the solution to a larger surface area over which toxins absorb. The increase in uric acid in the control solution was likely due to a slow dissolution rate.

Although uric acid was sufficiently absorbed, creatinine and ammonia were still present above physiological concentrations after 150 minutes. Ammonia was absorbed very quickly but saturated the AC within the first 5 minutes. Increasing the mass of AC should be used to increase creatinine and ammonia absorbance. This may be achieved by either using a higher concentration of AC in the deposition solution, or by using a larger surface area of sorbent mesh. Higher gauge meshes would not likely have a large impact on the ammonia absorption as it was limited by AC saturation and not by diffusion through the alginate matrix.

It is difficult to compare the sorbent performance between the sorbent mesh and encapsulated carbon technique as testing conditions are not standardized. It was nevertheless possible to compare the absorption of uric acid and creatinine against a chitosan coated activated carbon [47], polyhydroxy ethyl methacrylate activated carbon [48], and an albumin-coated activated carbon [46]. The standard unit of measurement for absorption is the mass of toxin absorbed per unit of mass of activated carbon, which typically increases with concentration of toxin. The sorbent

mesh outperformed the other immobilization techniques in this way. The carbon loading was nevertheless significantly smaller as well as the absorption per unit mass of material. This indicates that although the sorbent mesh is promising, future research must aim at increasing the carbon loading.

6) Volumetric Macro-Porosity

Un-cross-linked gels deteriorated in preliminary experiments when they were exposed to mixing conditions. Cross-linking strengthened the gel and significantly reduced this effect. Exposing the gel to the lowly-saline solution (when compared to the cross-linking solution) caused the gel to swell which is undesirable and must be taken into account when packaging the sorbent material.

The swollen-volumetric porosity of the gel was 0.51. Previous research indicated that heat and mass transfer is maximized at a porosity of 0.75 for stacked wire mesh [91]. The pressure drop in a fluid passing through a stacked wire mesh decreases with the square of the open area ratio of the material. Future efforts should therefore aim at increasing the porosity until it is between 0.75 and 1 depending on hydrodynamic and mass transfer criteria.

Chapter 8 General Conclusion

In this thesis, a novel electrophoretic deposition device was designed. The device was used to study the effects of viscosity grade on alginate deposition rates and the resulting gel characteristics which varied significantly. A sorbent material was developed for extracorporeal blood filtration applications by depositing an alginate-activated carbon solution onto a stainless steel wire mesh. The process was detailed and the material's performance was evaluated. From the above mentioned research it is possible to draw the following conclusions:

1) Viscosity grade affects alginate behaviour under electrophoretic deposition. The degree of cross-linking, swelling properties and contact angles were also affected in the resulting gel.

2) Cross-linking reduced the thickness of the alginate gel which increased the open-hole area of the mesh. Cross-linking improved the strength of the gel and significantly reduced the water fraction of the gel

3) Alginate-activated carbon gel pore sizes were significantly smaller than those of alginate gel alone. The pore size distribution was also narrower.

4) Using electrophoretic deposition, the activated carbon loading obtained from a 2% alginate – 1% activated carbon solution was 0.67% ± 0.0058%. Future efforts should aim at improving the carbon loading of the gel.

5) The novel sorbent material developed in this thesis absorbed creatinine, ammonia and uric acid in significant quantities, however the sorbent performance is still not on par with current materials and further optimization is still required.

8.1 Recommendations and Future Works

As this thesis was primarily a proof-of-concept, there are still many research questions to be answered and a large potential for improvement. The thesis showed that the novel sorbent material is functional, but is not yet viable. The following is recommended:

1) The effect of the electric field strength and cross-liking agent on the resulting gel properties should be evaluated, as well as the effects of varying the concentration of alginate powder and carbon powder in the deposition solution. Although increasing the relative concentration of carbon is expected to increase carbon loading, this is expected to plateau given high enough concentrations. As it is time consuming to suspend activated carbon in the alginate solution, it is important to find the plateau-concentration for industrial applications. The effects of the above on the mechanical properties of the gel should also be evaluated to ensure mechanical stability which is important for both clinical use and for transportation purposes.

2) The deposition time should be optimized to produce a stacked wire mesh material with the optimal porosity of 0.75. The effects of porosity on sorption

and hydrodynamic performance, although well discussed in literature for mass-transfer and hydrodynamic considerations, should be evaluated for the sorbent mesh. The use of smaller mesh gauges could vastly increase the specific surface area of the material. Nevertheless, preliminary experiments using a 50 gauge mesh showed that decreasing the size of the mesh was difficult owing to the clogging of the holes. Moreover, the thickness of the gel was too small to provide sufficient mechanical strength for the system. With proper optimization, however, it may be possible to overcome these challenges.

3) Sterilization must be evaluated for proper clinical testing to take place. The sorbent performance of the material should be evaluated using larger sized blood toxins, as they are not absorbed using current hemodialysis techniques, and the benefits are widely discussed in literature.

4) The method used to produce the novel sorbent material is versatile, and should be tested with other immobilizing hydrogels such as chitosan. Moreover, the electrophoretic deposition of hydrogels onto wire mesh substrates can be used to produce materials for a number of applications other than dialysis. Carbon-loaded gels could be used for water purification. Cells and proteins could easily be deposited to produce functional materials for recirculating bio-reactors when used in a stacked configuration, or for biosensors when used as a single mesh. Multi-layered depositions could be

used to produce complex devices such as high-surface-area glucose bio-fuel cells. A biodegradable mesh could be used as a tissue engineering scaffold that would facilitate the use of electric current to help induce cellular proliferation.

Bibliography

1. Agar, J.W.M., *Review: Understanding sorbent dialysis systems.* Nephrology, 2010. **15**(4): p. 406-411.

2. Nissenson, A.R., C. Ronco, G. Pergamit, M. Edelstein, and R. Watts, *Continuously functioning artificial nephron system: the promise of nanotechnology.* Hemodialysis international. International Symposium on Home Hemodialysis, 2005. **9**(3): p. 210-7.

3. Ash, S.R., *Sorbents in treatment of uremia: a short history and a great future.* Seminars in Dialysis, 2009. **22**(6): p. 615-622.

4. Ash, S.R., *Approaches to Quotidian Dialysis: The Allient Dialysis System.* Seminars in Dialysis, 2004. **17**(2): p. 164-166.

5. Davenport, A., V. Gura, C. Ronco, M. Beizai, C. Ezon, et al., *A wearable haemodialysis device for patients with end-stage renal failure: a pilot study.* The Lancet. **370**(9604): p. 2005-2010.

6. Wittebole, X. and P. Hantson, *Use of the molecular adsorbent recirculating system (MARS (TM)) for the management of acute poisoning with or without liver failure.* Clinical Toxicology, 2011. **49**(9): p. 782-793.

7. Ronco, C., A. Davenport, and V. Gura, *The future of the artificial kidney: moving towards wearable and miniaturized devices.* Nefrologia, 2011. **31**(1): p. 9-16.

8. Winchester, J.F., *Dialysis and hemoperfusion in poisoning.* Advances in renal replacement therapy, 2002. **9**(1): p. 26-30.

9. Holubek, W.J., R.S. Hoffman, D.S. Goldfarb, and L.S. Nelson, *Use of hemodialysis and hemoperfusion in poisoned patients.* Kidney International, 2008. **74**(10): p. 1327-1334.

10. Winchester, J.F. and C. Ronco, *Sorbent augmented hemodialysis systems: are we there yet?* Journal of the American Society of Nephrology, 2010. **21**(2): p. 209-211.

11. Twardowski, Z.J., *History of hemodialyzers' designs.* Hemodialysis International, 2008. **12**(2): p. 173-210.

12. Winchester, J.F., J. Silberzweig, C. Ronco, V. Kuntsevich, D. Levine, et al., *Sorbents in acute renal failure and end-stage renal disease: Middle molecule and cytokine removal.* Blood Purification, 2004. **22**(1): p. 73-77.

13. F.J. Winchester, C.R., J. Salsberg, E. Yousha, J.A. Brady, L.D. Cowgill, M. Choquette, R. Albright, J. CLemmer, V. Davankov, M. Tsyurupa, L. Pavlova, M. Pavlov, G. Cohen, W. Horl, F. Gotch, N.W. Levin, *Sorbent Augmented Dialysis Systems.* Hemodialysis Technology, 2002. **137**: p. 170-180.

14. Thomas M.S. Chang, J.F.C., Paul Barré, Andrew Gonda, John H. Dirks, Mortimer Levy, and Colin Lister, *Microcapsule artificial kidney: treatment of patients with acute drug intoxication.* Canadian Medical Association Journal, 1973. **108**(4): p. 429-433.

15. Chang, T.M.S., *A Comparison of Semipermeable Microcapsules and Standard Dialysers for Use in Separation.* Separation & Purification Reviews, 1974. **3**(2): p. 245-262.

16. Levine, S.N. and W.C. LaCourse, *Materials and design consideration for a compact artificial kidney.* Journal of Biomedical Materials Research, 1967. **1**(2): p. 275-284.

17. Tyagi, P.K., J.F. Winchester, and D.A. Feinfeld, *Extracorporeal removal of toxins.* Kidney International, 2008. **74**(10): p. 1231-1233.

18. Roberts, M., *The regenerative dialysis (REDY) sorbent system.* Nephrology, 1998. **4**(4): p. 275-278.

19. Walter F. Baron, E.L.B., *Medical Physiology: A Cellular and Molecular Appreach*2004: Elsevier/Saunders.

20. Costanzo, L.S., *Physiology*2010, Philadelphia, PA: Saunders/Elsevier.

21. Eric P. Widmaier, H.R., Kevin T. Strang, *Human Physiology - The Mechanisms of Body Function*, ed. t. Edition2006, New York, NY: McGraw Hill.

22. Levin, A., B. Hemmelgarn, B. Culleton, S. Tobe, P. McFarlane, et al., *Guidelines for the management of chronic kidney disease.* Canadian Medical Association Journal, 2008. **179**(11): p. 1154-1162.

23. System, R.D., *2011 ADR Reference Tables: Economic Costs of ESRD*, k_econ_11.xls, Editor 2010, National Institute of Diabetes and Digestive and Kidney Diseases: Minneapolis.

24. Star, R.A., *Treatment of acute renal failure.* Kidney International, 1998. **54**(6): p. 1817-1831.

25. Sleisenger, *Acute Liver Failure*, in *Sleisenger & Fordtran's gastrointestinal and liver disease pathophysiology, diagnosis, management* L.S.F. Mark Feldman, Lawrence J. Brandt, Editor 2009, W B Saunders Co: St. Louis, Missouri.

26. Foundation, C.L. *Liver Diseases Myths*. 2011 [cited 2012 12/01/2012]; Available from: http://www.liver.ca/liver-disease/myths.aspx.

27. Prevention, C.f.D.C.a., *Number of first-listed diagnoses for discharges from short-stay hospitals, by ICD-9-CM code, sex, age, and geographic region: United States, 2009*, 2009det10_numberfirstdiagnoses.pdf, Editor 2009.

28. Pascher, A., I.M. Sauer, C. Hammer, J.C. Gerlach, and P. Neuhaus, *Extracorporeal liver perfusion as hepatic assist in acute liver failure: a review of world experience.* Xenotransplantation, 2002. **9**(5): p. 309-324.

29. Nakano, H., K. Boudjema, E. Alexandre, P. Imbs, M.P. Chenard, et al., *Protective effects of N-acetylcysteine on hypothermic ischemia-reperfusion injury of rat liver.* Hepatology, 1995. **22**(2): p. 539-545.

30. Rank, N., C. Michel, C. Haertel, C. Med, A. Lenhart, et al., *N-acetylcysteine increases liver blood flow and improves liver function in septic shock patients: Results of a prospective, randomized, double-blind study.* Critical Care Medicine, 2000. **28**(12): p. 3799-3807.

31. Lagasse, E., H. Connors, M. Al-Dhalimy, M. Reitsma, M. Dohse, et al., *Purified hematopoietic stem cells can differentiate into hepatocytes in vivo.* Nature Medicine, 2000. **6**(11): p. 1229-1234.

32. Vassilopoulos, G., P.R. Wang, and D.W. Russell, *Transplanted bone marrow regenerates liver by cell fusion.* Nature, 2003. **422**(6934): p. 901-904.

33. Fausto, N., *Liver regeneration.* Journal of Hepatology, 2000. **32**: p. 19-31.

34. Lee, W.M., R.M. Galbraith, G.H. Watt, R.D. Hughes, D.D. McIntire, et al., *Predicting survival in fulminant hepatic failure using serum gc protein concentrations.* Hepatology, 1995. **21**(1): p. 101-105.

35. George, J., *Artificial liver support systems.* The Journal of the Association of Physicians of India, 2004. **52**: p. 719-22.

36. Raja, R.M., M.S. Kramer, and J.L. Rosenbaum, *Recirculation peritoneal dialysis with sorbent redy cartridge.* Nephron, 1976. **16**(2): p. 134-142.

37. Ofsthun, N.J. and A.K. Stennett, *An Integrated Membrane/Sorbent PD Approach to a Wearable Artificial Kidney*, O. Dössel and W.C. Schlegel, Editors. 2009, Springer Berlin Heidelberg. p. 729-732.

38. Malik, D.J., G.L. Warwick, M. Venturi, M. Streat, K. Hellgardt, et al., *Preparation of novel mesoporous carbons for the adsorption of an inflammatory cytokine (IL-1β).* Biomaterials, 2004. **25**(15): p. 2933-2940.

39. Collins, A.J., *Cardiovascular mortality in end-stage renal disease.* The American Journal of the Medical Sciences, 2003. **325**(4): p. 163-167.

40. Freemont, A.J., *Imaging in the dialysis patient: the pathology of dialysis.* Seminars in Dialysis, 2002. **15**(4): p. 227-231.

41. Tomson, C., *Vascular calcification in chronic renal failure.* Nephron Clinical Practice, 2003. **93**(4): p. C124-C130.

42. Leypoldt, J.K., A.K. Cheung, C.E. Carroll, D.C. Stannard, B.J.G. Pereira, et al., *Effect of dialysis membranes and middle molecule removal on chronic hemodialysis patient survival.* American Journal of Kidney Diseases, 1999. **33**(2): p. 349-355.

43. Davankov, V., L. Pavlova, M. Tsyurupa, J. Brady, M. Balsamo, et al., *Polymeric adsorbent for removing toxic proteins from blood of patients with kidney failure.* Journal of Chromatography B: Biomedical Sciences and Applications, 2000. **739**(1): p. 73-80.

44. Ronco, C., A. Brendolan, J.F. Winchester, E. Golds, J. Clemmer, et al., *First clinical experience with an adjunctive hemoperfusion device designed specifically to remove β₂-microglobulin in hemodialysis.* Blood Purification, 001. **19**(2): p. 260-263.

45. Vanholder, R., R. De Smet, G. Glorieux, A. Argiles, U. Baurmeister, et al., *Review on uremic toxins: Classification, concentration, and interindividual variability.* Kidney International, 2003. **63**(5): p. 1934-1943.

46. Chang, T.M. and N. Malave, *The development and first clinical use of semipermeable microcapsules (artificial cells) as a compact artificial kidney. 1970.* Therapeutic Apheresis and Dialysis, 2000. **4**(2): p. 108-16.

47. Chandy, T. and C.P. Sharma, *Preparation and performance of chitosan encapsulated activated charcoal (ACCB) adsorbents for small molecules.* Journal of Microencapsulation, 1993. **10**(4): p. 475-486.

48. Lee, C.-J. and S.-T. Hsu, *Preparation of spherical encapsulation of activated carbons and their adsorption capacity of typical uremic toxins.* Journal of Biomedical Materials Research, 1990. **24**(2): p. 243-258.

49. Besra, L. and M. Liu, *A review on fundamentals and applications of electrophoretic deposition (EPD).* Progress in Materials Science, 2007. **52**(1): p. 1-61.

50. Hamaker, H.C., *Formation of a deposit by electrophoresis.* Transactions of the Faraday Society, 1940. **35**: p. 279-287.

51. Corni, I., M.P. Ryan, and A.R. Boccaccini, *Electrophoretic deposition: From traditional ceramics to nanotechnology.* Journal of the European Ceramic Society, 2008. **28**(7): p. 1353-1367.

52. Hamaker, H.C. and E.J.W. Verwey, *(C) Colloid stability. The role of the forces between the particles in electrodeposition and other phenomena.* Transactions of the Faraday Society, 1940. **35**(3): p. 0180-0185.

53. Grillon, F., D. Fayeulle, and M. Jeandin, *Quantitative image-analysis of electrophoretic coatings.* Journal of Materials Science Letters, 1992. **11**(5): p. 272-275.

54. Sarkar, P. and P.S. Nicholson, *Electrophoretic deposition (EPD): Mechanisms, kinetics, and application to ceramics.* Journal of the American Ceramic Society, 1996. **79**(8): p. 1987-2002.

55. Van der Biest, O.O. and L.J. Vandeperre, *Electrophoretic deposition of materials.* Annual Review of Materials Science, 1999. **29**: p. 327-352.

56. Boccaccini, A.R. and I. Zhitomirsky, *Application of electrophoretic and electrolytic deposition techniques in ceramics processing.* Current Opinion in Solid State & Materials Science, 2002. **6**(3): p. 251-260.

57. Besra, L., S.W. Zha, and M.L. Liu, *Preparation of NiO-YSZ/YSZ bi-layers for solid oxide fuel cells by electrophoretic deposition.* Journal of Power Sources, 2006. **160**(1): p. 207-214.

58. Ducheyne, P., W. Vanraemdonck, J.C. Heughebaert, and M. Heughebaert, *Structural-analysis of hydroxyapatite coatings on titanium.* Biomaterials, 1986. **7**(2): p. 97-103.

59. Zhitomirsky, I. and L. GalOr, *Electrophoretic deposition of hydroxyapatite.* Journal of Materials Science-Materials in Medicine, 1997. **8**(4): p. 213-219.

60. Roether, J.A., A.R. Boccaccini, L.L. Hench, V. Maquet, S. Gautier, et al., *Development and in vitro characterisation of novel bioresorbable and bioactive composite materials based on polylactide foams and Bioglass (R) for tissue engineering applications.* Biomaterials, 2002. **23**(18): p. 3871-3878.

61. Fritsche, A., M. Haenle, C. Zietz, W. Mittelmeier, H.-G. Neumann, et al., *Mechanical characterization of anti-infectious, anti-allergic, and bioactive coatings on orthopedic implant surfaces.* Journal of Materials Science, 2009. **44**(20): p. 5544-5551.

62. Boccaccini, A.R., S. Keim, R. Ma, Y. Li, and I. Zhitomirsky, *Electrophoretic deposition of biomaterials.* Journal of the Royal Society Interface, 2010. **7**: p. S581-S613.

63. Du, H., S. Kondu, and H.F. Ji, *Formation of ultrathin hydrogel films on microcantilever devices using electrophoretic deposition.* Micro & Nano Letters, IET, 2008. **3**(1): p. 12-17.

64. Jiang, T., Z. Zhang, Y. Zhou, Y. Liu, Z. Wang, et al., *Surface Functionalization of Titanium with Chitosan/Gelatin via Electrophoretic Deposition: Characterization and Cell Behavior.* Biomacromolecules, 2010. **11**(5): p. 1254-1260.

65. Zhang, Z., Y. Huang, and Z. Jiang, *Electrophoretic deposition forming of SiC-TZP composites in a nonaqueous sol media.* Journal of the American Ceramic Society, 1994. **77**(7): p. 1946-1949.

66. Prabhakaran, M.P., J. Venugopal, D. Kai, and S. Ramakrishna, *Biomimetic material strategies for cardiac tissue engineering.* Materials Science & Engineering C-Materials for Biological Applications, 2011. **31**(3): p. 503-513.

67. Feng, Q.L., R.W. Tan, Z.D. She, M.B. Wang, H. Jin, et al., *In vitro and in vivo degradation of an injectable bone repair composite.* Polymer Degradation and Stability, 2010. **95**(9): p. 1736-1742.

68. Choi, N.W., M. Cabodi, B. Held, J.P. Gleghorn, L.J. Bonassar, et al., *Microfluidic scaffolds for tissue engineering.* Nat Mater, 2007. **6**(11): p. 908-915.

69. Hunt, N.C., R.M. Shelton, and L. Grover, *An alginate hydrogel matrix for the localised delivery of a fibroblast/keratinocyte co-culture.* Biotechnology Journal, 2009. **4**(5): p. 730-737.

70. Li, L., A.E. Davidovich, J.M. Schloss, U. Chippada, R.R. Schloss, et al., *Neural lineage differentiation of embryonic stem cells within alginate microbeads.* Biomaterials, 2011. **32**(20): p. 4489-4497.

71. Leor, J., N. Landa, L. Miller, M.S. Feinberg, R. Holbova, et al., *Effect of injectable alginate implant on cardiac remodeling and function after recent and old infarcts in rat.* Circulation, 2008. **117**(11): p. 1388-1396.

72. Hernandez, R.M., G. Orive, A. Murua, and J.L. Pedraz, *Microcapsules and microcarriers for in situ cell delivery.* Advanced Drug Delivery Reviews, 2010. **62**(7-8): p. 711-730.

73. Becker, T.A., D.R. Kipke, and T. Brandon, *Calcium alginate gel: A biocompatible and mechanically stable polymer for endovascular embolization.* Journal of Biomedical Materials Research, 2001. **54**(1): p. 76-86.

74. Zimmermann, U., B. Manz, M. Hillgartner, H. Zimmermann, D. Zimmermann, et al., *Cross-linking properties of alginate gels determined by using advanced NMR imaging and Cu2+ as contrast agent.* European Biophysics Journal with Biophysics Letters, 2004. **33**(1): p. 50-58.

75. Machida-Sano, I., Y. Matsuda, and H. Namiki, *In vitro adhesion of human dermal fibroblasts on iron cross-linked alginate films.* Biomedical Materials, 2009. **4**(2).

76. Martinsen, A., G. Skjakbraek, and O. Smidsrod, *Alginate as Immobilization Material .1. Correlation between Chemical and Physical-Properties of Alginate Gel Beads.* Biotechnology and Bioengineering, 1989. **33**(1): p. 79-89.

77. Schneider, S., P.J. Feilen, O. Kraus, T. Haase, T.A. Sagban, et al., *Biocompatibility of Alginates for Grafting: Impact of Alginate Molecular Weight.* Artificial Cells, Blood Substitutes and Biotechnology, 2003. **31**(4): p. 383-394.

78. Sperger, D.M., S. Fu, L.H. Block, and E.J. Munson, *Analysis of composition, molecular weight, and water content variations in sodium alginate using solid-state NMR spectroscopy.* Journal of Pharmaceutical Sciences, 2011. **100**(8): p. 3441-52.

79. Imai, T., C. Kawasaki, T. Nishiyama, and M. Otagiri, *Comparison of the pharmaceutical properties of sustained-release gel beads prepared by alginate having different molecular size with commercial sustained-release tablet.* Pharmazie, 2000. **55**(3): p. 218-222.

80. Efentakis, M. and A. Koutlis, *Release of Furosemide from Multiple-Unit and Single-Unit Preparations Containing Different Viscosity Grades of Sodium Alginate.* Pharmaceutical Development and Technology, 2001. **6**(1): p. 91-98.

81. Efentakis, M. and G. Buckton, *The effect of erosion and swelling on the dissolution of theophylline from low and high viscosity sodium alginate matrices.* Pharmaceutical Development & Technology, 2002. **7**(1): p. 69-77.

82. Yokoyama, F., T. Fujino, K. Kimura, Y. Yamashita, K. Nagata, et al., *Formation of optically anisotropic alginic acid gels under DC electric fields.* European Polymer Journal, 1998. **34**(2): p. 229-234.

83. Shi, X.W., C.Y. Tsao, X.H. Yang, Y. Liu, P. Dykstra, et al., *Electroaddressing of cell populations by co-deposition with calcium alginate hydrogels.* Advanced Functional Materials, 2009. **19**(13): p. 2074-2080.

84. Cheong, M. and I. Zhitomirsky, *Electrodeposition of alginic acid and composite films.* Colloids and Surfaces a-Physicochemical and Engineering Aspects, 2008. **328**(1-3): p. 73-78.

85. Grandfield, K., F. Sun, M. FitzPatrick, M. Cheong, and I. Zhitomirsky, *Electrophoretic deposition of polymer-carbon nanotube-hydroxyapatite composites.* Surface & Coatings Technology, 2009. **203**(10-11): p. 1481-1487.

86. White, A.A., S.M. Best, and I.A. Kinloch, *Hydroxyapatite-carbon nanotube composites for biomedical applications: A review.* International Journal of Applied Ceramic Technology, 2007. **4**(1): p. 1-13.

87. Lam, C.W., J.T. James, R. McCluskey, S. Arepalli, and R.L. Hunter, *A review of carbon nanotube toxicity and assessment of potential occupational and environmental health risks.* Critical Reviews in Toxicology, 2006. **36**(3): p. 189-217.

88. Liu, C.H., X.L. Guo, H.T. Cui, and R. Yuan, *An amperometric biosensor fabricated from electro-co-deposition of sodium alginate and horseradish peroxidase.* Journal of Molecular Catalysis B-Enzymatic, 2009. **60**(3-4): p. 151-156.

89. Dyga, R. and M. Placzek, *Efficiency of heat transfer in heat exchangers with wire mesh packing.* International Journal of Heat and Mass Transfer, 2010. **53**(23-24): p. 5499-5508.

90. Xu, J., J. Tian, T.J. Lu, and H.P. Hodson, *On the thermal performance of wire-screen meshes as heat exchanger material.* International Journal of Heat and Mass Transfer, 2007. **50**(5-6): p. 1141-1154.

91. Tian, J., T. Kim, T.J. Lu, H.P. Hodson, D.T. Queheillalt, et al., *The effects of topology upon fluid-flow and heat-transfer within cellular copper structures.* International Journal of Heat and Mass Transfer, 2004. **47**(14-16): p. 3171-3186.

92. Yang, K.S., Z. Jiang, and J. Shik Chung, *Electrophoretically Al-coated wire mesh and its application for catalytic oxidation of 1,2-dichlorobenzene.* Surface and Coatings Technology, 2003. **168**(2): p. 103-110.

93. Satterfield, C.N., *Heterogeneous catalysis in industrial practice*1996: Krieger Pub.

94. Vorob'eva, M.P., A.A. Greish, A.V. Ivanov, and L.M. Kustov, *Preparation of catalyst carriers on the basis of alumina supported on metallic gauzes.* Applied Catalysis A: General, 2000. **199**(2): p. 257-261.

95. Yao, J., J.S. Choi, K.S. Yang, D.Z. Sun, and J.S. Chung, *Wire-mesh honeycomb catalysts for selective catalytic reduction of NO with NH3.* Korean Journal of Chemical Engineering, 2006. **23**(6): p. 888-895.

96. Zhai, X., Z. Chen, J. Yao, H. Wang, and J. Li, *Preparation, characterization and kinetics of V(2)O(5)-MoO(3)/TiO(2)/Al(2)O(3) catalyst on wire-mesh honeycomb for the selective catalytic reduction of NO with NH(3)*. 2009 International Conference on Energy and Environment Technology, Vol 3, Proceedings2009. 469-472.

97. Yang, K.S., G. Mul, J.S. Choi, J.A. Moulijn, and J.S. Chung, *Development of TiO2/Ti wire-mesh honeycomb for catalytic combustion of ethyl acetate in air.* Applied Catalysis A: General, 2006. **313**(1): p. 86-93.

98. Yang, K.S., G. Mul, and J.A. Moulijn, *Electrochemical generation of hydrogen peroxide using surface area-enhanced Ti-mesh electrodes.* Electrochimica Acta, 2007. **52**(22): p. 6304-6309.

99. Yanagida, S., A. Nakajima, Y. Kameshima, N. Yoshida, T. Watanabe, et al., *Preparation of a crack-free rough titania coating on stainless steel mesh by electrophoretic deposition.* Materials Research Bulletin, 2005. **40**(8): p. 1335-1344.

100. Kołodziej, A., M. Jaroszyński, B. Janus, T. Kleszcz, J. Łojewska, et al., *An experimental study of the pressure drop in fluid flows through wire gauzes.* Chemical Engineering Communications, 2009. **196**(8): p. 932-949.

101. Azizi, F. and A.M. Al Taweel, *Hydrodynamics of liquid flow through screens and screen-type static mixers.* Chemical Engineering Communications, 2011. **198**(5): p. 726-742.

102. Duprat, F. and G. Lopez Lopez, *Comparison of performance of heat regenerators: Relation between heat transfer efficiency and pressure drop.* International Journal of Energy Research, 2001. **25**(4): p. 319-329.

103. Kołodziej, A. and J. Łojewska, *Mass transfer for woven and knitted wire gauze substrates: Experiments and modelling.* Catalysis Today, 2009. **147, Supplement**(0): p. S120-S124.

104. Ma, R., X. Pang, and I. Zhitomirsky, *Electrodeposition of biopolymer films containing haemoglobin.* Surface Engineering, 2011. **27**(9): p. 693-697.

105. Ma, R. and I. Zhitomirsky, *Electrophoretic deposition of chitosan-albumin and alginate-albumin films.* Surface Engineering, 2011. **27**(1): p. 51-56.

106. Van der Biest, O., L. Vandeperre, S. Put, G. Anne, and J. Vleugels, *Laminated and functionally graded ceramics by electrophoretic deposition*, in *Layered, Functional Gradient Ceramics, and Thermal Barrier Coatings: Design, Fabrication and Applications*, M.J.E.H.P. Anglada, Editor 2007. p. 49-58.

107. Bai, Y., K.A. Kim, I.S. Park, S.J. Lee, T.S. Bae, et al., *In situ composite coating of titania-hydroxyapatite on titanium substrate by micro-arc oxidation coupled with electrophoretic deposition processing.* Materials Science and Engineering B-Advanced Functional Solid-State Materials, 2011. **176**(15): p. 1213-1221.

108. Cho, J., S. Schaab, J. Roether, and A. Boccaccini, *Nanostructured carbon nanotube/TiO₂ composite coatings using electrophoretic deposition (EPD).* Journal of Nanoparticle Research, 2008. **10**(1): p. 99-105.

109. Sarkar, P., X. Huang, and P.S. Nicholson, *Zirconia/alumina functionally gradiented composites by electrophoretic deposition techniques.* Journal of the American Ceramic Society, 1993. **76**(4): p. 1055-1056.

110. Draget, K.I., G. Skjåk Bræk, and O. Smidsrød, *Alginic acid gels: the effect of alginate chemical composition and molecular weight.* Carbohydrate Polymers, 1994. **25**(1): p. 31-38.

111. Mancini, F., L. Montanari, D. Peressini, and P. Fantozzi, *Influence of Alginate Concentration and Molecular Weight on Functional Properties of Mayonnaise.* LWT - Food Science and Technology, 2002. **35**(6): p. 517-525.

112. Morris, E.R., A.N. Cutler, S.B. Ross-Murphy, D.A. Rees, and J. Price, *Concentration and shear rate dependence of viscosity in random coil polysaccharide solutions.* Carbohydrate Polymers, 1981. **1**(1): p. 5-21.

113. Vold, I.M.N., K.A. Kristiansen, and B.E. Christensen, *A Study of the chain stiffness and extension of alginates, in vitro epimerized alginates, and periodate-oxidized alginates using size-exclusion chromatography combined with light scattering and viscosity detectors.* Biomacromolecules, 2006. **7**(7): p. 2136-2146.

114. Simchi, A., F. Pishbin, and A.R. Boccaccini, *Electrophoretic deposition of chitosan.* Materials Letters, 2009. **63**(26): p. 2253-2256.

115. Efentakis, M. and G. Buckton, *The Effect of Erosion and Swelling on the Dissolution of Theophylline from Low and High Viscosity Sodium Alginate Matrices.* Pharmaceutical Development and Technology, 2002. **7**(1): p. 69-77.

116. Polk, A., B. Amsden, K. De Yao, T. Peng, and M.F.A. Goosen, *Controlled release of albumin from chitosan—alginate microcapsules.* Journal of Pharmaceutical Sciences, 1994. **83**(2): p. 178-185.

117. ACARTURK, S.T., F., *Calcium alginate microparticles for oral administration: I: effect of sodium alginate type on drug release and drug entrapment efficiency.* Journal of Microencapsulation, 1999. **16**(3): p. 275-290.

118. Webb, K., V. Hlady, and P.A. Tresco, *Relative importance of surface wettability and charged functional groups on NIH 3T3 fibroblast attachment, spreading, and cytoskeletal organization.* Journal of Biomedical Materials Research, 1998. **41**(3): p. 422-430.

119. Steele, J.G., C. McFarland, B.A. Dalton, G. Johnson, M.D.M. Evans, et al., *Attachment of human bone cells to tissue culture polystyrene and to unmodified polystyrene: the effect of surface chemistry upon initial cell attachment.* Journal of Biomaterials Science, Polymer Edition, 1994. **5**(3): p. 245-257.

120. Iuliano, D.J., S.S. Saavedra, and G.A. Truskey, *Effect of the conformation and orientation of adsorbed fibronectin on endothelial cell spreading and the strength of adhesion.* Journal of Biomedical Materials Research, 1993. **27**(8): p. 1103-1113.

121. Grinnell, F. and M.K. Feld, *Adsorption characteristics of plasma fibronectin in relationship to biological activity.* Journal of Biomedical Materials Research, 1981. **15**(3): p. 363-381.

122. Bae, J.-S., E.-J. Seo, and I.-K. Kang, *Synthesis and characterization of heparinized polyurethanes using plasma glow discharge.* Biomaterials, 1999. **20**(6): p. 529-537.

123. Heng, P.W.S., H.Y. Lee, L.W. Chan, and A.V. Dolzhenko, *Influence of viscosity and uronic acid composition of alginates on the properties of alginate films and microspheres produced by emulsification.* Journal of Microencapsulation, 2006. **23**(8): p. 912-927.

124. *Activated Charcoal Cell Culture Tested Product Information*, Sigma-Aldrich: Saint Louis. p. 1.

125. Soares, J.P., J.E. Santos, G.O. Chierice, and E.T.G. Cavalheiro, *Thermal behavior of alginic acid and its sodium salt.* Eclética Química, 2004. **29**: p. 57-64.

126. Kim, T., S. Cho, and S. Kim, *Adsorption equilibrium and kinetics of copper ions and phenol onto modified adsorbents.* Adsorption, 2011. **17**(1): p. 135-143.

127. Bergé-Lefranc, D., H. Pizzala, R. Denoyel, V. Hornebecq, J.-L. Bergé-Lefranc, et al., *Mechanism of creatinine adsorption from physiological solutions onto mordenite.* Microporous and Mesoporous Materials, 2009. **119**(1–3): p. 186-192.

128. Shoichet, M.S., R.H. Li, M.L. White, and S.R. Winn, *Stability of hydrogels used in cell encapsulation: An in vitro comparison of alginate and agarose.* Biotechnology and Bioengineering, 1996. **50**(4): p. 374-381.

129. Lanza, R., R. Langer, and J. Vacanti, *Index*, in *Principles of Tissue Engineering (Third Edition)*, L. Robert, L. Robert, and V. Joseph, Editors. 2007, Academic Press: Burlington. p. 1291-1307.

130. Kratz, A., M. Ferraro, P.M. Sluss, and K.B. Lewandrowski, *Case records of the Massachusetts General Hospital. Weekly clinicopathological exercises. Laboratory reference values.* The New England journal of medicine, 2004. **351**(15): p. 1548-63.